Supplementary Information for

HrrSA orchestrates a systemic response to heme and determines prioritisation of terminal cytochrome oxidase expression

Marc Keppel[1#], Max Hünnefeld[1#], Andrei Filipchyk[1#], Ulrike Viets[1], Cedric-Farhad Davoudi[1], Aileen Krüger[1], Eugen Pfeifer[2], Christina Mack[1], Tino Polen[1], Meike Baumgart[1], Michael Bott[1], and Julia Frunzke[1*]

[1]Institute of Bio- und Geosciences, IBG-1: Biotechnology, Forschungszentrum Jülich, 52425 Jülich, Germany
[2]Microbial Evolutionary Genomics, Institute Pasteur, 75015 Paris, France

*Corresponding author:
Julia Frunzke; Email: j.frunzke@fz-juelich.de; Phone: +49 2461 615430

[#]These authors contributed equally to this work.

This PDF file includes:

Figure S1: Schematic overview of the convolution profiling.
Figure S2: Assessment of significance for the reported peak intensity values.
Figure S3: Global binding pattern of HrrA in the *C. glutamicum* genome in response to hemin addition.
Figure S4: Distribution of distances from HrrA binding peaks centers to the closest gene start site (transcription start site, TSS).
Figure S5: HrrA binding to selected target promotor regions.
Figure S6: Derivation of a HrrA binding motif revealed a weakly conserved palindromic sequence.
Figure S7: Visual inspection of *C. glutamicum* cells before and after addition of heme.
Figure S8: Growth assays revealed an increased sensitivity of Δ*hrrA* cells against oxidative stress.
Figure S9: Binding affinity of HrrA to selected target promoters.
Figure S10: Time-resolved differential gene expression analysis.
Figure S11: Correlation of HrrA binding and expression change.
Figure S12: HrrA coordinates expression of *ctaA* and *ctaB* in response to heme.

Table S1: Bacterial strains and plasmids used in this study.
Table S2: Oligonucleotides used in this study.
Table S5: Pearson correlation for the gene expression values (TPM) between the two biological replicates.

SI References

Other supplementary materials for this manuscript include the following separate files:

Table S3: Full Dataset, binding peaks HrrA and transcriptome analysis of *C. glutamicum* wild type and Δ*hrrA.*
Table S4: Filtered dataset of time resolved transcriptome analysis of *C. glutamicum* wild type and Δ*hrrA* with genes showing at least two-fold alteration.

Supplementary Figures

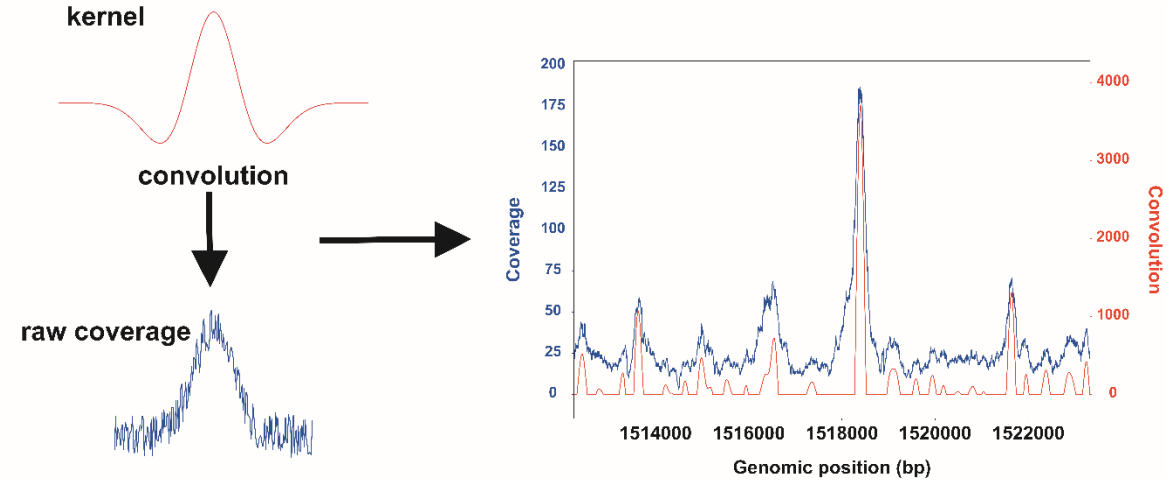

Figure S1: Schematic overview of the convolution profiling. Read coverage was convolved with negative second order Gaussian kernel. The convolved read coverage was then scanned to discover the local maxima (peaks).

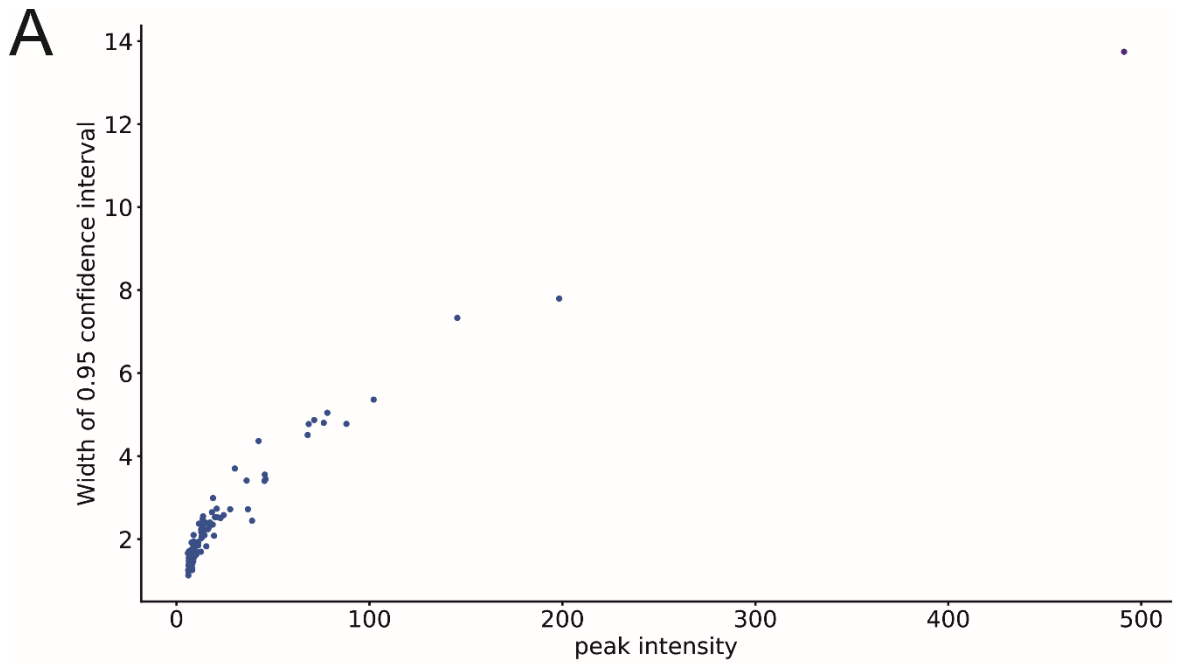

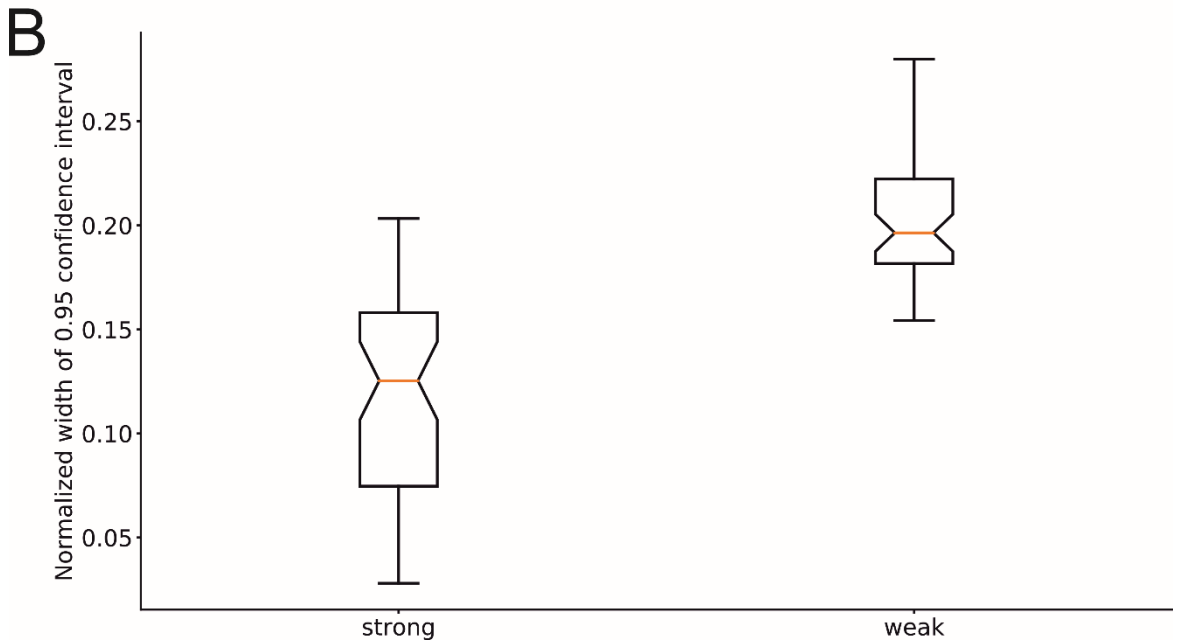

Figure S2: Assessment of significance for the reported peak intensity values. (A) The error of peak intensity value (0.95 confidence intervals width) linearly depends on its absolute value. The stronger the peak the less the confidence in its absolute value. In contrast, the relative error normalized to peak intensity is similar for peaks of various strength, hence can be used as universal measure for significance assessment. (B) Distribution of the normalized confidence intervals width (NCIW) among the detected peaks. The distribution is represented as box plots with box edges at 1st and 3rd quantiles and box whiskers at minimum and maximum values. For the weak peaks (peak intensity <10) average NCIW is around 0.2 and limited by 0.28, while for the strong ones the average NCIW is around 0.13 and limited by 0.2. The upper limits were taken for the final estimation, as the most conservative confidence evaluation was pursued.

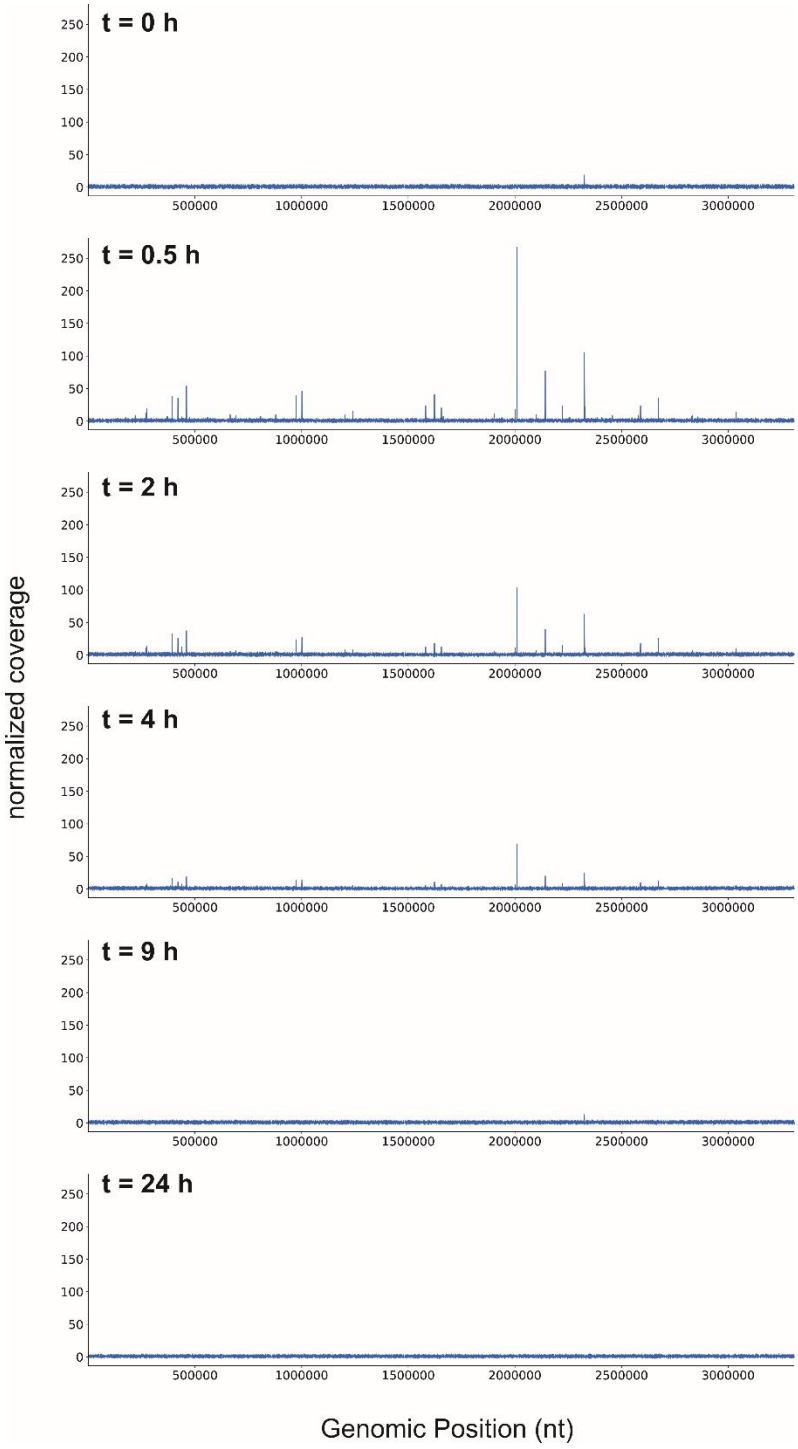

Figure S3: Global binding pattern of HrrA in the *C. glutamicum* genome in response to hemin addition. Genomic coverage (number of reads covering a particular genomic position) was normalized to the average coverage of the regions not harbouring binding peaks. Thus, depicted peak intensities are comparable between different time points. The strain *C. glutamicum*::*hrrA*-C-*twinstrep* was cultivated in CGXII minimal medium (lacking $FeSO_4$) supplemented with 2% (w/v) glucose and 4 µM hemin was added at 0 h. Cells were harvested at different time points as described in Figure 1.

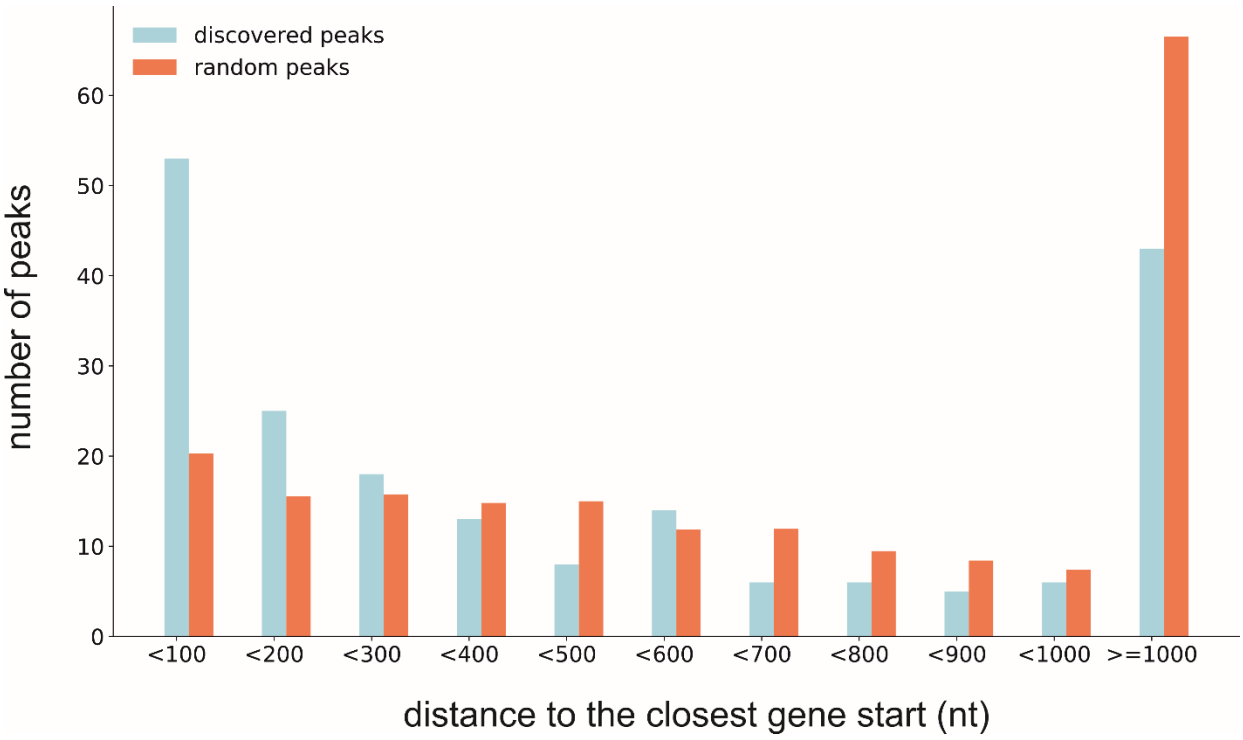

Figure S4: Distribution of distances from HrrA binding peaks centres to the closest downstream gene start site (transcription start site, TSS). As a background (red color), random peaks of the same width as real ones were generated. Random peak generation was performed 100 times and resulting distance distributions were then averaged into a single background distribution. Peaks with a distance of <100 nt can also be found up to 60 nt downstream of the TSS.

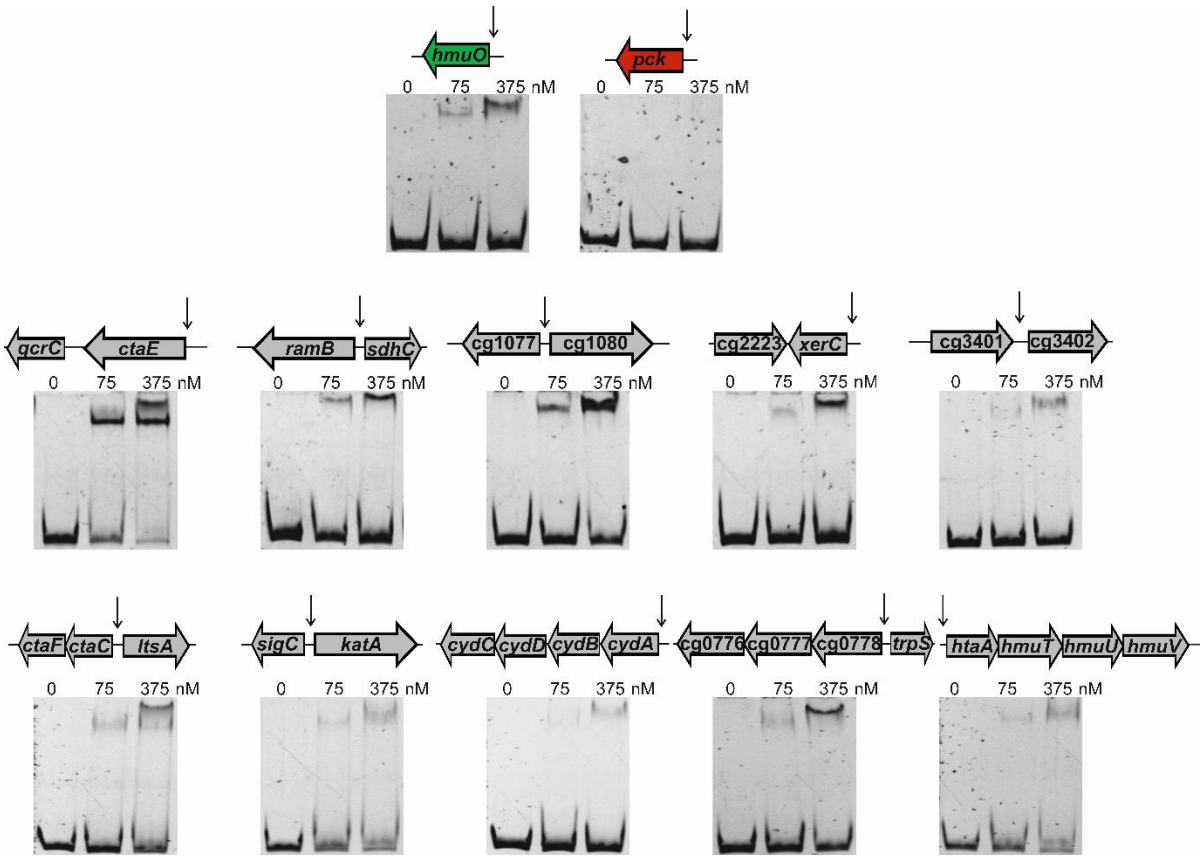

Figure S5: HrrA binding to selected target promotor regions. Protein-DNA interactions were validated by electrophoretic mobility shift assays (EMSA) using 15 nM DNA fragments covering 50 bp up- and downstream of the maximal ChAP-Seq peak height and an increasing protein monomer concentration of 0, 75 and 375 nM. The genomic location of the maximal peak height found in the ChAP-Seq experiments is indicated by an arrow. As control, the promoter regions of *hmuO* (positive control) and *pck* (negative control) were used.

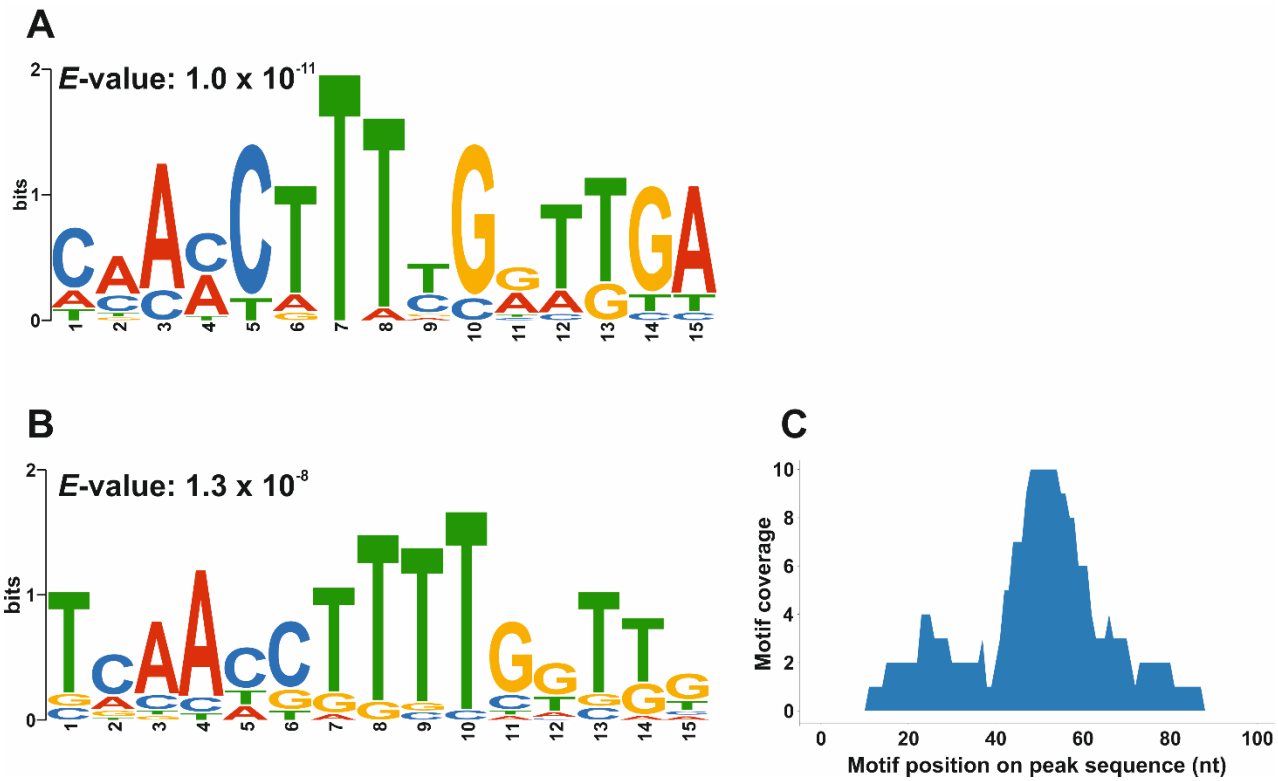

Figure S6: Derivation of a HrrA binding motif revealed a weakly conserved palindromic sequence. Sequences of all peaks with at least two-fold increased coverage (T_0) (A) or 100 bp of the tested EMSA DNA fragments (Figure S5) (B) were used for a MEME v.5 analysis (http://meme-suite.org). (C) Shown is the position of identified motif sequences within the analysed peak sequences used in (B). The majority of HrrA motifs centre at the position of the peak maximum (at 50 nt).

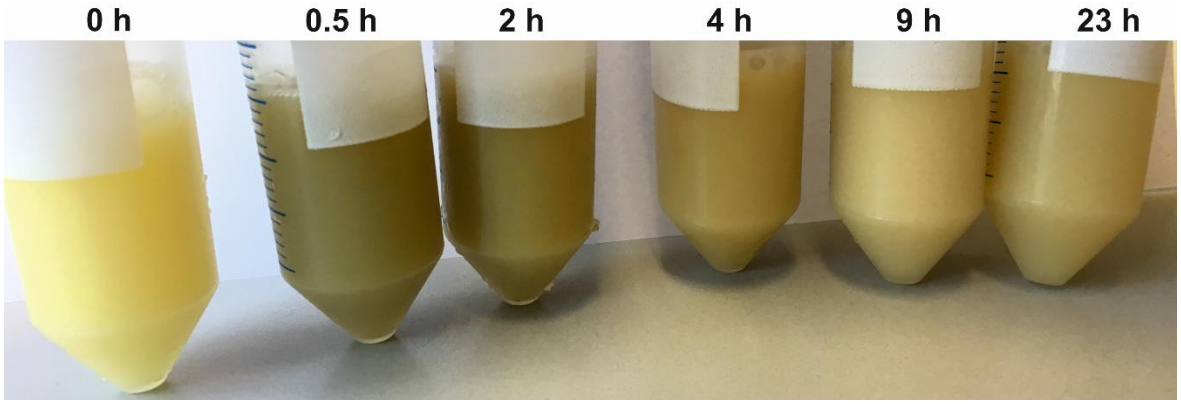

Figure S7: Visual inspection of *C. glutamicum* cells before and after addition of heme. Iron-starved *C. glutamicum* wild type cells were cultivated in CGXII medium (2 % (w/v) glucose, without $FeSO_4$) and cells were harvested at different time points before and after the addition of 4 µM heme. Cell pellets were subsequently resuspended in Tris buffer (100 mM Tris-HCl, 1 mM EDTA, pH 8.0) and adjusted to an OD_{600} of 3.5.

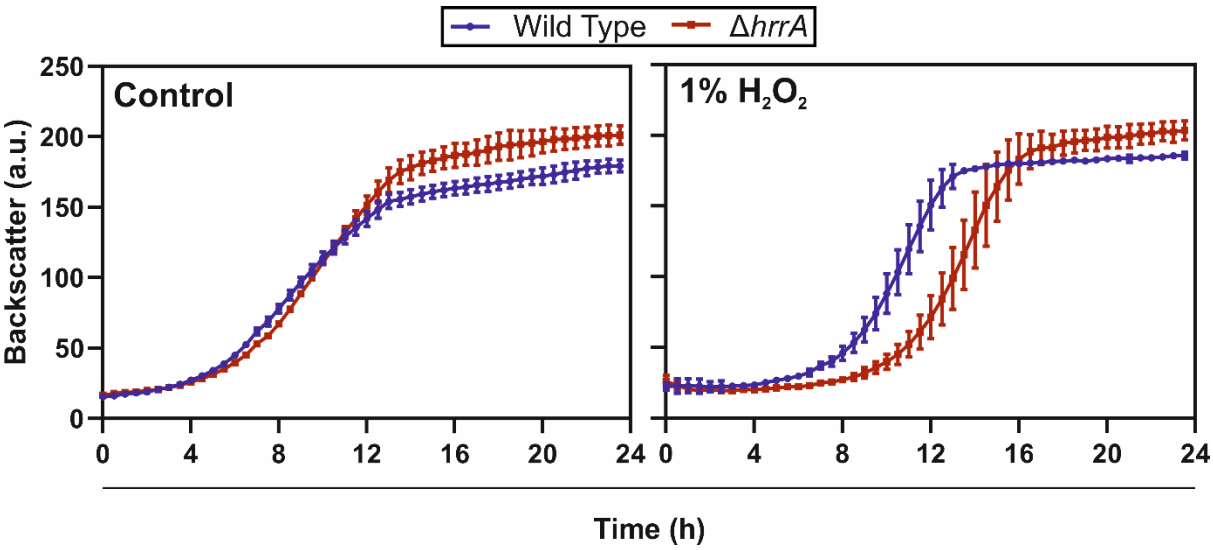

Figure S8: Growth assays revealed an increased sensitivity of *C. glutamicum* Δ*hrrA* against oxidative stress. Iron-starved *C. glutamicum* wild type as well as the mutant strain Δ*hrrA* were inoculated to an OD_{600} of 1 in CGXII medium (2% (w/v) glucose, 4 µM hemin, without $FeSO_4$) and subsequently incubated for 15 min at RT either with 1% (v/v) H_2O_2 or without. This incubation time of 15 min served as avoidance of misleading backscatter measurements due to foam generation. After the incubation, cells were transferred to microtiter plates and cultivated in a microbioreactor cultivation system. Growth curves shown are based on backscatter measurements (expressed in arbitrary units (a.u.)) of three biological replicates. The error bars represent the standard deviation of these replicates.

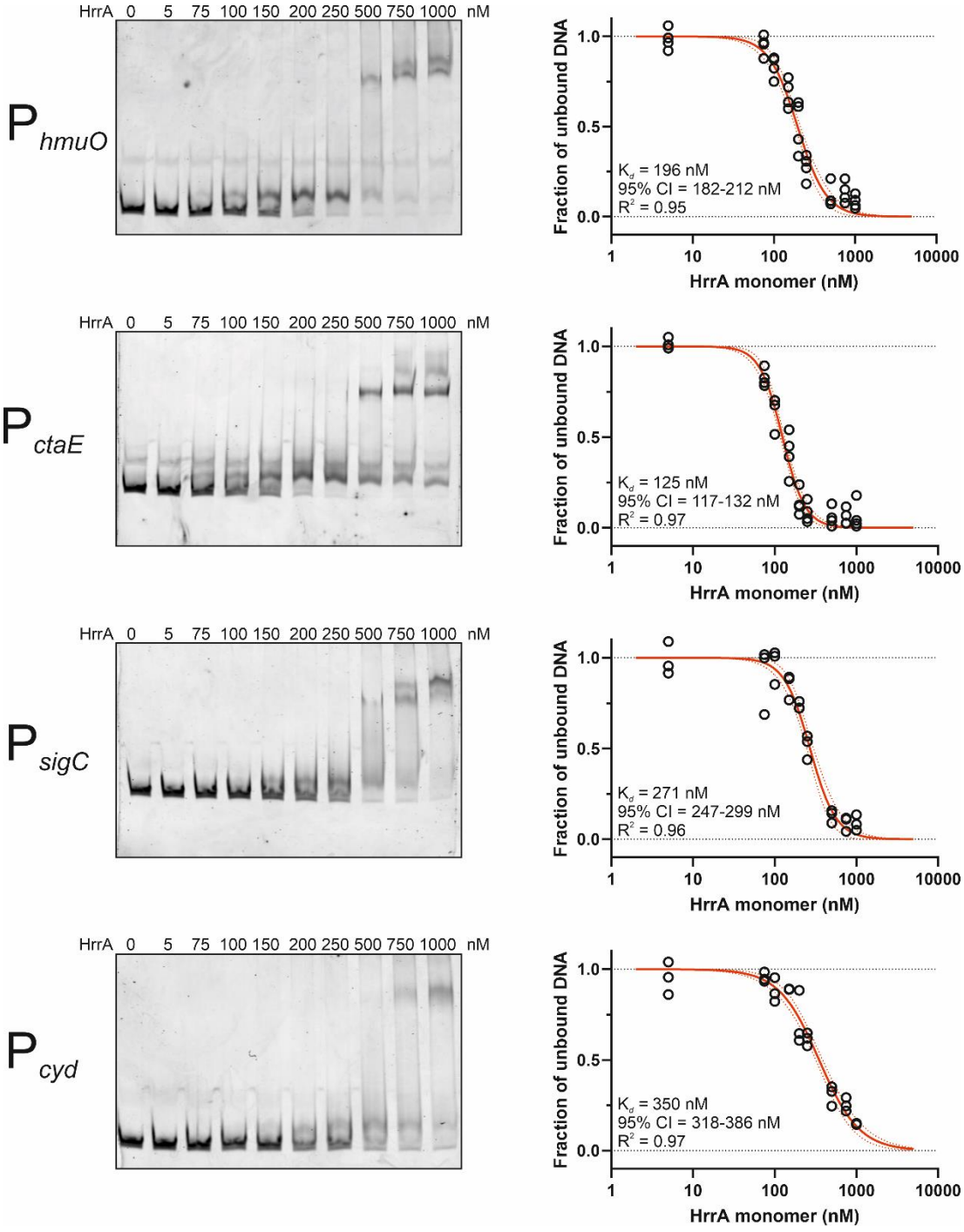

Figure S9: Binding affinity of HrrA to selected target promoters. Depicted are representative images of quantitative EMSAs used for analysis of protein-DNA interaction and the calculation of HrrA affinities to the different promoters. For the analysis, 10 nM Cy3-labelled 98-105 bp DNA fragments containing the maximal ChAP-Seq peak height were used with increasing amounts of HrrA (given as monomers). Determination of unbound DNA in EMSA studies allowed the calculation of HrrA binding affinities to different target promoters. Quantification of unbound DNA band intensities was performed using Image Studio Lite (Licor, Bad Homburg, Germany) and apparent K_d values were calculated using GraphPad Prism 7. The calculation of apparent K_d – values is based on 3-4 gels each. Black dotted lines represent top and bottom constraints for the fit. Red dotted lines represent the 95% confidence level. CI, confidence interval.

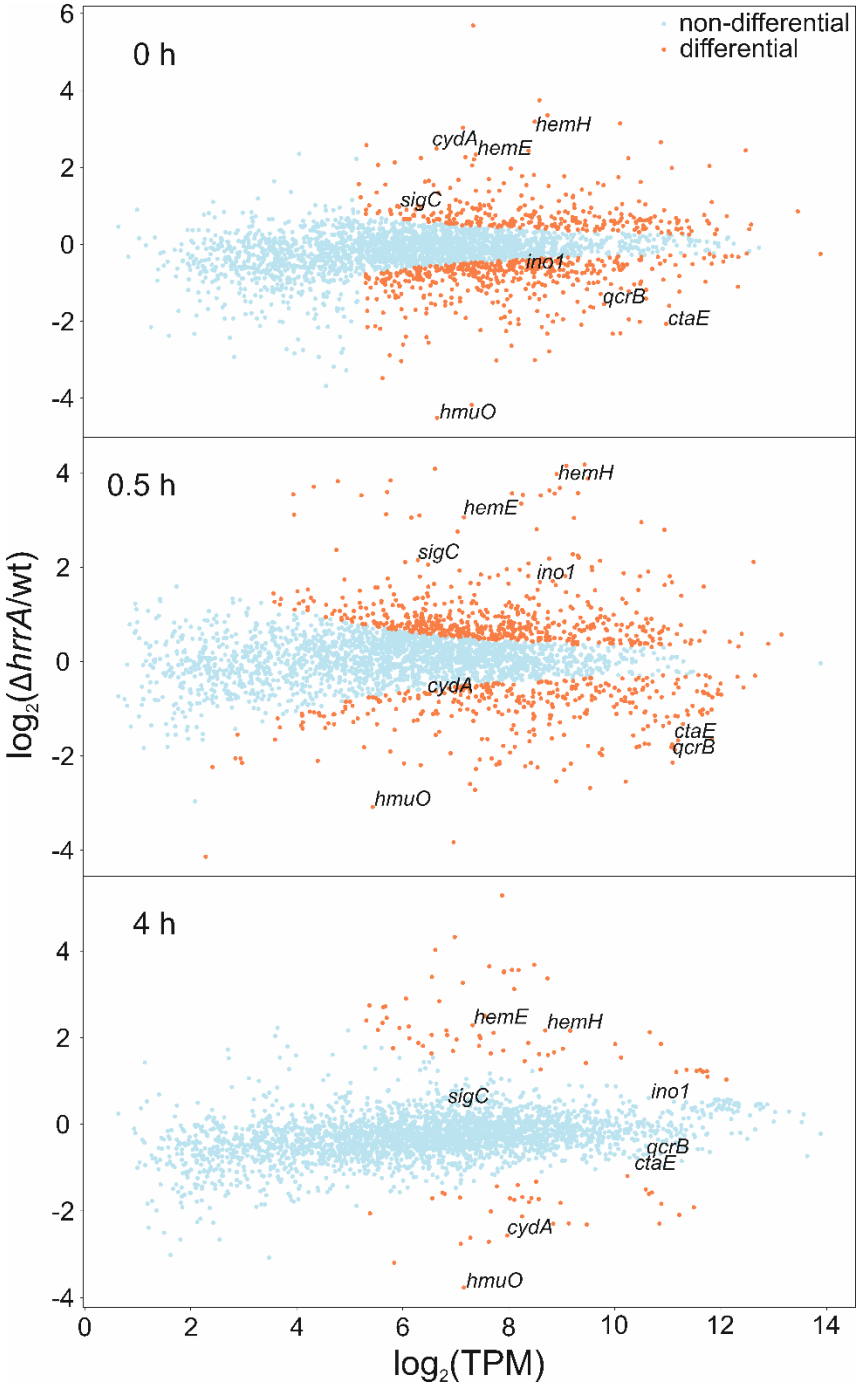

Figure S10: Time-resolved differential gene expression analysis. Shown is the $\log_2$ fold change in gene expression (Δ*hrrA* versus wild type) along with a $\log_2$ mean expression (expression averaged for Δ*hrrA* and WT samples) in transcripts per million (TPM). Orange dots represent significantly differentially expressed genes with an empirical FDR <0.05 (see material and methods). Wild type and Δ*hrrA C. glutamicum* strains were grown in CGXII medium (without $FeSO_4$) supplemented with 2% (w/v) glucose and 4 µM hemin (T_0 is prior addition of hemin; for details on cultivation and sample preparation see material and methods).

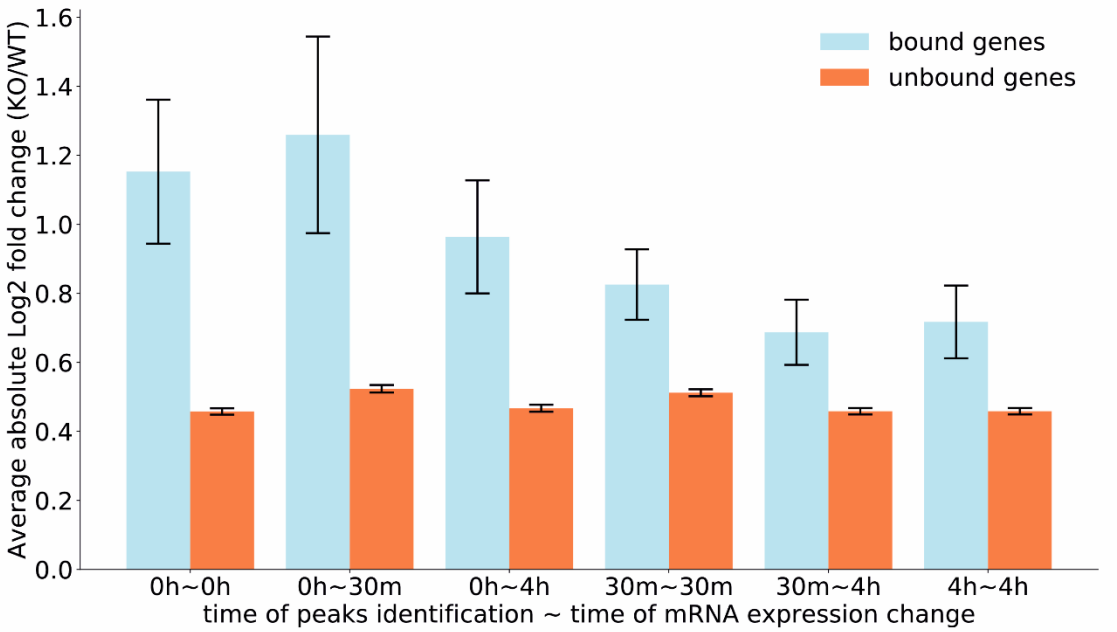

Figure S11: Correlation of HrrA binding and expression change. For the time-points 0h, 0.5h, 4h all the *C. glutamicum* protein-coding genes with decent expression (>10 TPM in Δ*hrrA* and WT samples) were split into groups: bound by HrrA (the ones which have an HrrA binding peak within 800 nt region upstream or 200 nt downstream to the transcription start site) and unbound. For these groups mean absolute log2 fold change (Δ*hrrA*/WT) was calculated for the time-points 0h, 0.5h, 4 h along with standard error of the mean.

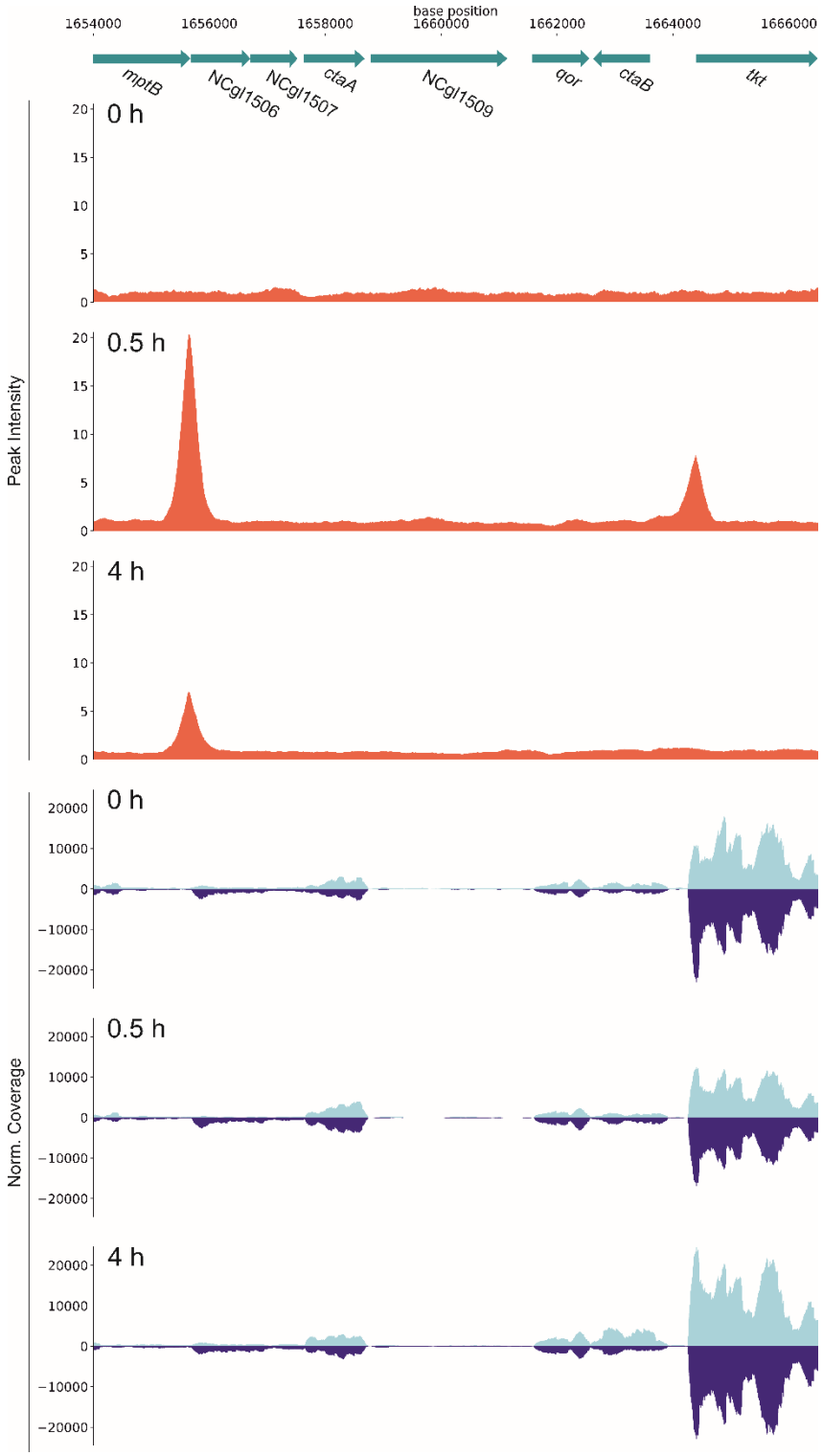

Figure S12: HrrA coordinates expression of *ctaA* and *ctaB* in response to heme. Shown are the ChAP-Seq (orange) and RNA-Seq (blue) results focusing on the *ctaA* and *ctaB* locus in the genome of *C. glutamicum.* Depicted is the genomic region between *mptb* (cg1766) and *tkt* (cg1774). For the cultivation, CGXII medium supplemented with 2% (w/v) glucose and 4 µM hemin was inoculated with iron starved cells from a stationary culture and adjusted to an OD_{600} of 3.5. Samples were analysed at the indicated time points as described in material and methods.

Supplementary Tables

Table S1: Bacterial strains and plasmids used in this study. Oligonucleotides used for the construction of the plasmids are listed in Table S2.

Strain	Relevant characteristics	Reference
Escherichia coli		
DH5α	*fhuA2 lac(del)U169 phoA glnV44 Φ80' lacZ(del)M15 gyrA96 recA1 relA1 endA1 thi-1 hsdR17*; for general cloning purposes	Invitrogen
BL21(DE3)	B F$^-$ *ompT gal dcm lon hsdS$_B$*($r_B^-m_B^-$) λ(DE3 [*lacI lacUV5-T7p07 ind1 sam7 nin5*]) [*malB*$^+$]$_{K\text{-}12}$(λ^S); overexpression of proteins.	(1)
Corynebacterium glutamicum		
***C. glutamicum* ATCC 13032**	Biotin-auxotrophic wild type strain	(2)
C. glutamicum* Δ*hrrA	Derivative of ATCC 13032 with in-frame deletion of the *hrrA* gene (cg3247).	(3)
C. glutamicum*::*hrrA*-C-*twinstrep	Derivative of ATCC 13032 encoding a C-terminally twinstrep-tagged version of *hrrA* (cg3247).	This study

Plasmids		
Name	**Resistance**	**Source**
pK19 *mob sacB*	Kanamycin	(4)
pK19 *mob sacB_hrrA*-C-*twinstrep*	Kanamycin	This study

Table S2: Oligonucleotides used in this study.

#	Name	Sequence
Construction of pK19 *mob sacB_hrrA*-C-*twinstrep*		
1	hrrA-LF-twin-strep_fw	CAAGCTTGCATGCCTGCAGGTCGACGCGGAATCGACGTCATCTTG
2	hrrA-LF-twin-strep_rv	ACCTAAAGCCTTGCAGCAACCCCCGCTATTTTTCGAACTGCGGGTGG
3	hrrA-RF_fw	GAGCCACCCGCAGTTCGAAAAATAGCGGGGGTTGCTGCAAGGC
4	hrrA-RF_rv	ATTCGAGCTCGGTACCCGGGGATCCCCGGAATCAATACACCGGC
Amplification of DNA probes for EMSAs		
5	P_{hmuO} (EMSA) fw	GAGAAATCCTCACGCTCAC
6	P_{hmuO} (EMSA) fw-Cy3	Cy3-GAGAAATCCTCACGCTCAC
7	P_{hmuO} (EMSA) rv	GGTGGGAGCCCCAAAGTTG
8	P_{ctaE} (EMSA) fw	CCCAAAGTGGTTTCCGCAGG
9	P_{ctaE} (EMSA) fw-Cy3	Cy3-CCCAAAGTGGTTTCCGCAGG
10	P_{ctaE} (EMSA) rv	ACGCCTTTTATTCGGGTTC
11	P_{pck} (EMSA) fw	CTTTCTATGGAGATGATCG
12	P_{pck} (EMSA) rv	CGATTTAAATGGACCCTAAAC
13	P_{ramB} (EMSA) fw	CCTGCGCAAAGTTGCTCCCTG
14	P_{ramB} (EMSA) rv	CTCACAGGATACCGATCCGAAC
15	P_{cg1080} (EMSA) fw	CGCTCCTCTGTGGGATTTGTC
16	P_{cg1080} (EMSA) rv	GCCTTCACTCCCTCAAAC
17	P_{xerC} (EMSA) fw	CTTAGGCTTGCCTCACACAC
18	P_{xerC} (EMSA) rv	AATGCGGAAATGCCATAAAACC
19	P_{cg3402}(EMSA) fw	CATAGGGGTATAGCCTTGAG
20	P_{cg3402}(EMSA) rv	CAGTGTGCGCAGGTCATGCC
21	P_{ctaC}(EMSA) fw	GGAATACCTAAAGTCTAGGC
22	P_{ctaC}(EMSA) rv	GTAGGAACGTAGGGGGTAAG
23	$P_{sigC/katA}$(EMSA) fw	GGTCACCATAAAGGTGTGTAG
24	$P_{sigC/katA}$(EMSA) fw-Cy3	Cy3-GGTCACCATAAAGGTGTGTAG
25	$P_{sigC/katA}$(EMSA) rv	GCCACCAAATAATCAGCCC
26	P_{cyd} (EMSA) fw	GTTCCCGCTCACAGCTTAAC
27	P_{cyd} (EMSA) fw-Cy3	Cy3-GTTCCCGCTCACAGCTTAAC
28	P_{cyd} (EMSA) rv	GGTGACTTGTCAACAAGGGG
29	P_{trpS} (EMSA) fw	GACTTGTTTACCCAAGCAATAC
30	P_{trpS} (EMSA) rv	CCGGTGAGGCAACATTTACC
31	P_{htaA} (EMSA) fw	GTCATGATGGCGTCTCGGGC
32	P_{htaA} (EMSA) rv	GTAATCAACGCACAAATG

Table S5: Pearson correlation for the gene expression values (TPM) between the two biological replicates. Transcriptome expression estimates for all the three time-points and both KO and WT conditions show high reproducibility. The genes with low expression (combined expression in replicates < 5 TPM) were not included in this analysis.

Time Point	WT	KO
0 h	0.9987	0.9994
0.5 h	0.9990	0.9984
4 h	0.9974	0.9964

References

1. Studier, F.W. and Moffatt, B.A. (1986) Use of bacteriophage T7 RNA polymerase to direct selective high-level expression of cloned genes. *J. Mol. Biol.*, **189**, 113-130.
2. Kalinowski, J., Bathe, B., Bartels, D., Bischoff, N., Bott, M., Burkovski, A., Dusch, N., Eggeling, L., Eikmanns, B.J., Gaigalat, L. *et al.* (2003) The complete *Corynebacterium glutamicum* ATCC 13032 genome sequence and its impact on the production of L-aspartate-derived amino acids and vitamins. *J Biotechnol*, **104**, 5-25.
3. Frunzke, J., Gätgens, C., Brocker, M. and Bott, M. (2011) Control of heme homeostasis in *Corynebacterium glutamicum* by the two-component system HrrSA. *J Bacteriol*, **193**, 1212-1221.
4. Schäfer, A., Tauch, A., Jager, W., Kalinowski, J., Thierbach, G. and Pühler, A. (1994) Small mobilizable multi-purpose cloning vectors derived from the *Escherichia coli plasmids* pK18 and pK19: selection of defined deletions in the chromosome of *Corynebacterium glutamicum*. *Gene*, **145**, 69-73.

HrrSA orchestrates a systemic response to heme and determines prioritization of terminal cytochrome oxidase expression

Marc Keppel[1#], Max Hünnefeld[1#], Andrei Filipchyk[1#], Ulrike Viets[1], Cedric-Farhad Davoudi[1], Aileen Krüger[1], Christina Mack[1], Eugen Pfeifer[2], Tino Polen[1], Meike Baumgart[1], Michael Bott[1], and Julia Frunzke[1]*

[1]Institute of Bio- und Geosciences, IBG-1: Biotechnology, Forschungszentrum Jülich, 52425 Jülich, Germany

[2]Microbial Evolutionary Genomics, Institute Pasteur, 75015 Paris, France

*Corresponding author:

Julia Frunzke; Email: j.frunzke@fz-juelich.de; Phone: +49 2461 615430

[#]These authors contributed equally to this work.

Keywords: Heme signaling, *Corynebacterium glutamicum*, *Corynebacterium diphtheriae*, two-component systems, bacterial transcription, regulatory networks, ChIP-Seq, HrrSA

Abstract

Heme is a multifaceted molecule. While serving as a prosthetic group for many important proteins, elevated levels are toxic to cells. The complexity of this stimulus has shaped bacterial network evolution. However, only a small number of targets controlled by heme-responsive regulators have been described to date. Here, we performed chromatin affinity purification and sequencing to provide genome-wide insights into *in vivo* promoter occupancy of HrrA, the response regulator of the heme-regulated two-component system HrrSA of *Corynebacterium glutamicum*. Time-resolved profiling revealed dynamic binding of HrrA to more than 200 different genomic targets encoding proteins associated with heme biosynthesis, the respiratory chain, oxidative stress response and cell envelope remodeling. By repression of the extracytoplasmic function sigma factor *sigC*, which activates the *cydABCD* operon, HrrA prioritizes the expression of genes encoding the cytochrome bc_1-aa_3 supercomplex. This is also reflected by a significantly decreased activity of the cytochrome aa_3 oxidase in the Δ*hrrA* mutant. Furthermore, our data reveal that HrrA also integrates the response to heme-induced oxidative stress by activating *katA* encoding the catalase. These data provide detailed insights in the systemic strategy that bacteria have evolved to respond to the versatile signaling molecule heme.

Introduction

Heme (iron bound protoporphyrin IX) is a versatile molecule that is synthesized and used by virtually all aerobic eukaryotic and prokaryotic cells (1). It serves as the prosthetic group of hemoglobins, hydroxylases, catalases, peroxidases, and cytochromes (2) and is therefore essential for many cellular processes, such as electron transfer, respiration and oxygen metabolism (3). Furthermore, salvaged heme represents the most important iron source for a variety of pathogenic bacteria (4,5), and also non-pathogenic bacteria can meet their iron demand by degradation of environmental heme. This becomes evident from the diverse set of heme uptake systems and heme oxygenases that catalyze the degradation of the protoporphyrin ring to biliverdin and the concomitant release of carbon monoxide and iron (6).

While heme represents an essential cofactor for a variety of proteins, this molecule also exhibits severe toxicity at high concentrations. Therefore, organisms have evolved sophisticated regulatory networks to tightly control heme uptake, detoxification (including export), synthesis and degradation (4). Several heme-regulated transcription factors have been described, including the heme activator protein (Hap) 1, which is an activator of genes required for aerobic growth of the yeast *Saccharomyces cerevisiae* (7); the transcription factor BACH1 (BTB and CNC homology 1), which is conserved in mammalian cells (8,9); and the rhizobial Irr protein, which is a heme-regulated member of the Fur family of transcriptional regulators (10-12).

In Gram-positive bacteria, two-component systems (TCSs) appear to play a prevalent role in heme-responsive signaling (13,14), as exemplified by the heme sensor system HssRS of *Staphylococcus aureus* and *Bacillus anthracis,* which controls the expression of the *hrtBA* operon, encoding a heme efflux system in both species (15,16). Remarkably, several members of the *Corynebacteriaceae* family, including the human pathogen *Corynebacterium diphtheriae* and the biotechnological platform strain *C. glutamicum,* have two paralogous TCSs, namely, HrrSA and ChrSA, dedicated to heme-responsive control of gene expression (17-20). The kinases HrrS and ChrS were recently shown to perceive transient changes in heme availability by direct intramembrane interactions with heme (21,22). Heme binding triggers autophosphorylation of the sensor kinase, followed by transfer of the phosphoryl group to the cognate response regulators HrrA and ChrA. In *C. glutamicum*, significant cross-phosphorylation was observed between the closely related systems; however, this crosstalk is proofread by a highly specific phosphatase activity of the kinases toward the cognate response regulators under non-inducing conditions (23). While the ChrSA system appears to be mainly involved in rapid activation of the HrtBA detoxification system (19), previous data suggest that HrrSA coordinates a homeostatic response to heme (18). In recent studies, six direct target operons have been described for HrrA, including genes encoding enzymes involved in heme synthesis (*hemE*, *hemA* and *hemH*), heme utilization (*hmuO*, encoding a heme oxygenase) and the *ctaE-qcrCAB* operon, encoding components of the heme-containing cytochrome bc_1-aa_3 supercomplex of the respiratory chain (18). Expression of *hrrA* as well as *hmuO* is, furthermore, repressed by the global iron-dependent regulator DtxR in *C. glutamicum* under conditions of sufficient iron supply (24,25) thereby linking iron and heme regulatory networks in this organism.

The branched electron transport chain of *C. glutamicum* consists of the cytochrome bc_1-aa_3 supercomplex (encoded by *ctaD*, the *ctaCF* operon, and the *ctaE-qcrCAB* operon) and the

cytochrome *bd* oxidase, encoded by the first two genes of the *cydABDC* operon (26). Although both the cytochrome *aa*$_3$ oxidase and the *bd* oxidase are involved in the establishment of a proton-motive force (PMF), the *aa*$_3$ oxidase is an active proton pump that is responsible for the increased proton translocation number (6 H^+/2 e^-) of the cytochrome *bc*$_1$-*aa*$_3$ supercomplex compared to that of the *bd* oxidase (2 H^+/2 e^-) (26). The presence of the cytochrome *bc*$_1$-*aa*$_3$ supercomplex is a characteristic feature of almost all actinobacteria, because members of this phylum lack a soluble cytochrome *c* and instead harbor a diheme cytochrome *c*$_1$ that directly shuttles electrons from the *bc*$_1$ complex to the *aa*$_3$ oxidase (27-32). Furthermore, both terminal oxidases differ in heme content, as the *bc*$_1$-*aa*$_3$ supercomplex harbors six heme molecules, while the *bd* oxidase harbors only three. Surprisingly, not much is known about the regulation of terminal oxidases in *C. glutamicum*. In addition to the described activation of the *ctaE-qcr* operon by HrrA, the hydrogen peroxide-sensitive regulator OxyR was described as a repressor of the *cydABCD* operon (33,34). Furthermore, the ECF sigma factor SigC (σ^C) activates expression of the *cydABCD* operon (33,35). For σ^C, a speculated stimulus is a defective electron transfer in the *aa*$_3$ oxidase (35) and such a defect was observed under copper-deprivation or when heme *a* insertion was disturbed, which resulted in activation of the σ^C regulon (36,37).

Interestingly, the regulons of prokaryotic heme regulators described thus far comprise only a low number of direct target genes, which are mostly involved in heme export (e.g., *hrtBA*) or degradation (*hmuO*). This current picture of prokaryotic heme signaling, however, does not match the complexity of the cellular processes influenced by heme. In this study, we performed a time-resolved and genome-wide binding profiling of HrrA in *C. glutamicum* using chromatin affinity purification and sequencing (ChAP-Seq) of HrrA in *C. glutamicum* showing the transient HrrA promoter occupancy of more than 200 genomic targets in response to heme. The obtained results emphasize that HrrSA is a global regulator of heme homeostasis, which also integrates the response to oxidative stress and cell envelope remodeling. Transcriptome analysis (RNA-Seq) at different time points after heme induction revealed HrrA to be an important regulator of the respiratory chain by coordinating the expression of components of both quinol oxidation branches as well as menaquinol reduction. Remarkably, HrrA was found to prioritize the expression of operons encoding the cytochrome *bc*$_1$-*aa*$_3$ supercomplex by repressing *sigC* expression.

Methods

Bacterial strains and growth conditions

Bacterial strains used in this study are listed in Table S1. The *C. glutamicum* strain ATCC 13032 was used as wild type (29) and cultivations were performed in liquid BHI (brain heart infusion, Difco BHI, BD, Heidelberg, Germany), as complex medium or CGXII (38) containing 2 % (w/v) glucose as minimal medium. The cells were cultivated at 30°C; if appropriate, 25 µg/ml kanamycin was added. *E. coli* (DH5α and BL21 (DE3)) was cultivated in Lysogeny Broth (Difco LB, BD, Heidelberg, Germany) medium at 37°C in a rotary shaker and for selection, 50 µg/ml kanamycin was added to the medium.

Recombinant DNA work and cloning techniques

Cloning and other molecular methods were performed according to standard protocols (39). As template, chromosomal DNA of *C. glutamicum* ATCC 13032 was used for PCR amplification of DNA fragments and was prepared as described previously (40). All sequencing and synthesis of oligonucleotides was performed by Eurofins Genomics (Ebersberg, Germany). For ChAP sequencing, the native *hrrA* was replaced with a twin-strep-tagged version of this gene using a two-step homologous recombination system. This system is based on the suicide vector pK19 *mob-sacB* (41,42), containing 500 bps flanking each site of the targeted sequence inside the *C. glutamicum* genome. The pK19*mob-sacB hrrA*-C-*twinstrep* plasmid was constructed using Gibson assembly of PCR products (primers indicated in Table S2) and the cut pK19 vector (43).

ChAP Sequencing – Sample preparation

The preparation of DNA for ChAP sequencing was adapted from (44). The *C. glutamicum* strain ATCC 13032::*hrrA*-C-twinstrep was used for the time series experiment. A preculture was inoculated in liquid BHI medium from a fresh BHI agar plate and incubated for 8-10 h at 30°C in a rotary shaker. Subsequently, cells were transferred into a second preculture in CGXII medium containing 2 % (w/v) glucose and 0 µM $FeSO_4$ to starve the cells from iron. Protocatechuic acid (PCA), which was added to the medium, allowed the uptake of trace amounts of iron. From an overnight culture, six main cultures were inoculated to an OD_{600} of 3.0 in 1 l CGXII medium containing 4 µM hemin as sole iron source. For the time point t = 0, the cells were added to 1 l fresh CGXII containing no additional iron source. After 0 h, 0.5 h, 4 h, 9 h and 24 h, cells corresponding to an OD_{600} of 3.5 in 1 l were harvested by centrifugation at 4 °C, 5000 *x g* and washed once in 20 ml CGXII. Subsequently, the cell pellet was resuspended in 20 ml CGXII containing 1 % (v/v) formaldehyde to crosslink the regulator protein to the DNA. After incubation for 20 min at RT, the cross linking was stopped by addition of glycine (125 mM), followed by additional incubation of 5 min at RT. After that, the cells were washed three times in buffer A (100 mM Tris-HCl, 1 mM EDTA, pH=8.0) and the pellets stored overnight at -80 °C. For cell disruption, the pellet was resuspended buffer A containing "cOmplete" protease inhibitor cocktail (Roche, Germany) and disrupted using a French press cell (SLM Ainco, Spectronic Instruments, Rochester, NY) five times at 207 MPa. The DNA was fragmented to ~500 bp by sonication (Branson Sonifier 250, Branson Ultrasonics Corporation, Connecticut, USA) and the supernatant was collected after ultra-centrifugation (150.000 x *g*, 4 °C, 1 h). The DNA bound by the twin-Strep-

tagged HrrA protein was purified using Strep-Tactin XT Superflow column material (IBA Lifesciences, Göttingen, Germany) according to the supplier's manual (applying the gravity flow protocol, 1.5 ml column volume). Washing of the column was performed with buffer W (100 mM Tris-HCl, 1 mM EDTA, 150 mM NaCl, pH 8,0) and the tagged protein was eluted with buffer E (100 mM Tris-HCl, 1 mM EDTA, 150 mM NaCl, pH 8.0, added 50 mM D-Biotin). After purification, 1 % (w/v) SDS was added to the elution fractions and the samples were incubated overnight at 65°C. For the digestion of protein, 400 µg/ml Proteinase K (AppliChem GmbH, Darmstadt, Germany) was added and incubated for 3 h at 55 °C. Subsequently, the DNA was purified as following: Roti-Phenol/Chloroform/Isoamyl alcohol (Carl Roth GmbH, Karlsruhe, Germany) was added to the samples in a 1:1 ratio and the organic phase was separated using Phase Lock Gel (PLG) tubes (VWR International GmbH, Darmstadt, Germany) according to the supplier's manual. Afterwards, the DNA was precipitated by adding ice-cold ethanol (to a conc. of 70 % (v/v) and centrifugation at 16.000 x *g*, 4 °C for 10 min. The DNA was washed with ice-cold 70 % (v/v) ethanol, then dried for 3 h at 50 °C and eluted in dH_2O.

ChAP-Seq analysis - Sequencing

The obtained DNA fragments of each sample (up to 2 µg) were used for library preparation and indexing using the TruSeq DNA PCR-free sample preparation kit according to the manufacturer's instruction, yet skipping fragmentation of the DNA and omitting the DNA size selection steps (Illumina, Chesterford, UK). The resulting libraries were quantified using the KAPA library quant kit (Peqlab, Bonn, Germany) and normalized for pooling. Sequencing of pooled libraries was performed on a MiSeq (Illumina) using paired-end sequencing with a read-length of 2 x 150 bases. Data analysis and base calling were accomplished with the Illumina instrument software and stored as fastq output files. The sequencing data obtained for each sample were imported into CLC Genomics Workbench (Version 9, Qiagen Aarhus A/S) for trimming and base quality filtering. The output was mapped to accession NC_003450.3 BX927147 as *C. glutamicum* reference genome (www.ncbi.nlm.nih.gov/pubmed/12948626). Genomic coverage was convoluted with second order Gaussian kernel. The kernel was truncated at 4 sigmas (that is all kernel values positioned further then 4 sigmas from the center were set to zero) and expanded to the "expected peak width". The expected peak width was estimated *via* the following procedure: 1) all the peaks higher than 3-fold mean coverage were detected. 2) Points at which their coverage dropped below ½ of the maximal peak height were found and the distance between them was considered as a peak width. 3) The "estimated peak width" was set equal to the median peak width. The convolution profile was scanned in order to find points where first derivative changes its sign from positive to negative (Figure S1). Each such point was considered as a potential peak and was assigned with a convolution score (that is convolution with second order Gaussian kernel centred at the peak position). Furthermore, we explored the distribution of the convolution scores. It appeared to resemble normal distribution, but with a heavy right tail. We assumed that this distribution is indeed bimodal of normal distribution (relatively low scores) representing 'noise' and a distribution of 'signal' (relatively high scores). We fit the Gaussian curve to the whole distribution (via optimize.fit function from SciPy package (45)) and set a score thresholds equal mean + 4 sigmas of the fitted distribution. Further filtering with this threshold provided estimated FDR (false discovery rate) of 0.004-0.013 depending on a sample. Filtered peaks were normalized to allow inter-sample comparisons. Sum of coverages of the detected peaks was negated from

the total genomic coverage. The resulting difference was used as normalization coefficient; that is peak intensities were divided by this coefficient.

ChAP-Seq analysis – Estimation of confidence intervals

To compare peak intensities between the samples, we assessed the significance levels of the detected intensity values by an extensive *in silico* simulation of ChAP-seq experiments along with further peak-detection analyses.

The simulation consisted of the following steps: The reads were artificially generated from *C. glutamicum* genome (NC003450.3) with the error rate (number of nucleotide mismatches) equal to the average error rate of the real HrrA ChAP-seq reads (estimated from the mapping statistics). The reads were taken from randomly selected spots in the genome (simulation of the non-peak coverage) and from the regions of the detected HrrA binding peaks with the probabilities proportional to the original peak intensities. Thus, we tried to emulate the original binding architecture. We also added a small amount (10% of the total simulated reads) of the sequences heavily affected by mismatches (25% mismatches for the original *C. glutamicum* sequences), as we wanted to account for around 10% of the unmapped reads in the original HrrA ChAP-seq experiments. Finally, the simulated reads were subjected to the computational peak-detection pipeline with the same parameters as in the original analyses. As a result, we obtained the peak intensity values for the detected peaks.

In total, we simulated 200 ChAP-seq samples, each containing 1.14M reads (the average amount of reads in the original samples). For each of the detected peaks we estimated the variation of the reported peak intensity among all the simulations. That is, for each peak intensity we estimated 0.95 confidence interval, as a difference between 97.5 and 2.5 percentiles. We discovered a strong positive correlation (0.94 Pearson) between the width of the confidence intervals and mean intensity (Figure S2A). Therefore, we then normalized the width of the confidence intervals to the mean intensity values. The normalized confidence interval width (NCIW) appears to be a convenient metric as it is similar for all peaks, weakly dependent on their intensity. However, for the strongest peaks (peak intensity > 10) the NCIW is limited by 0.2, while for the weaker ones by 0.28 (Figure S2B). Then we convert NCIW upper limits to the minimum confident fold changes by the following rule: min_fold = (1+NCIW/2)/(1-NCIW/2). Thus, we conclude that for the stronger peaks minimum confident fold change (p-value < 0.05) is ~1.23, while for the weaker peaks - ~1.33.

RNA Sequencing – Sample preparation

For RNA sequencing, *C. glutamicum* wild type and the Δ*hrrA* mutant strain were cultivated under the same conditions as described for ChAP Sequencing. Both strains did not contain any plasmids and, hence, were cultivated without addition of antibiotics in biological duplicates. After 0 h (no heme), 0.5 h and 4 h, cells corresponding to an OD_{600} of 3 in 0.1 l were harvested in falcon tubes filled with ice by centrifugation at 4 °C and 5000 *x g* for 10 minutes and the pellets were stored at -80 °C. For the preparation of the RNA, the pellets were resuspended in 800 µl RTL buffer (QIAGEN GmbH, Hilden, Germany) and the cells disrupted by 3 x 30 s silica bead beating, 6000 rt/min (Precellys 24, VWR International GmbH, Darmstadt, Germany). After ultra-centrifugation

(150.000 x *g*, 4 °C, 1 h), the RNA was purified using the RNeasy Mini Kit (QIAGEN GmbH, Hilden, Germany) according to the supplier's manual. Subsequently, the ribosomal RNA was removed by running twice the workflow of the Ribo-Zero rRNA Removal Kit [Bacteria] (Illumina, California, USA) in succession. Between steps, the depletion of rRNA as well as the mRNA quality was analysed using the TapeStation 4200 (Agilent Technologies Inc, Santa Clara, USA). After removal of rRNA, the fragmentation of RNA, cDNA strand synthesis and indexing was carried out using the TruSeq Stranded mRNA Library Prep Kit (Illumina, California, USA) according to the supplier's manual. Afterwards, the cDNA was purified using Agencourt AMPure XP magnetic beads (Beckman Coulter, Indianapolis, USA). The resulting libraries were quantified using the KAPA library quant kit (Peqlab, Bonn, Germany) and normalized for pooling.

RNA-seq analysis

Sequencing reads quality was explored with the FastQC (46) tool. Since reads appeared to be of a good quality and did not harbor significant fraction of adapters or overrepresented sequences, no pre-processing was undertaken. Identical reads were collapsed with a custom script in order to prevent gene levels' misquantification caused by PCR overamplification. Reads were mapped to the *Corynebacterium glutamicum* genome (BX927147) with Bowtie2 (47). Bowtie2 was run with the following parameters: bowtie2 -1 [path to the reads, 1st mate] -2 [path to the reads, 2nd mate] -S [path to the mappings] –phred33 –sensitive-local –local –score-min C,90 –rdg 9,5 –rfg 9,5 -a –no-unal -I 40 -X 400 –no-mixed –ignore-quals.

The reads mapped to multiple locations were split proportionally between parental genes. That is if 3 reads are mapped to gene A and gene B, expression of gene A is 10 and expression of gene B is 5, then 2 reads will go to gene A and 1 read to gene B. For each *C. glutamicum* gene (48) we assigned an expression value equal to the average read coverage over the gene region. These expression values were then normalized to TPM (transcripts per million) values (49).

Furthermore, we analyzed which genes are significantly differentially expressed between conditions. We set combinatorial thresholds on normalized GEC (gene expression change) [|expr1-expr2|/(expr1+expr2)] and MGE (mean gene expression) [log2((expr1+expr2)/2)] where "expr1" is gene expression for the first condition and "expr2" for the second. Thresholds were set in a way to achieve maximal sensitivity while keeping FDR (false discovery rate) less than 0.05. FDR was estimated as GECintra/(GECintra + GECinter); where GECintra is a number of genes passed the thresholds based on intrasample GEC (that is gene expression change between the replicates for the same condition), GECinter is a number of genes passed the thresholds based on intersample GEC (that is gene expression change between two different conditions). Threshold function for GEC was defined as: 1 | if MGE < C; 2**(-A*MGE) + B | if MGE >= C; where A, B, C are parameters to be adjusted. Parameters A, B, C were adjusted with genetic algorithm optimization approach to achieve maximal sensitivity in discovery of differentially expressed genes while keeping FDR below 0.05.

Sequencing and sequence analysis

Pooled libraries were sequenced on a MiSeq (Illumina, California, USA) generating paired-end reads with a length of 2 × 75 bases. Data analysis and base calling were performed with the Illumina instrument software and stored as fastq output files.

Measurement of cell-associated hemin

C. glutamicum was cultivated in 4 µM hemin as described above (see ChAP Sequencing). To measure the cell-associated heme pool, CGXII minimal medium supplemented with 2 % (w/v) glucose and 4 µM heme was inoculated to an OD_{600} of 3.5. Samples were taken 0.5, 2, 4, 9 and 24 hours after addition of heme. Cells were harvested, resuspended in 100 mM Tris-HCl (pH 8) and adjusted to an OD_{600} of 100. Cells cultivated in 4 µM $FeSO_4$ supplemented medium were taken as a control and harvested at the same time points. Absolute spectra of cells reduced with a spatula tip of sodium dithionite were measured at room temperature using the Jasco V560 with a silicon photodiode detector in combination with 5 mm light path cuvettes. Absorption values at 406 nm were normalized by subtracting the measured absorption values of Fe-cultivated cells.

Electrophoretic mobility shift assays (EMSA)

The promotor regions of HrrA target genes (100 bp) were chosen based on the ChAP-Seq analyses and covered the maximal HrrA peak area (for primers see Table S2). For quantitative measurements, Cy3-labelled oligonucleotides were used for the generation of the DNA fragments. Before addition of the DNA, HrrA was phosphorylated by incubation for 60 min with MBP-HrrSΔ1-248 in a ratio of 2:1 and 5 mM ATP. Binding assays were performed in a total volume of 20 µl using 15 nM DNA and increasing HrrA concentrations (75 nM and 375 nM) for the qualitative analyses and 10 nM DNA with increasing HrrA concentrations from 5-1000 nM for quantitative analyses, respectively. The binding buffer contained 20 mM Tris-HCl (pH 7.5), 50 mM KCl, 10 mM MgCl2, 5% (v/v) glycerol, 0.5 mM EDTA and 0.005% (w/v) Triton X-100. After incubation for 20 min at room temperature, the reaction mixtures were loaded onto a 10 % native polyacrylamide gel and subsequently separated and documented using a Typhoon TrioTM scanner (GE healthcare). The band intensities of unbound DNA were quantified using Image Studio Lite (Licor, Bad Homburg, Germany). The band intensities were normalized to the lane containing no DNA and plotted against the HrrA concentration in $\log_{10}$ scale. Apparent K*d* values were calculated based on at least 3 gels each using a sigmoidal fit and the software GraphPad Prism 8. For the sigmoidal fit, Y=0 and Y=1 were set as top and bottom constraints. The turning point of the curve was defined as the apparent K_d.

TMPD oxidase assay

C. glutamicum wild type strain and the Δ*hrrA* mutant were cultivated to an OD_{600} of 4 in CGXII minimal with or without the addition of 4 µM hemin. Subsequently, cells were disrupted in a homogenisator Precellys® (VWR International GmbH, Darmstadt, Germany) using zirconia/silica-beads (Ø 0.1 mm, Roth, Karlsruhe) in 100 mM Tris-HCl (pH 7.5) buffer. Ultracentrifugation at 200,000 x *g* for 1 h was used for membrane isolation. The pellet was resuspended in 100 mM Tris-HCl buffer and the protein concentration was determined using a BCA assay. The N,N,N',N'-Tetramethyl-*p*-phenylenediamine (TMPD) oxidase activity in the membrane faction was measured spectrophotometrically at 562 nm in a TECAN Reader (Thermo Fisher Scientific, Massachusetts, US) by injecting 200 µM TMPD (37). An extinction coefficient of 10.5 mM^{-1} cm^{-1} was used (50). One unit of activity was defined as 1 µmol of TMPD oxidized per minute. As a control for autooxidation, a sample containing only 100 mM Tris-HCl buffer was recorded after

TMPD addition and substracted from the actual rates. Significance was evaluated by an unpaired t-test with a 95% confidence interval.

Results

Genome-wide profiling of HrrA promoter occupancy

In previous studies, a number of direct HrrA target operons were described in *C. glutamicum* and *C. diphtheriae,* suggesting an important role of the HrrSA TCS in the control of heme homeostasis (17-20). It has to be noted, that the membrane embedded HrrS sensor kinase is also activated by endogenously synthesized heme (21) and that the addition of external heme leads to a boost of the HrrSA response. In this study, we investigated the genome-wide binding profile of HrrA using chromatin affinity purification of twin-Strep-tagged HrrA combined with DNA sequencing (ChAP-Seq). Importanty, qPCR experiments confirmed wild-type level expression of the twin-Strep-tagged version of HrrA.

To obtain insights into the stimulus-dependent DNA association and dissociation, *C. glutamicum* cells were grown in iron-depleted glucose minimal medium, and samples were obtained before (T_0) and 0.5, 2, 4, 9 and 24 h after the addition of 4 µM hemin. HrrA was purified, and the bound DNA fragments were sequenced (Figure 1A). We obtained substantial enrichment of known HrrA targets in response to heme (e.g. after 0.5 hours: 5-fold *hmuO*, 54-fold *hemE*, 105-fold *ctaE*; Figure 1B, C, D, respectively) and identified more than 200 previously unknown HrrA-bound regions in the *C. glutamicum* genome (Table S3).

As expected, the highest number of peaks was identified at the first time point after the heme pulse (0.5 h), with 199 peaks meeting our applied threshold (distance of <800 bp to the closest downstream or <200 bp to the closest upstream transcription start site (TSS)). In comparison, only 15 peaks showed a more than two-fold enrichment before hemin addition (T_0, Table S3 and Figure S3). It has to be noted, that these 15 peaks detected at T_0 appear to be specific HrrA targets, since none of them was detected in an input control sample. Overall, these data illustrate the fast and transient DNA binding by HrrA in response to heme. In general, the majority of the discovered HrrA binding sites were close to TSSs (Figure S4). The binding of HrrA to 11 selected targets was confirmed by electrophoretic mobility shift assays (Figure S5), and a palindromic binding motif was deduced (Figure 2B and Figure S6).

The HrrA binding patterns depicted in Figure 1B-D are representative of many bound regions. Thirty minutes after the heme pulse, the average peak intensities increased approximately 2.5-fold in comparison to those at T_0 (Figure 2A). After 2 h of cultivation in hemin, the average peak intensity is declining and is, after 9 hours, already below the starting level at T_0 reaching a minimum in stationary phase (24 h). This is likely the result of the pre-cultivation and main cultivation under iron starvation conditions leading to a lowered intracellular heme pool. The dissociation of HrrA from its target promoters is, consequently, caused by rapid depletion of heme and a switch of HrrS from kinase to phosphatase state (23). Heme depletion was confirmed by spectroscopy of *C. glutamicum* cells (Figure 2A, dashed line) and was also obvious upon visual inspection (Figure S7). Of all peaks, that passed our threshold, 128 were upstream of genes encoding hypothetical proteins, while 150 could be assigned to genes with known or predicted function (Figure 2C). Furthermore, we assessed the significance levels of HrrA binding changes between samples from different conditions or/and time-points. It turned out, that for the

stronger peaks (peak intensity > 10) the minimum significant fold change (p-value < 0.05) is ~1.23, while for the weaker peaks (peak intensity < 10) it is ~1.33 (see Material and Methods).

To analyze the synchronicity in the HrrA regulon, peak intensities were correlated over time. A relatively high correlation between peak intensities for the time points 0.5, 2 and 4 h (Figure 2D) showed that, the system reacted proportionally for a majority of the binding sites and the strength of HrrA binding changed in response to heme availability. Relaxation of the system was observed after 9 h were peak intensities correlated well with T_0.

The HrrSA TCS coordinates heme homeostasis by integrating the response to oxidative stress and cell envelope remodeling

Our dataset confirmed the binding of HrrA to all previously known targets, including genes encoding components of heme biosynthesis (*hemE*, *hemH* and *hemA*), degradation (*hmuO*), and export (*hrtBA*) pathways and heme-containing complexes of the respiratory chain (*ctaE-qcrCAB* operon and *ctaD*). A comprehensive overview of all identified HrrA targets is presented in Table S3; selected target genes are listed in Table 1. Among the more than 180 novel targets identified in this study, we observed HrrA binding upstream of *ctaB*, which encodes a protoheme IX farnesyltransferase that catalyzes the conversion of heme *b* to heme *o* (26) and upstream of *ctaC*, which encodes subunit 2 of the cytochrome aa_3 oxidase. Remarkably, HrrA binding was also observed upstream of the *cydABDC* operon, which encodes the cytochrome *bd* oxidase of the respiratory chain. Altogether, this set of target genes highlights the global role of the HrrSA system in heme-dependent coordination of both branches of the respiratory chain. The HrrA regulon appeared to cover also the aspect of cofactor supply for the respiratory chain, as several HrrA targets encode enzymes involved in menaquinone reduction (*sdhCD*, *lldD* and *dld*).

Besides the known heme biosynthesis targets (*hemE*, *hemH* and *hemA*), HrrA binding was also observed upstream of a gene (*hemQ*) encoding a putative dismutase-family protein. However, in actinobacteria, it was proposed that these proteins do not possess chlorite dismutase activity but instead are essential for heme synthesis (51). Furthermore, we observed binding of HrrA upstream of the *chrSA* operon encoding the second TCS involved in heme-dependent regulation in *C. glutamicum*. This finding therefore confirmed the previously postulated cross-regulation of these TCS at the level of transcription (24,52).

Furthermore, HrrA binding was also observed upstream of several genes involved in the oxidative stress response, including *katA,* encoding catalase, *tusG*, encoding a trehalose uptake system (53), and upstream of *gapA* and *gapB* (glyceraldehyde-3-phosphate dehydrogenase, glycolytic and gluconeogenetic, respectively) (54,55). In line with these findings, the phenotypic analysis of a *C. glutamicum hrrA* mutant revealed a significantly higher sensitivity to oxidative stress (treatment with H_2O_2) in comparison to the wild type (Figure S8). These findings suggest that the HrrSA system not only controls heme biosynthesis and degradation but also integrates the response to heme-induced oxidative stress.

A further important class of HrrA targets is represented by genes associated with the regulation or maintenance of the *C. glutamicum* cell envelope. The gene products of these previously unknown HrrA targets are, for instance, involved in the synthesis of peptidoglycan (*murA*), the peptidoglycan precursor meso-2,6-diaminopimelate (mDAP), inositol-derived lipids (*ino1*) and arabinogalactan (*aftC*). Furthermore, HrrA binding was revealed upstream of a number of genes encoding global transcriptional regulators (e.g., *ramA*, *ramB*, and *amtR*), adding a further level of complexity to this systemic response to heme.

Temporal dynamics of promoter occupancy reveal hierarchy in the HrrA regulon

With the time-resolved and genome-wide analysis of HrrA binding, we were also able to visualize distinct binding patterns of HrrA in response to addition and depletion of heme. Consequently, we asked whether the binding patterns (ChAP-Seq coverage) could provide information regarding the apparent dissociation constant (K_d) of HrrA to specific genomic targets. We compared the *in vivo* binding patterns of HrrA to *ctaE*, *hmuO* and *cydAB* (Figure 1, Table S3). While a comparably high peak was observed upstream of the *ctaE* promoter – even before the addition of heme (T_0) – the binding of HrrA to the promoter of *hmuO* occurred with apparently high stimulus dependency and appeared to be rather transient, as HrrA was fully dissociated from this promoter 9 h after the addition of hemin (Figure 1BC).

Subsequently, we determined the *in vitro* affinity of phosphorylated HrrA to the promoter regions of *ctaE*, *cydAB* and *hmuO* (Table 2, Figure S9). Consistent with the ChAP-Seq data, we measured the highest affinity of HrrA to P_{ctaE} with an apparent K_d of 125 nM. We therefore hypothesize that the *ctaE* promoter is a prime target that is constitutively activated by HrrA (Table S3) to maintain high gene expression of the operon encoding the bc_1-aa_3 supercomplex. In line with this hypothesis, we also found a high HrrA binding peak upstream of the other operons encoding components of the bc_1-aa_3 supercomplex (*ctaD* and *ctaCF*, Table 1 and Table S3).

In contrast, we measured an almost 3-fold higher apparent K_d (350 nM) for P_{cydAB}, which was consistent with the relatively transient binding pattern observed for this target. With an apparent K_d of 196 nM, the *in vitro* binding affinity of HrrA to the *hmuO* promoter was rather high considering the genomic coverage measured in the ChAP-Seq analysis. However, *in vitro* analysis does not account for the widespread interference among regulatory networks *in vivo*. In the particular example of *hmuO*, the pattern of HrrA binding was likely the result of interference with the global regulator of iron homeostasis, DtxR, which has previously been described to repress *hmuO* expression by binding to adjacent sites (56). Taken together, these results suggest that *in vivo* promoter occupancy is not only influenced by the binding affinity of the regulator to the particular target, but also significantly shaped by network interference. Consequently, high *in vivo* promoter occupancy indicates high binding affinity, but conclusions based on weakly bound regions may be confounded by competition with other binding factors.

HrrA activates the expression of genes encoding components of both branches of the quinol oxidation pathway

To evaluate how HrrA binding affects the expression of individual target genes, we analyzed the transcriptome (RNA-Seq) of the *C. glutamicum* wild type strain (ATCC 13032) as well as a Δ*hrrA* mutant (Table S4). Analogous to the ChAP-Seq experiments, RNA-Seq analysis was performed prior to the addition of heme (T_0) as well as 0.5 and 4 h after the heme pulse (in medium containing no other iron source). The RNA-Seq analysis was performed in two independent biological replicates (for inter-replicate, see Table S5).

At T_0, before the addition of heme, already 212 genes showed a more that 2-fold altered expression level in Δ*hrrA* cells compared to wild type cells (Δ*hrrA*/wt). Directly after the addition of heme (0.5 h), the expression of 309 genes changed more than 2-fold. (Table S4, Figure 3A, orange dots). Of these genes, 174 were upregulated and 135 were downregulated in the *hrrA* deletion strain. 4 h after addition of heme, only 167 genes exhibited a greater than 2-fold increase or decrease (scatter plots for additional time points are presented in Figure S10).

The *hrrA* expression decreased after 0.5 h upon the addition of heme, which was likely caused by DtxR repression in response to increased intracellular iron levels (Figure 3B) (24). In contrast, after 4 h of cultivation, *hrrA* levels significantly increased, reflecting the depletion of heme as an alternative iron source and dissociation of DtxR. Furthermore, differential gene expression analysis revealed HrrA to be an activator of all genes encoding components of the respiratory chain (*ctaE*, *ctaD*, *ctaF* and *cydAB*) and as a repressor of heme biosynthesis (*hemA*, *hemE* and *hemH)* (Figure 3C). The impact on the cytochrome bc_1-aa_3 supercomplex was also confirmed by measuring the activity of the aa_3 oxidase, which was about 2-fold reduced in a *hrrA* mutant in comparison to the wild type when grown on heme (Figure 3D). Additionally, expression of *lldD* (L-lactate dehydrogenase) as well as *sdhCD* (succinate dehydrogenase) contributing to the reduced menaquinone pool was downregulated more than three-fold upon deletion of *hrrA*. In addition to these considerable differences between the wild type and the Δ*hrrA* mutant, we also observed decreased mRNA levels of genes involved in the oxidative stress response (e.g. *katA*) or cell envelope remodeling (e.g. *murA*) in the Δ*hrrA* mutant, suggesting HrrA to be an activator of these targets.

In some cases, promoter occupancy by HrrA did not result in altered expression levels of the particular target gene in a Δ*hrrA* mutant under the tested conditions (Table 1, Table S3). This finding is, however, not surprising considering the multiplicity of signals and regulators affecting gene expression. Under changing environmental conditions, transcription factor binding will not necessarily always be translated in an altered gene expression of the respective target. When we compare the results obtained from RNA-Seq and ChAP-Seq analysis, 269 genes out of 309 genes featuring an >2-fold change in gene expression did not show HrrA binding in their upstream promoter region. Looking at all HrrA targets (ChAP-Seq analysis) on a global scale, there is, nevertheless, a significantly higher impact on gene expression in a strain lacking *hrrA* for all targets bound by HrrA in comparison to non-targets (unbound, Figure S11). Overall, 109 out of 228 HrrA targets featured a significantly altered gene expression in the *hrrA* mutant (64 increased and 55 decreased).

HrrA determines the prioritization of terminal cytochrome oxidases by repression of *sigC*

The results from ChAP-Seq and RNA-Seq experiments highlight the important role of HrrA in the control of the respiratory chain, including cofactor supply. Our data revealed that HrrA activates the expression of genes encoding the cytochrome bc_1-aa_3 supercomplex (*ctaE-qcrCAB*, *ctaD*, *ctaCF*) and of *cydAB*, encoding the cytochrome *bd* branch of the respiratory chain (Figure 4, Table S3). Remarkably, the mRNA profiles of the corresponding operons exhibited significantly delayed activation of *cydAB* in response to heme, which was abolished in the Δ*hrrA* mutant (Figure 4). In contrast, *ctaE* expression was significantly higher in wild type cells, even before hemin addition (T_0), but showed a further induction after stimulus addition (T 0.5 h, Table S4). Notably, we also observed binding of HrrA upstream of *sigC*, encoding an ECF sigma factor that was shown to be involved in the activation of the *cydABDC* operon (35). The mRNA level of *sigC* increased more than two-fold in the Δ*hrrA* mutant, indicating HrrA to be a repressor of this gene (Figure 4). Consistent with this hypothesis, *sigC* expression was slightly decreased in response to the addition of heme, which correlated with increased HrrA peak intensity (Figure 4F). Additionally, the higher *cydAB* expression, observed in the Δ*hrrA* strain before addition of stimulus (Figure 4B) is likely the effect of increased *sigC* expression (Figure 4C). Dissociation of HrrA from P_{sigC} at a later time point (4 h after heme pulse) led to derepression of *sigC* coinciding with an increased expression of *cydAB* in the wild type. Because *cydAB* levels were constitutively low in the Δ*hrrA* mutant in response to heme, we hypothesized that activation by HrrA together with an additional boost by SigC (Figure 5) leads to delayed activation of *cydAB* after the heme pulse. This regulation enables cells to channel most of the available heme pool into the more efficient cytochrome bc_1-aa_3 supercomplex. The lower apparent K_d of HrrA for the *ctaE* promoter (125 nM) compared to P_{cydAB} (350 nM) or P_{sigC} (270 µM) also reflects this prioritization of HrrA targets (Table 2). Consequently, this almost 3-fold decrease in affinity (apparent K_d) increases the threshold for HrrSA activity to control these targets.

HrrA activates PTS-dependent and –independent glucose uptake

Besides the activation of all components constituting the respiratory chain, ChAP-Seq experiments and transcriptome analysis revealed HrrA as a direct activator of genes encoding components of the phosphotransferase (PTS) system (*ptsH* and *ptsG*) and of *iolT1* encoding inositol permease with a reported function as a PTS-independent glucose uptake system (57). Remarkably, the gene *ppgK*, encoding the polyphosphate glucokinase was among the targets with the highest HrrA peak and showed reduced expression in the 4 h sample (Table 1 and Table S4). These results emphasize that cellular respiration and glucose uptake is coordinated via the HrrSA system in response to cellular heme levels.

Discussion

In this work, we applied a genome-wide approach to study the "heme-responsive regulator" HrrA in *C. glutamicum* and identified more than 200 genomic target regions of this response regulator. This intriguingly diverse set of target genes, encoding enzymes involved in heme biosynthesis, heme-containing proteins, and components of the respiratory chain as well as proteins involved in oxidative stress response, glucose uptake and cell envelope remodeling, provided unprecedented insight into the systemic response to heme coordinated by the TCS HrrSA.

In Gram-positive bacteria, TCSs appear to play a central role in transient heme sensing, and heme-responsive systems have been described in several prominent pathogens, including *C. diphtheriae*, *S. aureus* and *B. anthracis* (15-18). However, for all prokaryotic heme regulatory systems, only a small number of target genes have been described to date, focusing on targets involved in degradation (*hmuO* (18,58)), heme export (*hrtBA* (19,59)) or heme biosynthesis (*hemA* (18,20)). Systems orthologous to HrrSA are present in almost all corynebacterial species and the high amino acid sequence identity shared by the response regulators (87 %, between *C. glutamicum* and *C. diphtheriae* HrrA) suggests that the important role of HrrSA in the control of heme homeostasis is conserved. In many corynebacteria, including *C. diphtheriae*, control of heme homeostasis is shaped by the tight interplay of HrrSA with a second heme-dependent system, ChrSA. While the present study emphasized that HrrSA governs a large and complex homeostatic response, the only known target of the response regulator ChrA in *C. glutamicum* is the divergently located operon *hrtBA* encoding a heme export system. There is, however, also evidence for a cross-regulation between the TCSs, not only by cross-phosphorylation but also on the transcriptional level (23,24). In *C. diphtheria*, evidence for more overlap between the regulons of the TCSs has been provided, since both response regulators were shown to control a common set of target genes including *hrtBA*, *hemA* and *hmuO* (20,60). Genome-wide analysis of these systems have, however, not been performed so far and in vitro protein-DNA interaction studies may not necessarily reflect the in vivo promoter preferences of these highly similar systems.

Coping with heme stress

While being an essential cofactor for many proteins, heme causes severe toxicity to cells at high levels (4). In mammalian cells, the BACH1 regulator is inactivated by heme binding and plays a key role in maintaining the balance of the cellular heme pool (8,61). Heme oxygenases are targets of various heme-dependent regulators (18,62,63), and consistent with this principle, the mammalian *HMOX1* gene, encoding an NADPH-dependent oxygenase, is regulated by BACH1 (61). Other identified BACH1 targets are involved in redox regulation, the cell cycle, and apoptosis as well as subcellular transport processes (9,64,65).

Although neither the regulator nor the constitution of the regulon is conserved, the responses of BACH1 and HrrSA share a similar logic. Analogous to eukaryotic BACH1, we observed HrrA-mediated activation of genes involved in the oxidative stress response, including *katA*, which appears to be required to counteract oxidative stress caused by elevated heme levels (Figure S8).

Remarkably, HrrA binding was also observed upstream of both *gapA* and *gapB*, which encode glyceraldehyde-3-phosphate dehydrogenases (GapDHs) involved in glycolysis and

gluconeogenesis, respectively. Previous studies in baker's yeast and mammalian cells have revealed that oxidative stress may block glycolysis by inhibiting GapDH (55,66). Furthermore, GapDH of *C. diphtheriae* was recently shown to be redox-controlled by S-mycothiolation (67). Slight activation of *gapA* by HrrA may thus counteract an impaired glycolytic flux under conditions of heme stress.

Furthermore, several HrrA targets play a role in the biosynthesis and remodeling of the corynebacterial cell envelope, including *ino1*, which is required for the synthesis of inositol-derived lipids (68), *lysC,* providing the peptidoglycan precursor meso-2,6-diaminopimelate (mDAP), and *murA* (Table 1). Taken together, these insights emphasize the important role of the HrrSA system in the control of heme stress responses.

From networks to function

Genome-wide analysis of regulatory networks may provide important hints towards the physiological function of genes. An example is provided by the HrrA-dependent regulation of cg2079 (*hemQ*), described in this study (Table 1). In actinobacteria, it was recently proposed that these proteins inherit an essential role in heme biosynthesis (51,69). The finding that HrrA binds to the promoter of this gene and represses its expression supports a role of HemQ in heme biosynthesis in *C. glutamicum.* Among the direct targets of HrrA are many further targets encoding proteins of unknown function, including several ABC transport systems with a potential role in heme uptake or export. Therefore, this dataset provides guidance for further functional analysis of these HrrA targets to decipher their role in heme homeostasis.

Coordinated control of the respiratory chain

Among the most significantly affected targets in the Δ*hrrA* mutant were many genes encoding components of the respiratory chain (26). These genes comprise all the genes constituting the cytochrome bc_1-aa_3 branch of the respiratory chain (*ctaE-qcrCAB*, *ctaCF* and *ctaD*) (70); genes encoding the cytochrome *bd* branch (*cydAB* (26)); *ctaA* (71) and *ctaB* (72), encoding enzymes responsible for heme *a* synthesis; and *lldD* and *dld*, encoding lactate dehydrogenases that contribute to the reduced menaquinone pool (26) (Figure 4, Figure S12 and Table S3).

In a recent study, Toyoda and Inui described the ECF sigma factor σ^C to be an important regulator of both branches of the *C. glutamicum* respiratory chain. The *ctaE-qcrCAB* operon was shown to be significantly downregulated after σ^C overexpression due to binding of the sigma factor to the antisense strand of the promoter (35). Here, we demonstrated that this repression is counteracted by HrrA, which not only represses *sigC* but also activates *ctaE-qcrCAB* expression. While the two proteins have antagonistic effects on the expression of the supercomplex, both σ^C and HrrA positively regulate the *cyd* operon, encoding the cytochrome *bd* branch of the respiratory chain (Figure 5).

Interestingly, a hierarchy in the regulon was reflected by the differences in the apparent K_d values of HrrA with P_{cydA} and P_{sigC}, which were two-fold lower than those with the promoter of *ctaE.* These findings were also consistent with the ChAP-Seq experiments, where the peaks upstream of *ctaE* and *ctaD* were among the highest peaks at T_0 and after 0.5 h (Figure 4A). These data suggest that under conditions of sufficient heme supply, production of the cytochrome bc_1-aa_3

supercomplex is preferred, which is highly effective but requires the incorporation of six heme molecules (in contrast to only three molecules for the synthesis of the *bd* oxidase). Repression of *sigC* by HrrA and the relatively low affinity to the *cydAB* promoter results in delayed production of the *bd* branch. Under the applied aerobic conditions, available heme is thus first channeled to the cytochrome bc_1-aa_3 supercomplex before the cytochrome *bd* oxidase is used, which is less efficient but has a higher oxygen affinity. Remarkably, HrrA was also found to activate expression of genes involved in PTS-dependent (*ptsH* and *ptsG*) and –independent (*iolT1*) glucose uptake thereby ensuring a high glucose uptake rate under conditions of active cellular respiration.

Interference with other regulatory networks

Deletion of the *hrrA* gene led to more than 2-fold upregulation of 174 genes, while 135 genes were downregulated after the addition of heme. Several other genes were significantly affected but to a lesser extent. Remarkably, among the direct target genes controlled by HrrA, we identified several prominent global regulators, including the regulators of acetate metabolism *ramA* and *ramB* (73,74), and *amtR* encoding the master regulator of nitrogen control (75). Furthermore, *cpdA* encoding a cAMP phosphodiesterase playing a key role in the control of cellular cAMP levels in *C. glutamicum* (76) was found to be under direct control of HrrA. These examples illustrate the profound influence of HrrA on cellular networks and the systemic response cells have programmed to respond to heme availability.

Conclusion

Genome-wide analyses of targets controlled by prokaryotic transcription factors will change our view on many systems we believe to know. In this study, we provide an unprecedented insight into the systemic response to heme coordinated by the TCS HrrSA. Given the many properties of this molecule, the complexity of this response is actually not surprising but paves the way for further functional analysis of HrrA targets with so far unknown functions in heme homeostasis.

Data availability

The custom-developed software used in this study is publicly available at GitHub repository under the link https://github.com/afilipch/afp.

All sequencing data were deposited in the GEO database under the accession numbers GSE121962 (ChAP-Seq) and GSE120924 (RNA-Seq).

Supplementary Data

Supplementary Data are available at NAR online.

Funding

The authors acknowledge financial support by the German Research Foundation (FR 2759/4-1), the European Research Council (ERC-StG-2017, grant 757563) and by the Helmholtz Association (W2/W3-096).

Acknowledgements

We thank Eva Davoudi for fruitful discussions and critical reading of the manuscript. We thank Helga Etterich for her practical help with the sequencing experiments.

Conflict of Interest

The authors declare that there is no conflict of interest.

References

1. Ponka, P. (1999) Cell biology of heme. *The American journal of the medical sciences*, **318**, 241-256.
2. Layer, G., Reichelt, J., Jahn, D. and Heinz, D.W. (2010) Structure and function of enzymes in heme biosynthesis. *Protein science : a publication of the Protein Society*, **19**, 1137-1161.
3. Ajioka, R.S., Phillips, J.D. and Kushner, J.P. (2006) Biosynthesis of heme in mammals. *Biochimica et biophysica acta*, **1763**, 723-736.
4. Anzaldi, L.L. and Skaar, E.P. (2010) Overcoming the heme paradox: heme toxicity and tolerance in bacterial pathogens. *Infection and immunity*, **78**, 4977-4989.
5. Huang, W. and Wilks, A. (2017) Extracellular Heme Uptake and the Challenge of Bacterial Cell Membranes. *Annual review of biochemistry*, **86**, 799-823.
6. Wilks, A. (2002) Heme oxygenase: evolution, structure, and mechanism. *Antioxid Redox Signal*, **4**, 603-614.
7. Hickman, M.J. and Winston, F. (2007) Heme levels switch the function of Hap1 of *Saccharomyces cerevisiae* between transcriptional activator and transcriptional repressor. *Molecular and cellular biology*, **27**, 7414-7424.
8. Ogawa, K., Sun, J., Taketani, S., Nakajima, O., Nishitani, C., Sassa, S., Hayashi, N., Yamamoto, M., Shibahara, S., Fujita, H. *et al.* (2001) Heme mediates derepression of Maf recognition element through direct binding to transcription repressor Bach1. *The EMBO journal*, **20**, 2835-43.
9. Warnatz, H.J., Schmidt, D., Manke, T., Piccini, I., Sultan, M., Borodina, T., Balzereit, D., Wruck, W., Soldatov, A., Vingron, M. *et al.* (2011) The BTB and CNC homology 1 (BACH1) target genes are involved in the oxidative stress response and in control of the cell cycle. *J Biol Chem*, **286**, 23521-23532.
10. Qi, Z., Hamza, I. and O'Brian, M.R. (1999) Heme is an effector molecule for iron-dependent degradation of the bacterial iron response regulator (Irr) protein. *Proc Natl Acad Sci U S A*, **96**, 13056-13061.
11. Qi, Z. and O'Brian, M.R. (2002) Interaction between the bacterial iron response regulator and ferrochelatase mediates genetic control of heme biosynthesis. *Mol Cell*, **9**, 155-162.
12. O'Brian, M.R. (2015) Perception and Homeostatic Control of Iron in the Rhizobia and Related Bacteria. *Annual review of microbiology*, **69**, 229-245.

13. Torres, V.J., Stauff, D.L., Pishchany, G., Bezbradica, J.S., Gordy, L.E., Iturregui, J., Anderson, K.L., Dunman, P.M., Joyce, S. and Skaar, E.P. (2007) A *Staphylococcus aureus* regulatory system that responds to host heme and modulates virulence. *Cell host & microbe*, **1**, 109-119.
14. Mike, L.A., Choby, J.E., Brinkman, P.R., Olive, L.Q., Dutter, B.F., Ivan, S.J., Gibbs, C.M., Sulikowski, G.A., Stauff, D.L. and Skaar, E.P. (2014) Two-component system cross-regulation integrates *Bacillus anthracis* response to heme and cell envelope stress. *PLoS Pathog*, **10**, e1004044.
15. Stauff, D.L. and Skaar, E.P. (2009) The heme sensor system of *Staphylococcus aureus*. *Contributions to microbiology*, **16**, 120-135.
16. Stauff, D.L. and Skaar, E.P. (2009) *Bacillus anthracis* HssRS signalling to HrtAB regulates haem resistance during infection. *Mol Microbiol*, **72**, 763-778.
17. Bibb, L.A., Kunkle, C.A. and Schmitt, M.P. (2007) The ChrA-ChrS and HrrA-HrrS signal transduction systems are required for activation of the *hmuO* promoter and repression of the *hemA* promoter in *Corynebacterium diphtheriae*. *Infection and immunity*, **75**, 2421-2431.
18. Frunzke, J., Gatgens, C., Brocker, M. and Bott, M. (2011) Control of heme homeostasis in *Corynebacterium glutamicum* by the two-component system HrrSA. *Journal of bacteriology*, **193**, 1212-1221.
19. Heyer, A., Gatgens, C., Hentschel, E., Kalinowski, J., Bott, M. and Frunzke, J. (2012) The two-component system ChrSA is crucial for haem tolerance and interferes with HrrSA in haem-dependent gene regulation in *Corynebacterium glutamicum*. *Microbiology (Reading, England)*, **158**, 3020-3031.
20. Burgos, J.M. and Schmitt, M.P. (2016) The ChrSA and HrrSA Two-Component Systems Are Required for Transcriptional Regulation of the hemA Promoter in Corynebacterium diphtheriae. *J Bacteriol*, **198**, 2419-2430.
21. Keppel, M., Davoudi, E., Gätgens, C. and Frunzke, J. (2018) Membrane Topology and Heme Binding of the Histidine Kinases HrrS and ChrS in *Corynebacterium glutamicum*. *Front Microbiol*, **9**.
22. Ito, Y., Nakagawa, S., Komagata, A., Ikeda-Saito, M., Shiro, Y. and Nakamura, H. (2009) Heme-dependent autophosphorylation of a heme sensor kinase, ChrS, from *Corynebacterium diphtheriae* reconstituted in proteoliposomes. *FEBS letters*, **583**, 2244-2248.
23. Hentschel, E., Mack, C., Gatgens, C., Bott, M., Brocker, M. and Frunzke, J. (2014) Phosphatase activity of the histidine kinases ensures pathway specificity of the ChrSA and HrrSA two-component systems in Corynebacterium glutamicum. *Mol Microbiol*, **92**, 1326-1342.
24. Keppel, M., Piepenbreier, H., Gatgens, C., Fritz, G. and Frunzke, J. (2019) Toxic but tasty - temporal dynamics and network architecture of heme-responsive two-component signaling in Corynebacterium glutamicum. *Mol Microbiol*, **111**, 1367-1381.
25. Wennerhold, J. and Bott, M. (2006) The DtxR regulon of *Corynebacterium glutamicum*. *J. Bacteriol.*, **188**, 2907-2918.
26. Bott, M. and Niebisch, A. (2003) The respiratory chain of *Corynebacterium glutamicum*. *Journal of biotechnology*, **104**, 129-153.
27. Kao, W.C., Kleinschroth, T., Nitschke, W., Baymann, F., Neehaul, Y., Hellwig, P., Richers, S., Vonck, J., Bott, M. and Hunte, C. (2016) The obligate respiratory supercomplex from Actinobacteria. *Biochimica et biophysica acta*, **1857**, 1705-1714.
28. Niebisch, A. and Bott, M. (2001) Molecular analysis of the cytochrome bc_1-aa_3 branch of the *Corynebacterium glutamicum* respiratory chain containing an unusual diheme cytochrome c_1. *Archives of microbiology*, **175**, 282-294.
29. Kalinowski, J., Bathe, B., Bartels, D., Bischoff, N., Bott, M., Burkovski, A., Dusch, N., Eggeling, L., Eikmanns, B.J., Gaigalat, L. *et al.* (2003) The complete *Corynebacterium glutamicum* ATCC 13032 genome sequence and its impact on the production of L-aspartate-derived amino acids and vitamins. *Journal of biotechnology*, **104**, 5-25.

30. Ikeda, M. and Nakagawa, S. (2003) The *Corynebacterium glutamicum* genome: features and impacts on biotechnological processes. *Appl Microbiol Biotechnol*, **62**, 99-109.
31. Sone, N., Nagata, K., Kojima, H., Tajima, J., Kodera, Y., Kanamaru, T., Noguchi, S. and Sakamoto, J. (2001) A novel hydrophobic diheme c-type cytochrome. Purification from *Corynebacterium glutamicum* and analysis of the QcrCBA operon encoding three subunit proteins of a putative cytochrome reductase complex. *Biochimica et biophysica acta*, **1503**, 279-290.
32. Niebisch, A. and Bott, M. (2003) Purification of a cytochrome *bc*-aa_3 supercomplex with quinol oxidase activity from *Corynebacterium glutamicum*. Identification of a fourth subunity of cytochrome aa_3 oxidase and mutational analysis of diheme cytochrome c_1. *J. Biol. Chem.*, **278**, 4339-4346.
33. Teramoto, H., Inui, M. and Yukawa, H. (2013) OxyR acts as a transcriptional repressor of hydrogen peroxide-inducible antioxidant genes in Corynebacterium glutamicum R. *Febs J*, **280**, 3298-3312.
34. Milse, J., Petri, K., Ruckert, C. and Kalinowski, J. (2014) Transcriptional response of Corynebacterium glutamicum ATCC 13032 to hydrogen peroxide stress and characterization of the OxyR regulon. *J Biotechnol*, **190**, 40-54.
35. Toyoda, K. and Inui, M. (2016) The extracytoplasmic function sigma factor sigma(C) regulates expression of a branched quinol oxidation pathway in *Corynebacterium glutamicum*. *Molecular microbiology*, **100**, 486-509.
36. Morosov, X., Davoudi, C.F., Baumgart, M., Brocker, M. and Bott, M. (2018) The copper-deprivation stimulon of *Corynebacterium glutamicum* comprises proteins for biogenesis of the actinobacterial cytochrome bc_1-aa_3 supercomplex. *J Biol Chem*.
37. Davoudi, C.F., Ramp, P., Baumgart, M. and Bott, M. (2019) Identification of Surf1 as an assembly factor of the cytochrome bc_1-aa_3 supercomplex of Actinobacteria. *Biochimica et biophysica acta. Bioenergetics*, **1860**, 148033.
38. Keilhauer, C., Eggeling, L. and Sahm, H. (1993) Isoleucine synthesis in *Corynebacterium glutamicum*: molecular analysis of the *ilvB-ilvN-ilvC* operon. *Journal of bacteriology*, **175**, 5595-5603.
39. Sambrook J., R.D. (2001) *Molecular Cloning: A Laboratory Manual, 3rd edn.* . NY: Cold Spring Harbor Laboratory Press.
40. Eikmanns, B.J., Thum-Schmitz, N., Eggeling, L., Ludtke, K.U. and Sahm, H. (1994) Nucleotide sequence, expression and transcriptional analysis of the Corynebacterium glutamicum gltA gene encoding citrate synthase. *Microbiology*, **140 (Pt 8)**, 1817-1828.
41. Niebisch, A. and Bott, M. (2001) Molecular analysis of the cytochrome bc_1-aa_3 branch of the *Corynebacterium glutamicum* respiratory chain containing an unusual diheme cytochrome c_1. *Arch. Microbiol.*, **175**, 282-294.
42. Schäfer, A., Tauch, A., Jager, W., Kalinowski, J., Thierbach, G. and Pühler, A. (1994) Small mobilizable multi-purpose cloning vectors derived from the *Escherichia coli plasmids* pK18 and pK19: selection of defined deletions in the chromosome of *Corynebacterium glutamicum*. *Gene*, **145**, 69-73.
43. Gibson, D.G., Young, L., Chuang, R.Y., Venter, J.C., Hutchison, C.A., 3rd and Smith, H.O. (2009) Enzymatic assembly of DNA molecules up to several hundred kilobases. *Nature methods*, **6**, 343-345.
44. Pfeifer, E., Hünnefeld, M., Popa, O., Polen, T., Kohlheyer, D., Baumgart, M. and Frunzke, J. (2016) Silencing of cryptic prophages in *Corynebacterium glutamicum*. *Nucleic acids research*, **44**, 10117-10131.
45. Jones, E., Oliphant, T. and Peterson, P. (2001) SciPy: Open source scientific tools for Python *http://www.scipy.org/*.
46. Andrews, S. (2010) FASTQC. A quality control tool for high throughput sequence data.

47. Langmead, B. and Salzberg, S.L. (2012) Fast gapped-read alignment with Bowtie 2. *Nature methods*, **9**, 357-359.
48. Baumgart, M., Unthan, S., Kloss, R., Radek, A., Polen, T., Tenhaef, N., Muller, M.F., Kuberl, A., Siebert, D., Bruhl, N. *et al.* (2018) *Corynebacterium glutamicum* Chassis C1*: Building and Testing a Novel Platform Host for Synthetic Biology and Industrial Biotechnology. *ACS synthetic biology*, **7**, 132-144.
49. Pachter, L. (2011) Models for transcript quantification from RNA-Seq. *Conference Proceedings*.
50. Sakamoto, J., Shibata, T., Mine, T., Miyahara, R., Torigoe, T., Noguchi, S., Matsushita, K. and Sone, N. (2001) Cytochrome c oxidase contains an extra charged amino acid cluster in a new type of respiratory chain in the amino-acid-producing Gram-positive bacterium *Corynebacterium glutamicum*. *Microbiology*, **147**, 2865-2871.
51. Dailey, H.A. and Gerdes, S. (2015) HemQ: An iron-coproporphyrin oxidative decarboxylase for protoheme synthesis in Firmicutes and Actinobacteria. *Archives of biochemistry and biophysics*, **574**, 27-35.
52. Frunzke, J., Gätgens, C., Brocker, M. and Bott, M. (2011) Control of heme homeostasis in *Corynebacterium glutamicum* by the two-component system HrrSA. *J Bacteriol*, **193**, 1212-1221.
53. Alvarez-Peral, F.J., Zaragoza, O., Pedreno, Y. and Arguelles, J.C. (2002) Protective role of trehalose during severe oxidative stress caused by hydrogen peroxide and the adaptive oxidative stress response in *Candida albicans*. *Microbiology*, **148**, 2599-2606.
54. Kuehne, A., Emmert, H., Soehle, J., Winnefeld, M., Fischer, F., Wenck, H., Gallinat, S., Terstegen, L., Lucius, R., Hildebrand, J. *et al.* (2015) Acute Activation of Oxidative Pentose Phosphate Pathway as First-Line Response to Oxidative Stress in Human Skin Cells. *Mol Cell*, **59**, 359-371.
55. Ralser, M., Wamelink, M.M., Latkolik, S., Jansen, E.E., Lehrach, H. and Jakobs, C. (2009) Metabolic reconfiguration precedes transcriptional regulation in the antioxidant response. *Nat Biotechnol*, **27**, 604-605.
56. Wennerhold, J. and Bott, M. (2006) The DtxR regulon of *Corynebacterium glutamicum*. *Journal of bacteriology*, **188**, 2907-2918.
57. Lindner, S.N., Seibold, G.M., Henrich, A., Kramer, R. and Wendisch, V.F. (2011) Phosphotransferase system-independent glucose utilization in *Corynebacterium glutamicum* by inositol permeases and glucokinases. *Appl Environ Microbiol*, **77**, 3571-3581.
58. Bibb, L.A., King, N.D., Kunkle, C.A. and Schmitt, M.P. (2005) Analysis of a heme-dependent signal transduction system in *Corynebacterium diphtheriae*: deletion of the *chrAS* genes results in heme sensitivity and diminished heme-dependent activation of the *hmuO* promoter. *Infection and immunity*, **73**, 7406-7412.
59. Bibb, L.A. and Schmitt, M.P. (2010) The ABC transporter HrtAB confers resistance to hemin toxicity and is regulated in a hemin-dependent manner by the ChrAS two-component system in *Corynebacterium diphtheriae*. *Journal of bacteriology*, **192**, 4606-4617.
60. Bibb, L.A. and Schmitt, M.P. (2010) The ABC transporter, HrtAB, confers resistance to hemin toxicity and is regulated in a hemin-dependent manner by the ChrAS two-component system in *Corynebacterium diphtheriae*. *J. Bacteriol.*
61. Sun, J., Hoshino, H., Takaku, K., Nakajima, O., Muto, A., Suzuki, H., Tashiro, S., Takahashi, S., Shibahara, S., Alam, J. *et al.* (2002) Hemoprotein Bach1 regulates enhancer availability of heme oxygenase-1 gene. *The EMBO journal*, **21**.
62. Ratliff, M., Zhu, W., Deshmukh, R., Wilks, A. and Stojiljkovic, I. (2001) Homologues of neisserial heme oxygenase in gram-negative bacteria: degradation of heme by the product of the *pigA* gene of *Pseudomonas aeruginosa*. *J Bacteriol*, **183**, 6394-6403.
63. Schmitt, M.P. (1997) Transcription of the *Corynebacterium diphtheriae hmuO* gene is regulated by iron and heme. *Infection and immunity*, **65**, 4634-4641.

64. Hintze, K.J., Katoh, Y., Igarashi, K. and Theil, E.C. (2007) Bach1 repression of ferritin and thioredoxin reductase1 is heme-sensitive in cells and in vitro and coordinates expression with heme oxygenase1, beta-globin, and NADP(H) quinone (oxido) reductase1. *J Biol Chem*, **282**, 34365-34371.
65. Dhakshinamoorthy, S., Jain, A.K., Bloom, D.A. and Jaiswal, A.K. (2005) Bach1 competes with Nrf2 leading to negative regulation of the antioxidant response element (ARE)-mediated NAD(P)H:quinone oxidoreductase 1 gene expression and induction in response to antioxidants. *J Biol Chem*, **280**, 16891-16900.
66. Kuehne, A., Emmert, H., Soehle, J., Winnefeld, M., Fischer, F., Wenck, H., Gallinat, S., Terstegen, L., Lucius, R., Hildebrand, J. *et al.* (2015) Acute Activation of Oxidative Pentose Phosphate Pathway as First-Line Response to Oxidative Stress in Human Skin Cells. *Molecular Cell*, **59**, 359-371.
67. Hillion, M., Imber, M., Pedre, B., Bernhardt, J., Saleh, M., Loi, V.V., Maaß, S., Becher, D., Astolfi Rosado, L., Adrian, L. *et al.* (2017) The glyceraldehyde-3-phosphate dehydrogenase GapDH of *Corynebacterium diphtheriae* is redox-controlled by protein S-mycothiolation under oxidative stress. *Scientific reports*, **7**, 5020.
68. Baumgart, M., Luder, K., Grover, S., Gatgens, C., Besra, G.S. and Frunzke, J. (2013) IpsA, a novel LacI-type regulator, is required for inositol-derived lipid formation in *Corynebacteria* and *Mycobacteria*. *BMC Biol*, **11**, 122.
69. Dailey, H.A., Dailey, T.A., Gerdes, S., Jahn, D., Jahn, M., O'Brian, M.R. and Warren, M.J. (2017) Prokaryotic Heme Biosynthesis: Multiple Pathways to a Common Essential Product. *Microbiology and molecular biology reviews : MMBR*, **81**.
70. Niebisch, A. and Bott, M. (2003) Purification of a cytochrome *bc-aa*3 supercomplex with quinol oxidase activity from *Corynebacterium glutamicum*. Identification of a fourth subunity of cytochrome aa3 oxidase and mutational analysis of diheme cytochrome c1. *The Journal of biological chemistry*, **278**, 4339-4346.
71. Mueller, J.P. and Taber, H.W. (1989) Isolation and sequence of *ctaA*, a gene required for cytochrome aa_3 biosynthesis and sporulation in *Bacillus subtilis*. *J Bacteriol*, **171**, 4967-4978.
72. Svensson, B., Lubben, M. and Hederstedt, L. (1993) *Bacillus subtilis* CtaA and CtaB function in haem *A* biosynthesis. *Mol Microbiol*, **10**, 193-201.
73. Auchter, M., Cramer, A., Huser, A., Ruckert, C., Emer, D., Schwarz, P., Arndt, A., Lange, C., Kalinowski, J., Wendisch, V.F. *et al.* (2011) RamA and RamB are global transcriptional regulators in *Corynebacterium glutamicum* and control genes for enzymes of the central metabolism. *J Biotechnol*, **154**, 126-139.
74. Shah, A., Blombach, B., Gauttam, R. and Eikmanns, B.J. (2018) The RamA regulon: complex regulatory interactions in relation to central metabolism in Corynebacterium glutamicum. *Appl Microbiol Biotechnol*, **102**, 5901-5910.
75. Burkovski, A. (2007) Nitrogen control in *Corynebacterium glutamicum*: proteins, mechanisms, signals. *Journal of microbiology and biotechnology*, **17**, 187-194.
76. Schulte, J., Baumgart, M. and Bott, M. (2017) Identification of the cAMP phosphodiesterase CpdA as novel key player in cAMP-dependent regulation in *Corynebacterium glutamicum*. *Mol Microbiol*, **103**, 534-552.

Tables

Table 1: Selected target genes of HrrA. This table summarizes results from the HrrA ChAP-Seq analysis of the *C. glutamicum* strain ATCC 13032::*hrrA*-C-twinstrep and the transcriptome analysis of *C. glutamicum* wild type and strain Δ*hrrA* (complete datasets are provided in Table S3 and S4, respectively). For both experiments, cells were grown on glucose minimal medium and 4 M heme (see Material and Methods).

Locus tag	Gene name	Annotation	Dist. TSS[a]	Peak intensity[b]	log_2(Δ*hrrA*/wt)[c] T 0.5h	log_2(Δ*hrrA*/wt)[c] T 4h
Heme homeostasis/metabolism						
cg2445	***hmuO***	Heme oxygenase	43	5.4	-3.1	-3.8
cg0516	***hemE***	Uroporphyrinogen decarboxylase	17	54	3.1	2.2
cg0497	***hemA***	Glutamyl-tRNA reductase	-162	13	0.7	1.0
cg0517	***hemY***	Protoporphyrinogen oxidase	429	3.0	2.8	1.6
cg2079	***hemQ* (?)**	Putative chlorite dismutase-family protein, conserved		19	2.8	1.8
cg3156	***htaD***	Secreted heme transport-associated protein	-108	15	-0.3	-1.1
cg1734	***hemH***	Ferrochelatase	21	41	4.0	2.2
cg3247	***hrrA***	Heme-dependent response regulator	108	3.7	n.d.	n.d.
cg2201	***chrS***	Heme-dependent histidine kinase (*chrSA* operon)	32	2.5	-0.4	1.3
cg2202	***hrtB***	Heme exporter (*hrtBA* operon)	78	2.5	-1.0	4.3
Respiratory chain						
cg2406	***ctaE***	Cytochrome aa_3 oxidase, subunit 3	307	105	-1.7	-0.8
cg2780	***ctaD***	Cytochrome aa_3 oxidase, subunit 1	197	36	-1.1	-0.9
cg1301	***cydA***	Cytochrome *bd* oxidase	192	11	-0.7	-2.6
cg2409	***ctaC***	Cytochrome *aa*3 oxidase, subunit 2	47	22	-1.4	-1.0
cg1773	***ctaB***	Protoheme IX farnesyltransferase	667	7.9	0.4	-1.4
cg0445	***sdhC***	Succinate:menaquinone oxidoreductase, cytochrome b subunit	83	38	-1.7	-1.6
cg3226		L-lactate permease, operon with *lldD*	533	5.5	-1.7	0.9
Glucose uptake						
cg2121	***ptsH***	Phosphocarrier protein HPr, general component of PTS	-70	2.1	-1.2	-0.3
cg1537	***ptsG***	Glucose-specific EIIABC component EIIGlc of PTS	70	1.6	-1.1	-0.1
cg2091	***ppgG***	Polyphosphate glucokinase	199	266	0.2	-0.8
cg0223	***iolT1***	Myo-Inositol transporter 1, alternative glucose uptake system	73	2.0	-1.0	-0.7
Signal transduction						
cg0986	***amtR***	Master regulator of nitrogen control, repressor, TetR-family	366	1.8	0.3	0.1
Cg2461	***benR***	Transcriptional regulator, LuxR-family	229	5.6	-0.1	-1.2

cg2761	***cpdA***	cAMP phosphodiesterase	309	4.2	0.4	-0.5
cg0309	***sigC***	Extracytoplasmid-function σ factor, control of branched quinol oxidation pathway	29	19	2.1	0.6
cg0444	***ramB***	Transcriptional regulator, involved in acetate metabolism	83	38	-0.7	-0.6
cg2831	***ramA***	Transcriptional regulator, acetate metabolism, LuxR-family	-10	2.1	-0.5	0.6
Oxidative stress						
cg0310	***katA***	Catalase	132	19	-0.7	-1.2
cg0831	***tusG***	Trehalose uptake system, ABC-type, permease protein	-30	1.8	0.0	-0.2
cg1791	***gapA***	Glyceraldehyde-3-phos. dehydrogenase, glycolysis	86	3.9	-0.3	-0.4
cg1069	***gapB***	Glyceraldehyde-3-phos. dehydrogenase, gluconeogenesis	175	2.4	1.6	-0.1
Cell envelope						
cg2077	***aftC***	arabinofuranosyltransferase	271	3.0	-0.3	-0.2
cg3323	***ino1***	D-myo-inositol-1-phosphate synthase	-46	4.2	1.7	0.6
cg0337	***whcA***	WhiB homolog, role in SigH-mediated oxidative stress response	-21	2.1	-0.5	-0.7
cg0306	***lysC***	Aspartate kinase	32	13	0.7	0.1
cg0422	***murA***	UDP-N-acetylenolpyruvoylglucosamine reductase	591	3.5	-0.3	-0.1

[a)] Distance of the HrrA binding peak, identified via ChAP-Seq, to the start codon (transcription start site, TSS)

[b)] the corresponding peak intensity

[c)] Relative ratio of the transcript levels of the Δ*hrrA* deletion mutant compared to the wild type (log_2 fold change). The values are derived from a comparison between the two strains 0.5 and 4 h after hemin addition. The log_2(Δ*hrrA*/wt) value for was not determined for the deleted *hrrA* gene (n.d.).

Table 2: Apparent K_d values of HrrA to the promoters of *hmuO*, *ctaE*, *sigC* and *cydA*. The affinity of phosphorylated HrrA to the indicated regions was measured using purified protein in increasing concentrations and its ability to shift 10 nM DNA fragments of approximately 100 bp size covering the maximal ChAP-Seq peak (for detailed information, see Figure S9).

Promoter	Function	Apparent K_d value (nM)	95% confidence interval (nM)	R^2	Peak intensity after hemin addition (ChAP-Seq)
P_{hmuO}	Heme oxygenase	196	182-212	0.95	10
P_{ctaE}	Cytochrome aa_3 oxidase	125	117-132	0.97	53
P_{sigC}	ECF sigma factor σ^C	271	247-299	0.96	25
P_{cydA}	Cytochrome *bd* oxidase	350	318-386	0.96	18

Figures and Figure legends

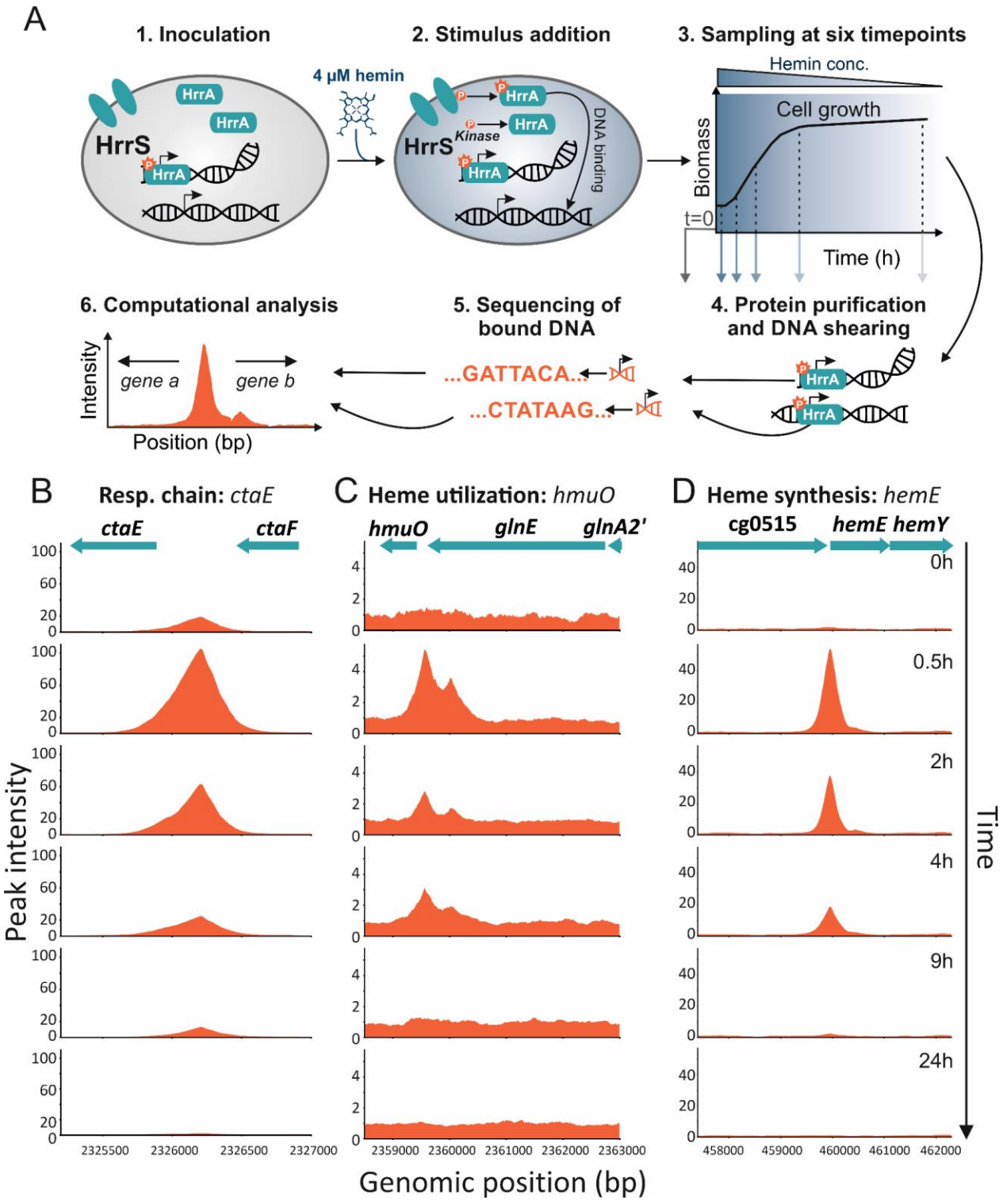

Figure 1: Genome-wide profiling of HrrA binding in response to addition of external heme. (A) ChAP-Seq analysis of the *C. glutamicum* strain ATCC 13032::*hrrA*-C-twinstrep grown in iron-depleted glucose minimal medium before and after addition of 4 µM hemin. The experimental approach is briefly depicted: Cells were harvested at the indicated time points, twin-Strep tagged HrrA was purified and co-purified DNA was sequenced to identify HrrA genomic targets. This approach resulted in the identification of more than 200 genomic regions bound by HrrA upon addition of hemin after 30 minutes. Exemplarily shown is the HrrA binding to regions upstream of operons involved in (B) the respiratory chain (*ctaE*), (C) heme degradation (*hmuO*) and (D) heme biosynthesis (*hemE*).

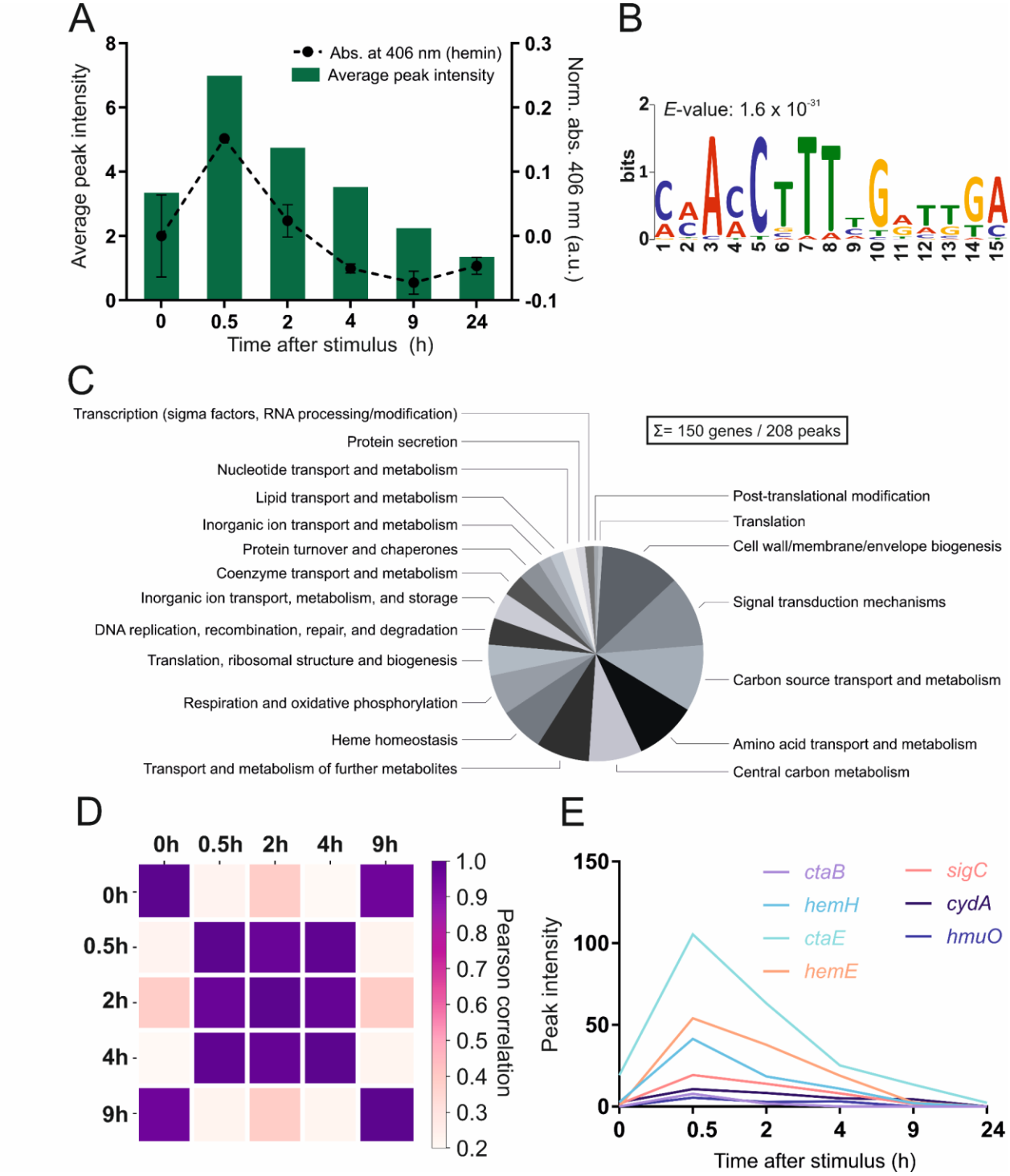

Figure 2: ChAP-Seq analysis revealed HrrA as a global regulator of heme homeostasis in *C. glutamicum*. (A) HrrA binding in response to the addition of hemin. The bar plot reflects the average peak intensities among detected peaks in ChAP-Seq experiments (<800 bp to the next TSS). The binding was correlated with the amount of cell-associated hemin (dashed line), measured at corresponding time points by spectroscopy as described in *Material and Methods*. (B) A binding motif was deduced from the sequences of the top 25 peaks ($T_{0.5}$) using MEME v.5 analysis (http://meme-suite.org). (C) Pie chart presenting HrrA targets, which can be attributed

to known functional categories (total of 272 genes, among which 128 encode proteins of unknown function, e.g., target genes within the CGP3 prophage region were excluded). For a complete overview of HrrA targets, see Table S3. (D) Proportional behavior of the HrrA regulon. For each peak that passed the threshold (distance of <800 bp to the closest downstream or <200 to the closest upstream transcription start site) at time point A, the highest peak in the same region (± 50 nucleotides from the center of the peak) was selected for time point B and *vice versa*. Thus, 'paired' peaks for these two time points were obtained, and the Pearson correlation of the intensities of all paired peaks was calculated for all six time points. (E) Peak intensities of selected HrrA targets over time, as identified by ChAP-Seq.

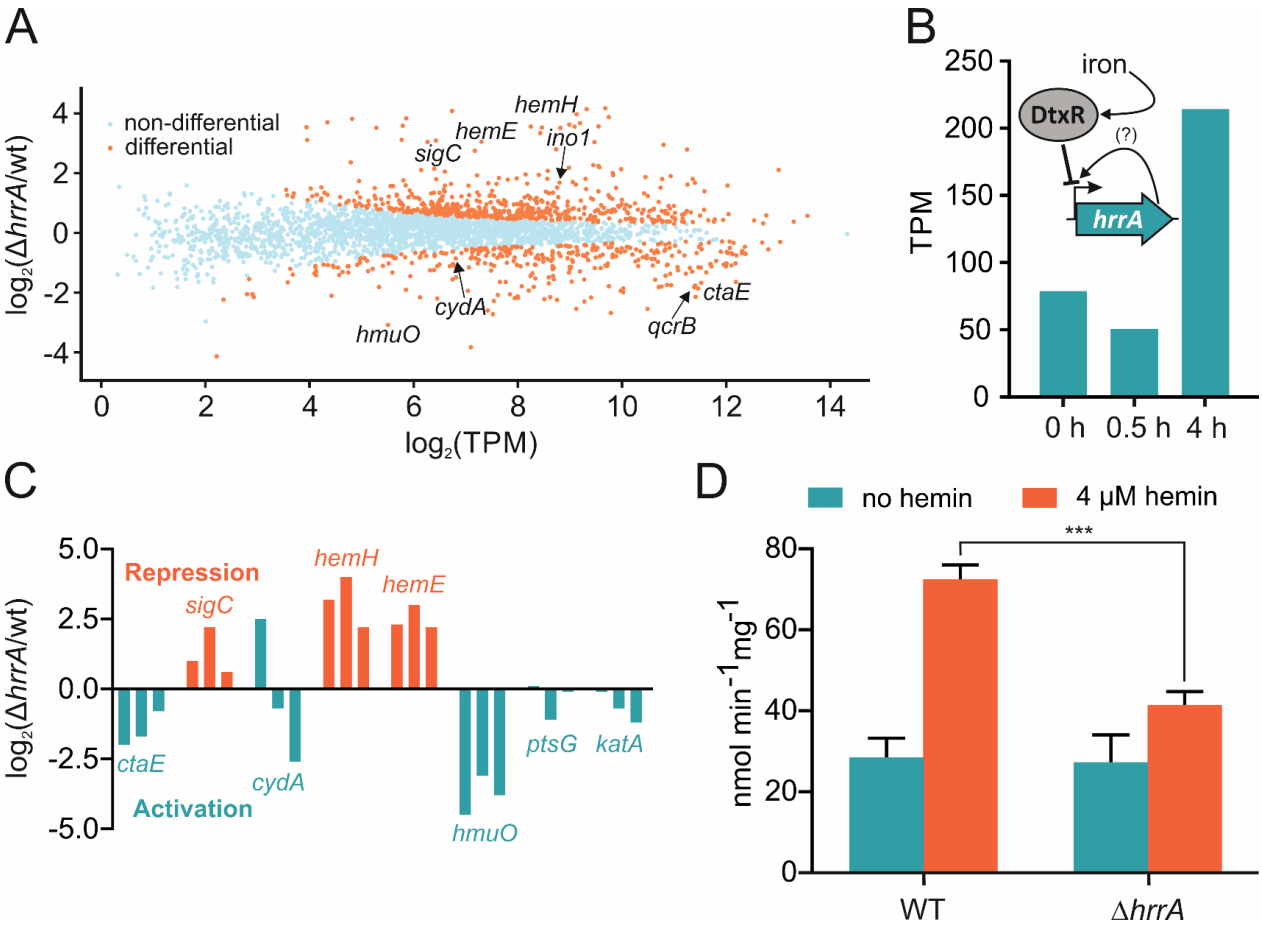

Figure 3: Differential gene expression analysis of wild type *C. glutamicum* and a Δ*hrrA* mutant. (A) Differential gene expression analysis (RNA-Seq) revealed 120 upregulated and 154 downregulated genes in the *hrrA* deletion strain compared to the wild type (in transcripts per million, TPM) after 30 minutes of cultivation in iron-depleted glucose minimal medium containing 4 µM heme. (B) Expression levels of *hrrA* (TPM) 0, 0.5 and 4 h after the addition of hemin. A scheme depicts HrrA autoregulation and iron-dependent DtxR repression (24). (C) Impact of *hrrA* deletion on the transcript levels of six selected target genes at three different time points (0 h, 0.5 h, 4 h; orange: HrrA acts as a repressor, turquoise: HrrA acts as an activator). (D) Measurement

of cytochrome aa_3 oxidase activity using the TMPD oxidase assay in *C. glutamicum* wild type and Δ*hrrA* grown with or without 4 µM heme.

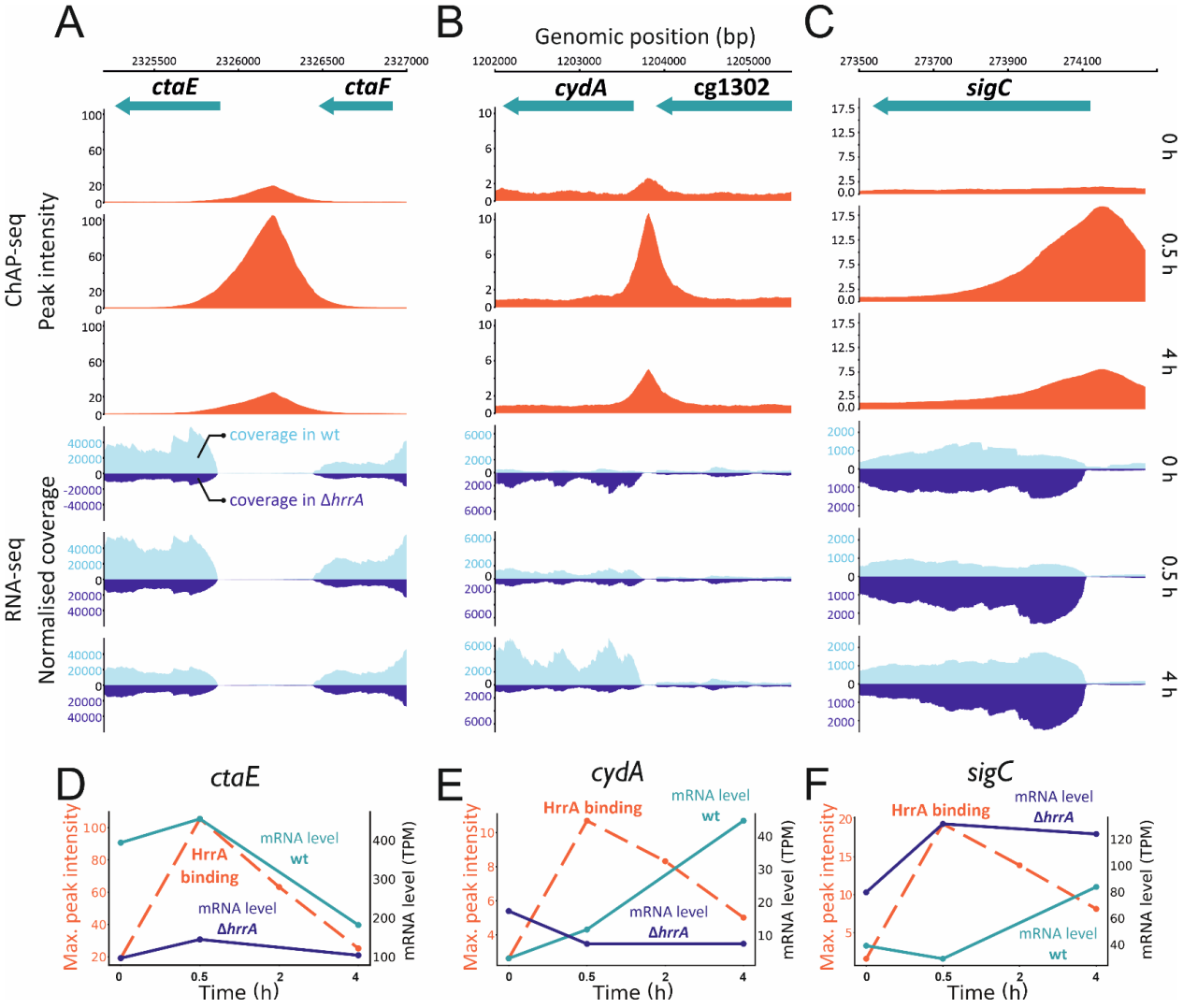

Figure 4: HrrA prioritizes the expression of genes encoding components of the bc_1-aa_3 supercomplex. Depicted are HrrA binding peaks as identified by ChAP-Seq analysis (Figure 1 and 2) in comparison to the normalized coverage of RNA-Seq results (wild type and the Δ*hrrA* mutant) for the genomic loci of *ctaE* (A, D), *sigC* (B, E) and *cydA* (C, F). D-F: HrrA binding (max. peak intensities measured by ChAP-Seq experiments) and the mRNA levels (in transcripts per million, TPM) of the respective genes in the Δ*hrrA* strain as well as in wild type *C. glutamicum* cells 0, 0.5 and 4 h after the addition of hemin.

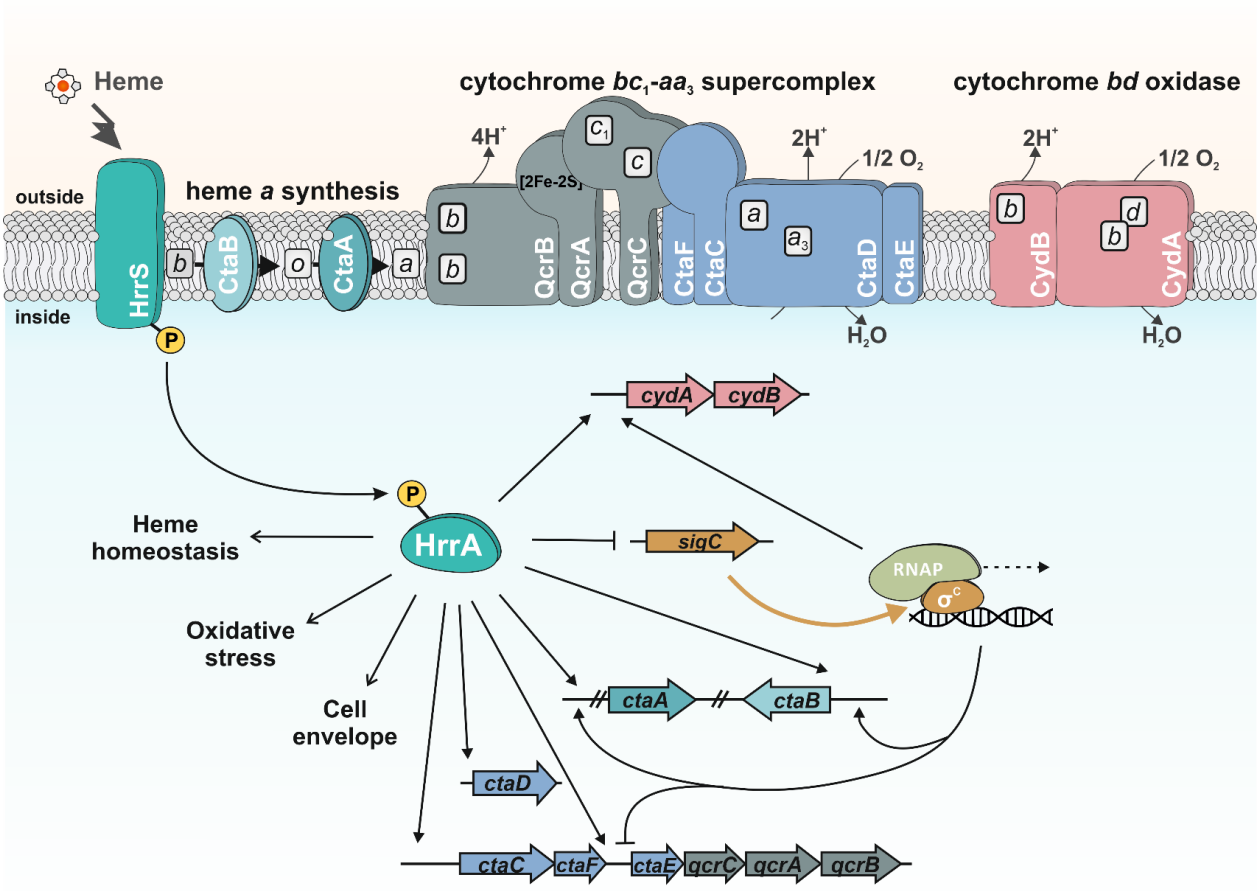

Figure 5: Model of heme-responsive control of components of the respiratory chain by HrrSA. The results of this study reveal HrrSA as a global regulator of heme homeostasis coordinating the expression of genes involved in heme biosynthesis, oxidative stress responses, glucose uptake and cell envelope remodeling. Genes encoding the components of the branched respiratory chain of C. glutamicum comprise an important part of the HrrA regulon. While HrrA acts as an activator of almost all components (*ctaE-qcrCAB*, *ctaB*, *cydAB*), it represses transcription of the *sigC* gene encoding an important sigma factor required for *cydAB* expression. This regulatory network architecture consequently confers prioritization to the synthesis of the more efficient proton pump, the cytochrome bc_1-aa_3 supercomplex. Bordered boxes, b, c, a, d: heme *b*, heme *c*, heme *a*, heme *d*.

ıplete Dataset of genome wide HrrA binding (ChAP-seq) and time resolved transcriptome analysis of *C. glutamicum* wild type and Δ*hrrA* (RNA-seq). For ChAP-seq analysis, the strain *C. glutamicum ::hrrA -C-twinstrep* was cultivated in CGXII minimal
lemented with 2% (w/v) glucose and 4 µM hemin, was harvested at different time points as described in Figure 1. For RNA-Seq, wild type cells and a Δ*hrrA* strain were cultivated accordingly and harvested 0 h, 0.5 h and 4 h after hemin addition.
nd C show the peak name, the gene locus (ID) and gene name. An annotation of the genes (column D) and the functional prediction (column V) were taken from Baumgart et al., 2018. Column E indicates the distance of the peak maximum to the
:tart site of the gene and column F indicates the distance to the transcription start site. In light grey (G-L), ChAP-seq peak intensities are indicated at 0 h, 0.5 h, 2 h, 4 h, 9 h and 24 h after hemin addition. In green (M-O) and red (P-R), the measured
›f the corresponding genes in the wild type strain (green) and a Δ*hrrA* strain (red) are shown (in transcripts per million, mean of two biological replicates). Column S-U show the log2-fold change of Δ*hrrA* in comparison to the wild type after 0 h, 0.5
:ubation in hemin containing medium.

Gene ID	Gene name	Annotation	Distance ATG	Distance to TS	ChAP-SeqT=0	T=0.5	T=2	T=4	T=9	T=24	mRNA wt t=0	mRNA wt t=0.5	mRNA wt t=4	mRNA DhrrA t	mRNA DhrrA t	mRNA DhrrA t	Log2 DhrrA/W	Log2 DhrrA/W	Log2 DhrrA/W
cg0074		putative sulfurtransferase, RHOD domain-containing protein	205	205	0,0	2,1	2,2	2,1	0,0	0,0	7,0	1,5	9,8	5,2	2,3	6,5	-0,4	0,6	-0,6
cg0075		hypothetical protein, conserved	79	-108	0,0	2,1	2,2	2,1	0,0	0,0	136,5	65,7	68,4	93,7	40,4	64,3	-0,5	-0,7	-0,1
cg0076		hypothetical protein	280	280	0,0	2,3	2,3	2,0	0,0	0,0	22,6	6,0	15,8	12,0	3,8	12,0	-0,9	-0,7	-0,4
cg0113	*ureA*	urease γ subunit (EC:3.5.1.5)	557	533	0,0	1,8	1,6	0,0	0,0	0,0	408,2	163,9	118,3	165,2	216,3	93,4	-1,3	0,4	-0,3
cg0128		putative secreted protein, signal peptide	166	166	0,0	1,7	1,9	1,6	0,0	0,0	10,6	6,9	17,4	5,8	12,5	13,0	-0,9	0,9	-0,4
cg0129	*putA*	proline dehydrogenase/δ-1-pyrroline-5-carboxylate dehydrogenase (EC:1.5.99.8)	90	8	0,0	1,7	1,9	1,6	0,0	0,0	179,4	90,1	179,3	132,3	113,6	95,6	-0,4	0,3	-0,9
cg0153	*hde*	putative esterase/lipase protein (EC:3.1.1.3)	302	302	0,0	3,8	3,7	2,5	0,0	0,0	20,5	18,0	30,6	21,5	21,4	15,9	0,1	0,3	-0,9
cg0163		putative N-acetylglucosaminyltransferase	428	322	0,0	2,0	1,9	1,6	0,0	0,0	165,9	302,2	181,6	56,6	50,7	87,6	-1,6	-2,6	-1,1
cg0204	*iolG*	putative oxidoreductase, myo-inositol 2-dehydrogenase (EC:1.1.1.18)	253	253	0,0	6,4	4,3	3,1	0,0	0,0	21,3	39,7	59,0	25,7	26,6	37,4	0,3	-0,6	-0,7
cg0222		putative membrane protein	410	275	0,0	3,2	3,1	2,4	0,0	0,0	43,0	28,1	37,7	22,1	25,2	22,0	-1,0	-0,2	-0,8
cg0223	*iolT1*	myo-Inositol transporter 1	158	73	0,0	2,0	1,9	1,7	0,0	0,0	18,4	11,8	37,5	14,9	6,0	23,0	-0,3	-1,0	-0,7
cg0247		hypothetical protein, conserved	180	180	0,0	2,2	1,7	1,5	0,0	0,0	40,4	21,2	28,5	37,2	34,6	23,3	-0,1	0,7	-0,3
cg0251		putative quinone oxidoreductase (EC:1.6.5.5)	71	-71	1,3	1,6	2,3	1,4	0,0	0,0	108,3	67,8	107,3	95,5	80,8	85,0	-0,2	0,3	-0,3
cg0284		Associated with mycolic acid metabolism	122	-159	0,0	1,8	2,0	0,0	0,0	0,0	95,7	76,4	103,8	109,7	85,9	88,3	0,2	0,2	-0,2
NCgl0236		putative transposase	169	110	1,3	1,3	1,3	1,3	1,2	1,0	0,0	0,1	0,0	0,0	0,1	0,3	0,0	-0,5	NA
cg0296	*dnaZX*	DNA polymerase III, subunits γ and τ (tau) (EC:2.7.7.7)	73	73	0,0	1,6	1,7	0,0	0,0	0,0	191,0	145,7	237,7	139,6	145,4	188,8	-0,5	0,0	-0,3
cg0304		putative membrane protein	214	35	0,0	13	11	5,9	0,0	0,0	96,2	39,6	71,9	90,0	67,5	53,8	-0,1	0,8	-0,4
cg0306	*lysC*	aspartate kinase (EC:2.7.2.4), deletion causes lysine-auxotrophy	32	32	0,0	13	11	5,9	0,0	0,0	601,5	598,3	692,6	722,9	970,1	764,5	0,3	0,7	0,1
cg0309	*sigC*	RNA polymerase σ factor, ECF-family, control of branched quinol oxidation pathway	29	29	1,5	19	14	8,1	1,7	0,0	39,1	29,2	83,7	79,7	131,6	124,0	1,0	2,2	0,6
cg0310	*katA*	catalase (EC:1.11.1.6)	175	132	1,5	19	14	8,1	1,7	0,0	1980,0	5988,3	1699,9	1847,3	3600,9	734,7	-0,1	-0,7	-1,2
cg0330	*cgtR1*	two component response regulator	24	24	0,0	3,0	2,7	1,9	0,0	0,0	25,8	15,3	19,7	13,8	19,7	16,5	-0,9	0,4	-0,3
cg0336	*pbp1a*	penicillin-binding protein 1A (EC:2.4.2.-)	533	243	0,0	2,1	2,0	1,6	0,0	0,0	413,5	221,9	224,6	224,0	153,7	194,9	-0,9	-0,5	-0,2
cg0337	*whcA (whiB4)*	negative role in SigH-mediated oxidative stress response, WhiB homolog	133	-21	0,0	2,1	2,0	1,6	0,0	0,0	1195,5	1024,2	1111,8	755,4	742,4	677,5	-0,7	-0,5	-0,7
cg0341	*phdA (fadD1)*	acyl:CoA ligase transmembrane protein; involved in degradation of aromatic compounds	175	175	0,0	2,6	2,7	2,0	1,5	0,0	5,0	3,3	9,8	4,5	2,2	3,7	-0,2	-0,6	-1,4
cg0390		putative permease, major facilitator-family	350	350	0,0	3,4	3,6	2,0	0,0	0,0	95,4	96,1	55,0	59,1	90,1	43,3	-0,7	-0,1	-0,3
cg0420		putative glycosyltransferase, horizontally transferred	641	641	0,0	7,3	4,9	4,4	0,0	0,0	192,3	99,2	161,1	50,3	62,0	41,3	-1,9	-0,7	-2,0
cg0420		putative glycosyltransferase, horizontally transferred	164	-164	0,0	3,0	2,4	2,3	0,0	0,0	192,3	99,2	161,1	50,3	62,0	41,3	-1,9	-0,7	-2,0
cg0422	*murA*	UDP-N-acetylglucosamine 1-carboxyvinyltransferase (EC:2.5.1.7), horizontally transferred	675	591	0,0	3,5	2,4	2,5	0,0	0,0	230,1	157,2	218,4	237,6	144,1	205,0	0,0	-0,1	-0,1
cg0424		putative glycosyltransferase, horizontally transferred	89	-97	0,0	2,2	1,5	0,0	0,0	0,0	194,0	149,5	254,4	183,3	135,3	216,8	-0,1	-0,1	-0,2
cg0437	*wzy*	putative membrane protein, involved in polysaccharide polymerization, horizontally transferred	312	60	0,0	4,0	3,4	2,7	0,0	0,0	154,8	119,9	212,2	88,7	124,0	160,7	-0,8	0,0	-0,4
cg0438		putative glycosyltransferase, horizontally transferred	35	3	0,0	2,3	1,7	0,0	0,0	0,0	416,0	360,2	458,3	385,8	399,8	263,8	-0,1	0,2	-0,8
cg0438		putative glycosyltransferase, horizontally transferred	79	29	0,0	2,3	1,7	1,8	0,0	0,0	416,0	360,2	458,3	385,8	399,8	263,8	-0,1	0,2	-0,8
cg0439		putative acetyl transferase EC:2.3.1.-, horizontally transferred	326	35	0,0	2,3	1,7	0,0	0,0	0,0	194,3	209,8	254,1	169,3	227,8	203,2	-0,2	0,1	-0,3
cg0439		putative acetyl transferase EC:2.3.1.-, horizontally transferred	281	-10	0,0	2,3	1,7	1,8	0,0	0,0	194,3	209,8	254,1	169,3	227,8	203,2	-0,2	0,1	-0,3
cg0444	*ramB*	transcriptional regulator, involved in acetate metabolism, MerR-family	213	198	3,1	38	33	16	3,1	0,0	673,0	725,4	470,9	353,7	439,9	319,0	-0,9	-0,7	-0,6
cg0445	*sdhC sdhCD*	succinate:menaquinone oxidoreductase, cytochrome b subunit	298	83	3,1	38	33	16	3,1	0,0	1917,1	2911,0	2339,4	392,3	884,6	760,6	-2,3	-1,7	-1,6
cg0453		putative membrane protein	4	-38	0,0	2,4	2,0	0,0	0,0	0,0	220,6	312,2	502,2	438,4	562,0	417,4	1,0	0,8	-0,3
cg0465		putative membrane protein, conserved	45	45	0,0	2,8	2,3	2,2	0,0	0,0	5,6	1,1	8,6	3,9	1,1	11,3	-0,5	-0,1	0,4
cg0466	*htaA*	secreted heme transport-associated protein	185	43	0,0	2,8	2,3	2,2	0,0	0,0	19,4	8,6	77,7	3,0	3,0	72,5	-2,7	-1,5	-0,1
cg0475		hypothetical protein, conserved	370	370	0,0	36	26	11	2,2	0,0	612,1	709,0	1603,6	1108,8	1378,3	1607,6	0,9	1,0	0,0
cg0495		putative phosphatase (EC:3.1.3.3)	434	44	0,0	7,1	13	8,1	0,0	0,0	39,2	24,8	46,5	30,9	33,6	33,7	-0,3	0,4	-0,5
cg0497	*hemA*	glutamyl-tRNA reductase, involved in heme biosynthesis	34	-162	0,0	7,1	13	8,1	0,0	0,0	115,4	487,8	136,3	636,4	765,8	274,8	2,5	0,7	1,0
cg0500	*qsuR*	transcriptional activator of qsuABCD genes, LysR-family	16	-40	0,0	4,8	4,1	2,9	0,0	0,0	38,8	25,7	20,4	22,2	20,1	14,0	-0,8	-0,4	-0,6
cg0501	*qsuA*	putative shikimate permease, MFS-type	260	80	0,0	4,8	4,1	2,9	0,0	0,0	59,3	85,9	25,4	44,9	50,4	24,8	-0,4	-0,8	0,0
cg0505		putative ribosomal protein L7/L12-family	7	7	0,0	1,9	1,6	1,4	0,0	0,0	79,4	59,2	81,2	126,7	93,2	41,2	0,7	0,7	-1,0
cg0516	*hemE*	uroporphyrinogen decarboxylase (EC:4.1.1.37), involved in heme biosynthesis	17	17	0,0	54	38	19	2,6	0,0	56,8	34,8	52,6	281,2	277,5	249,6	2,3	3,0	2,2
cg0517	*hemY*	protoporphyrinogen oxidase (EC:1.3.3.4), involved in heme biosynthesis	624	429	0,0	0,0	3,0	0,0	0,0	0,0	65,7	37,6	96,6	215,2	258,1	297,0	1,7	2,8	1,6
cg0524	*ccsB*	cytochrome c assembly membrane protein, CcsA-family	38	-38	0,0	2,2	2,2	1,5	0,0	0,0	95,5	234,0	292,9	112,7	300,6	375,5	0,2	0,4	0,4
cg0545	*pitA*	low-affinity phosphate transport protein, Pit-family	3	-158	0,0	1,6	1,4	0,0	1,4	0,0	105,9	51,6	206,8	138,9	81,9	289,6	0,4	0,7	0,5
cg0557		putative monooxygenase, FAD-binding	9	-9	0,0	3,0	3,2	2,3	0,0	0,0	24,4	25,0	28,3	33,8	55,8	42,7	0,5	1,2	0,6
cg0559	*ispB*	putative octaprenyl-diphosphate synthase protein (EC:2.5.1.-)	154	80	0,0	3,0	3,2	2,3	0,0	0,0	271,6	230,9	253,5	213,1	263,4	273,8	-0,4	0,2	0,1
cg0566	*gabT*	4-aminobutyrate aminotransferase, AT class II (EC:2.6.1.19)	748	748	0,0	3,9	2,6	1,7	0,0	0,0	3,2	4,1	3,2	3,0	3,4	3,0	-0,1	-0,3	-0,1
cg0614		hypothetical protein	654	654	0,0	2,1	1,5	1,6	0,0	0,0	78,5	197,6	53,7	73,5	143,1	33,6	-0,1	-0,5	-0,7
cg0630	*rplR*	50S ribosomal protein L18	141	-141	0,0	1,8	0,0	0,0	0,0	0,0	1311,6	798,0	3689,9	2113,2	2820,0	4967,9	0,7	1,8	0,4
cg0636	*creB*	putative membrane protein	54	5	0,0	6,6	4,2	4,2	0,0	0,0	50,9	50,2	18,7	42,2	31,1	13,1	-0,3	-0,7	-0,5
cg0636	*creB*	putative membrane protein	451	402	0,0	3,5	2,5	0,0	0,0	0,0	50,9	50,2	18,7	42,2	31,1	13,1	-0,3	-0,7	-0,5
cg0647	*secY*	preprotein translocase subunit	708	595	0,0	1,8	1,4	0,0	0,0	0,0	652,3	537,6	587,1	651,5	477,7	563,0	0,0	-0,2	-0,1
cg0656	*rplQ*	50S ribosomal protein L17	14	-14	0,0	2,9	2,1	1,8	0,0	0,0	1374,9	750,8	3061,1	1423,6	1461,5	4076,1	0,1	1,0	0,4
cg0671		hypothetical protein, conserved	710	710	0,0	3,2	2,6	2,5	0,0	0,0	7,9	1,9	8,9	3,5	4,1	3,2	-1,2	1,1	-1,5
cg0673	*rplM*	50S ribosomal protein L13	36	-177	0,0	2,0	1,7	1,4	0,0	0,0	1752,3	1550,6	4184,4	2711,6	2511,2	5649,7	0,6	0,7	0,4
cg0688		putative protein, conserved, UPF0031-family	17	17	0,0	3,9	3,8	2,7	1,4	0,0	49,4	41,5	114,3	65,5	75,2	90,1	0,4	0,9	-0,3
cg0752		putative secreted or membrane protein	504	381	0,0	1,9	1,5	1,5	0,0	0,0	111,5	135,6	286,1	158,2	186,8	387,3	0,5	0,5	0,4
cg0753		putative secreted protein	250	250	0,0	10	6,3	4,6	0,0	0,0	238,0	301,2	328,1	442,7	531,1	190,0	0,9	0,8	-0,8
cg0778		putative ABC-type iron-siderophore transporter, permease subunit	65	29	0,0	8,8	7,3	4,2	0,0	0,0	130,6	80,6	111,9	149,8	121,9	154,5	0,2	0,6	0,5
cg0779	*trpS*	tryptophanyl-tRNA synthetase (EC:6.1.1.2)	95	95	0,0	8,8	7,3	4,2	0,0	0,0	333,0	247,9	506,6	247,4	304,5	315,6	-0,4	0,3	-0,7
cg0780		putative membrane protein, ribonuclease BN-like-family	140	-140	0,0	2,0	0,0	0,0	0,0	0,0	459,5	359,3	184,0	211,0	218,1	149,2	-1,1	-0,7	-0,3
cg0823	*ntaA*	nitrilotriacetate monooxygenase component A (EC:1.14.13.-)	32	-32	1,2	1,5	1,2	1,2	1,1	1,2	5,3	1,8	5,6	4,2	2,1	3,0	-0,3	0,2	-0,9
cg0831	*tusG*	trehalose uptake system, ABC-type, permease protein	30	-30	0,0	1,8	1,4	0,0	0,0	0,0	146,7	129,7	452,5	130,2	128,9	403,2	-0,2	0,0	-0,2
cg0842		putative DNA helicase	58	58	0,0	1,7	1,4	0,0	0,0	0,0	21,8	22,1	121,0	35,8	42,5	90,8	0,7	0,9	-0,4

cg0875		hypothetical protein, conserved	54	-8	0,0	4,5	3,4	2,1	0,0	0,0	3,8	4,0	3,5	2,2	3,2	1,7	-0,8	-0,3	-1,1
cg0876	*sigH*	RNA polymerase σ70 factor, ECF-family	114	-17	0,0	4,5	3,4	2,1	0,0	0,0	208,6	342,9	347,9	249,1	313,8	260,4	0,3	-0,1	-0,4
cg0880		putative secreted protein	54	54	0,0	7,7	5,0	3,4	0,0	0,0	67,0	45,0	63,2	76,9	70,9	51,2	0,2	0,7	-0,3
cg0931		putative pyridoxal phosphate aminotransferase, AT class I (EC:2.6.1.1)	69	69	0,0	2,3	1,6	1,5	1,2	1,0	26,8	17,1	7,7	16,8	12,5	5,3	-0,7	-0,5	-0,5
cg0948	*serC*	phosphoserine aminotransferase, AT class IV EC:2.6.1.52, loss causes serine-auxotrophic	207	147	0,0	2,8	2,3	1,7	0,0	0,0	800,8	553,5	595,8	662,8	839,1	927,2	-0,3	0,6	0,6
cg0949	*gltA*	citrate synthase (EC:2.3.3.1)	519	140	0,0	2,8	2,3	1,7	0,0	0,0	4125,6	2270,2	2535,7	2959,2	1630,9	3228,6	-0,5	-0,5	0,3
cg0950	*fkpA*	(FKBP)-type peptidyl-prolyl cis-trans isomerase (EC:5.2.1.8)	692	630	0,0	10	6,5	4,0	0,0	0,0	689,3	547,7	1184,1	718,0	952,9	1436,1	0,1	0,8	0,3
cg0951	*accD3*	acetyl-coenzyme A carboxylase carboxyl transferase (EC:6.4.1.2)	69	-96	0,0	4,3	1,8	2,2	0,0	0,0	508,0	728,0	395,4	134,3	156,3	119,4	-1,9	-2,2	-1,7
cg0986	*amtR*	master regulator of nitrogen control, repressor, TetR-family	407	366	0,0	1,8	1,4	1,4	0,0	0,0	274,1	242,2	233,6	208,3	295,3	241,8	-0,4	0,3	0,1
cg0986	*amtR*	master regulator of nitrogen control, repressor, TetR-family	460	419	0,0	0,0	0,0	0,0	0,0	0,0	274,1	242,2	233,6	208,3	295,3	241,8	-0,4	0,3	0,1
cg1044		hypothetical protein, conserved	431	431	0,0	2,0	1,4	0,0	0,0	0,0	272,8	189,1	678,3	468,8	436,8	465,6	0,8	1,2	-0,5
cg1050		putative membrane protein	57	57	0,0	40	24	14	1,6	0,0	49,5	26,5	90,1	102,2	119,1	170,4	1,0	2,2	0,9
cg1051		hypothetical protein	149	-149	0,0	2,8	2,1	1,7	0,0	0,0	25,8	28,8	68,1	49,4	69,8	63,0	0,9	1,3	-0,1
cg1051		hypothetical protein	102	-102	0,0	2,8	2,1	0,0	1,2	0,0	25,8	28,8	68,1	49,4	69,8	63,0	0,9	1,3	-0,1
cg1052	*cmt3*	corynomycolyl transferase EC:2.3.1.122	277	233	0,0	2,8	2,1	1,7	0,0	0,0	220,6	155,6	176,1	172,6	220,6	96,2	-0,4	0,5	-0,9
cg1052	*cmt3*	corynomycolyl transferase EC:2.3.1.122	230	186	0,0	2,8	2,1	0,0	1,2	0,0	220,6	155,6	176,1	172,6	220,6	96,2	-0,4	0,5	-0,9
cg1069	*gapB (gapX)*	glyceraldehyde-3-phosphate dehydrogenase gluconeogenesis	295	215	0,0	2,4	2,1	1,4	0,0	0,0	75,8	96,1	538,2	89,4	304,8	503,9	0,2	1,7	-0,1
cg1069	*gapB (gapX)*	glyceraldehyde-3-phosphate dehydrogenase gluconeogenesis	255	175	0,0	2,4	2,1	1,4	0,0	0,0	75,8	96,1	538,2	89,4	304,8	503,9	0,2	1,7	-0,1
cg1077		putative permease of the major facilitator superfamily	33	33	4,1	47	28	15	2,4	0,0	4,4	2,8	7,2	23,0	25,6	21,1	2,4	3,2	1,5
cg1080		putative multicopper oxidase	50	17	4,1	47	28	15	2,4	0,0	26,9	12,1	52,1	130,4	206,2	200,5	2,3	4,1	1,9
NCgl0914		putative ABC transport system ATP-binding protein	450	382	0,0	3,4	2,3	1,9	0,0	0,0	33,5	24,2	100,2	51,3	44,2	71,0	0,6	0,9	-0,5

cg1105	*lysI*	L-lysine permease	553	553	0,0	3,8	2,5	2,1	0,0	0,0	23,3	14,4	13,7	20,3	17,9	11,2	-0,2	0,3	-0,3
cg1111	*eno*	enolase EC:4.2.1.11 phosphopyruvate hydratase	389	319	0,0	2,2	1,7	0,0	0,0	0,0	2231,6	1416,8	3740,6	2553,3	1758,9	3184,7	0,2	0,3	-0,2
cg1145	*fumC (fum)*	fumarase fumarate hydratase (EC:4.2.1.2)	115	78	0,0	2,2	1,3	1,3	0,0	0,0	664,9	719,6	1499,4	674,7	1209,2	1530,5	0,0	0,7	0,0
cg1147	*ssuI*	NADPH-dependent FMN reductase (EC:1.5.1.29) required for sulfonate and sulfonate ester utilization	203	-17	0,0	2,2	1,3	1,3	0,0	0,0	416,4	258,7	159,8	255,5	180,0	170,9	-0,7	-0,5	0,1
cg1157	*fbp*	fructose 1,6 bisphosphatase, class II (EC:3.1.3.11) essential for gluconeogenesis	869	767	0,0	2,0	1,3	0,0	0,0	0,0	825,0	876,1	861,3	518,3	842,0	903,0	-0,7	-0,1	0,1
cg1179		putative sensory box/GGDEF-family membrane protein	782	740	0,0	2,2	1,7	1,3	0,0	0,0	85,5	114,7	85,8	101,9	105,8	60,6	0,3	-0,1	-0,5
cg1288		putative multidrug efflux permease of the major facilitator superfamily	775	666	0,0	1,9	0,0	1,3	0,0	0,0	25,6	62,2	19,7	16,6	43,4	19,0	-0,6	-0,5	-0,1
cg1289		putative multidrug efflux permease of the major facilitator superfamily	534	534	0,0	2,0	1,3	1,4	0,0	0,0	13,2	31,6	13,4	8,2	24,3	13,7	-0,7	-0,4	0,0
cg1292		putative flavin-containing monooxygenase 3 (EC:1.14.13.8)	113	113	0,0	3,0	2,0	1,6	0,0	0,0	83,4	29,6	351,0	77,3	41,0	325,7	-0,1	0,5	-0,1
cg1301	*cydA*	cytochrome bd oxidase, subunit I	192	192	2,6	11	8,3	5,0	4,5	0,0	30,3	117,6	446,8	173,5	74,3	74,5	2,5	-0,7	-2,6
cg1316		putative superfamily II DNA/RNA helicases, SNF2-family	443	383	0,0	1,8	1,3	0,0	0,0	0,0	94,7	62,3	100,3	85,5	68,2	91,2	-0,1	0,1	-0,1
cg1334	*lysA*	diaminopimelate decarboxylase (EC:4.1.1.20)	114	-54	2,2	16	9,0	6,4	1,8	0,0	328,0	330,5	530,0	273,3	337,0	588,8	-0,3	0,0	0,2
cg1355	*prfA*	peptide chain release factor 1 RF-1	627	495	0,0	1,7	1,4	1,2	0,0	0,0	503,3	222,0	398,3	442,1	256,2	472,0	-0,2	0,2	0,2
cg1359		putative membrane protein, UDP-N-acetylmuramyl pentapeptide phosphotransferase/UDP-N-acetylglucosamine-1-pho	176	176	0,0	1,6	0,0	0,0	0,0	0,0	158,8	83,5	159,7	131,3	112,9	139,3	-0,3	0,4	-0,2
cg1454		putative aliphatic sulfonates uptake ABC transporter secreted solute-binding protein	274	248	0,0	1,5	0,0	0,0	0,0	0,0	84,5	130,3	101,3	124,8	145,9	67,8	0,6	0,2	-0,6
cg1456		putative signal-transduction protein containing cAMP-binding and CBS domain, conserved	154	-166	0,0	1,5	0,0	0,0	0,0	0,0	110,4	132,3	151,7	97,3	104,4	109,8	-0,2	-0,3	-0,5
cg1458	*odx*	oxaloacetate decarboxylase	144	-144	0,0	2,1	1,4	0,0	0,0	0,0	238,6	153,4	371,2	212,6	253,8	418,5	-0,2	0,7	0,2
cg1467		putative transcriptional regulator, TetR-family	250	116	0,0	1,9	1,2	1,1	0,0	0,0	16,7	12,1	4,5	9,8	10,9	5,3	-0,8	-0,1	0,2
cg1474		putative ATP/GTP-binding protein, large untranslated regions besides	138	-138	0,0	2,8	1,3	1,5	0,0	0,0	48,2	54,8	70,8	43,8	40,3	47,6	-0,1	-0,4	-0,6
cg1484		putative secreted protein	-64	-97	0,0	3,1	0,0	1,4	0,0	0,0	100,1	191,4	101,6	141,4	187,3	107,5	0,5	0,0	0,1
cg1484		putative secreted protein	-20	-53	0,0	3,1	1,9	1,4	0,0	0,0	100,1	191,4	101,6	141,4	187,3	107,5	0,5	0,0	0,1
cg1485		putative metal dependent phosphohydrolase, RelA/SpoT homolog	254	187	0,0	2,4	1,6	0,0	0,0	0,0	50,5	40,6	26,7	34,3	35,1	22,3	-0,6	-0,2	-0,3
cg1485		putative metal dependent phosphohydrolase, RelA/SpoT homolog	124	57	0,0	3,1	0,0	1,4	0,0	0,0	50,5	40,6	26,7	34,3	35,1	22,3	-0,6	-0,2	-0,3
cg1485		putative metal dependent phosphohydrolase, RelA/SpoT homolog	80	13	0,0	3,1	1,9	1,4	0,0	0,0	50,5	40,6	26,7	34,3	35,1	22,3	-0,6	-0,2	-0,3
cg1526		putative multidrug efflux permease of the major facilitator superfamily	46	-46	0,0	2,1	1,7	1,4	0,0	0,0	3,1	1,3	2,1	3,3	2,1	1,5	0,1	0,7	-0,6
cg1527		putative transcriptional regulator, HTH_3-family	83	83	0,0	2,1	1,7	1,4	0,0	0,0	29,9	28,7	21,3	23,8	27,6	15,2	-0,3	-0,1	-0,5
cg1531	*rpsA*	30S ribosomal protein S1, conserved	409	261	0,0	2,3	1,7	1,3	0,0	0,0	1779,3	1823,5	4049,0	1999,6	2520,4	5095,3	0,2	0,5	0,3
cg1537	*ptsG*	glucose-specific EIIABC component EIIGlc of PTS EC:2.7.1.69 fructose-specific enzyme II BC (EIIFru) component of PTS (EC:2.7.1.69)	325	70	0,0	1,6	1,4	0,0	0,0	0,0	2393,3	1757,4	1855,8	2649,0	825,0	1779,5	0,1	-1,1	-0,1
cg1538	*coaE*	dephospho-CoA kinase (EC:2.7.1.24)	144	144	0,0	3,7	2,4	1,8	0,0	0,0	829,0	534,1	501,4	693,8	494,2	355,0	-0,3	-0,1	-0,5
cg1568	ugpA	ABC-type sn-glycerol-3-phosphate transport system, permease protein, presumably regulated by RegX3	228	228	0,0	0,0	0,0	1,6	1,5	1,4	27,9	17,6	16,8	23,2	14,7	8,7	-0,3	-0,3	-1,0
cg1583	*argD*	acetylornithine aminotransferase, AT class II (EC:2.6.1.11)	191	191	0,0	1,5	1,4	0,0	0,0	0,0	129,9	110,1	178,2	401,3	1329,5	356,0	1,6	3,6	1,0
cg1603		hypothetical protein, conserved	35	35	0,0	3,6	1,9	1,4	0,0	0,0	274,0	374,8	334,0	213,7	355,6	309,2	-0,4	-0,1	-0,1
cg1628		putative hydrolase of the α/β superfamily	13	-62	0,0	4,9	2,9	2,0	0,0	0,0	60,3	198,4	19,6	41,0	362,6	31,7	-0,6	0,9	0,7
cg1629	*secA2*	preprotein translocase subunit SecA2, essential	225	193	0,0	4,9	2,9	2,0	0,0	0,0	119,5	101,9	164,4	94,7	127,1	143,8	-0,3	0,3	-0,2
cg1636		putative secreted protein	14	-110	0,0	4,1	1,7	1,3	0,0	0,0	86,6	130,8	152,6	88,4	167,2	132,1	0,0	0,4	-0,2
cg1639		putative membrane protein containing CBS domain	56	-56	0,0	1,6	1,0	1,2	0,0	0,0	89,2	106,8	125,5	73,0	116,4	110,1	-0,3	0,1	-0,2
cg1668		putative membrane protein	155	155	0,0	2,0	1,4	1,2	0,0	0,0	155,9	123,3	164,7	200,6	213,3	238,0	0,4	0,8	0,5
cg1691	*arc (mpa)*	AAA+ ATPase forming ring-shaped complexes, recognizes pupylated proteins, homolog in M. tuberculosis interacts with proteasome	74	74	0,0	1,9	1,3	0,0	0,0	0,0	452,4	360,3	200,9	361,6	307,9	161,6	-0,3	-0,2	-0,3
cg1695		putative plasmid maintenance system antidote protein, HTH-motif XRE-family	210	-37	0,0	24	13	5,8	3,0	0,0	302,1	434,4	172,6	171,1	211,4	62,1	-0,8	-1,0	-1,5
cg1695		putative plasmid maintenance system antidote protein, HTH-motif XRE-family	165	80	3,2	24	13	0,0	3,0	0,0	302,1	434,4	172,6	171,1	211,4	62,1	-0,8	-1,0	-1,5
cg1701	*metH*	homocysteine methyltransferase, methionine synthase EC:2.1.1.13	718	718	0,0	2,2	1,3	1,4	0,0	0,0	1376,3	1208,0	102,7	1037,7	859,8	175,3	-0,4	-0,5	0,8
cg1731		putative membrane protein implicated in regulation of membrane protease activity	126	126	0,0	4,5	2,6	2,0	1,4	0,0	470,8	324,9	753,6	401,6	493,1	521,4	-0,2	0,6	-0,5
cg1734	*hemH*	ferrochelatase (EC:4.99.1.1), essential	21	21	2,7	41	18	11	2,0	0,0	78,6	68,1	156,0	731,7	1086,0	692,5	3,2	4,0	2,2
cg1736		putative membrane protein	87	-60	0,0	8,3	4,7	3,1	0,0	0,0	48,2	30,3	37,3	38,3	35,7	26,1	-0,3	0,2	-0,5
cg1737	*acn*	aconitase aconitate hydratase (EC:4.2.1.3), loss results in glutamate/glutamine auxotrophy	267	-59	0,0	8,3	4,7	3,1	0,0	0,0	2242,6	3962,9	1878,7	1175,0	3469,1	1605,0	-0,9	-0,2	-0,2
cg1767		putative ABC-type multidrug transport system, ATPase component	27	27	0,0	21	13	7,0	0,0	0,0	41,4	16,3	48,6	130,8	139,3	129,6	1,7	3,1	1,4
cg1773	*ctaB*	polyprenyltransferase cytochrome oxidase assembly factor	789	667	0,0	7,9	1,8	0,0	0,0	0,0	96,0	73,4	313,9	73,8	101,1	115,2	-0,4	0,5	-1,4
cg1791	*gapA (gap)*	glyceraldehyde-3-phosphate dehydrogenase glycolysis EC:1.2.1.12	269	86	2,9	3,9	3,0	2,3	2,2	0,0	6401,7	3734,5	6577,6	9354,4	3023,4	5159,7	0,5	-0,3	-0,4
cg1801	*rpe*	ribulose-phosphate 3-epimerase (EC:5.1.3.1)	67	67	0,0	2,6	1,6	1,2	0,0	0,0	350,8	379,0	445,3	356,6	384,5	414,8	0,0	0,0	-0,1
cg1841	*aspS*	aspartyl-tRNA synthetase (EC:6.1.1.12)	189	79	0,0	1,7	0,0	0,0	0,0	0,0	355,0	264,9	550,4	258,2	268,4	550,7	-0,5	0,0	0,0
cg1842		putative secreted metalloprotease	43	43	0,0	1,7	0,0	0,0	0,0	0,0	542,0	357,4	234,1	400,4	324,9	223,1	-0,4	-0,1	-0,1
cg1893	*act4*	putative N-acetyltransferase CGP3 region	462	267	0,0	2,2	1,4	1,3	0,0	0,0	139,7	88,8	103,4	122,9	101,9	75,5	-0,2	0,2	-0,5
cg1894		hypothetical protein CGP3 region	124	-124	0,0	2,2	1,4	1,3	0,0	0,0	276,3	246,1	250,9	213,1	251,2	186,7	-0,4	0,0	-0,4
cg1898		hypothetical protein CGP3 region	743	590	0,0	2,9	1,9	1,7	0,0	0,0	2,2	0,3	1,0	1,7	0,0	0,8	-0,3	NA	-0,4
cg1905		hypothetical protein CGP3 region	286	139	0,0	2,1	2,0	1,4	0,0	0,0	573,4	901,6	1744,0	487,4	967,2	1131,7	-0,2	0,1	-0,6
NCgl1628		hypothetical protein CGP3 region	961	776	0,0	1,6	1,1	0,0	0,0	0,0	26,4	15,5	46,2	25,4	30,5	32,9	-0,1	1,0	-0,5
cg1918		putative secreted protein CGP3 region	682	682	0,0	1,8	1,5	0,0	0,0	0,0	140,4	93,9	103,1	75,1	55,2	70,8	-0,9	-0,8	-0,5
cg1923		hypothetical protein CGP3 region	156	-156	0,0	1,9	1,3	0,0	0,0	0,0	3,1	2,9	2,8	3,1	3,2	2,8	0,0	0,1	0,0
cg1925		hypothetical protein CGP3 region	348	348	0,0	2,4	1,2	1,3	0,0	0,0	118,4	79,7	49,7	95,8	118,5	48,2	-0,3	0,6	0,0
cg1926		hypothetical protein CGP3 region	170	170	0,0	2,0	1,4	0,0	0,0	0,0	47,7	33,5	29,6	25,1	52,5	23,4	-0,9	0,6	-0,3
cg1926		hypothetical protein CGP3 region	130	130	0,0	2,0	1,4	0,0	0,0	0,0	47,7	33,5	29,6	25,1	52,5	23,4	-0,9	0,6	-0,3
cg1959	*priP*	prophage DNA primase CGP3 region	16	-180	0,0	3,3	1,9	1,8	0,0	0,0	4,8	2,6	2,7	3,6	2,6	2,0	-0,4	0,0	-0,4
cg1981		hypothetical protein CGP3 region	556	556	0,0	2,4	0,0	0,0	0,0	0,0	12,9	7,0	6,1	9,4	5,7	4,4	-0,5	-0,3	-0,5
cg1981		hypothetical protein CGP3 region	476	476	0,0	0,0	1,5	1,6	0,0	0,0	12,9	7,0	6,1	9,4	5,7	4,4	-0,5	-0,3	-0,5
cg1981		hypothetical protein CGP3 region	438	438	0,0	0,0	1,5	1,6	0,0	0,0	12,9	7,0	6,1	9,4	5,7	4,4	-0,5	-0,3	-0,5
cg1981		hypothetical protein CGP3 region	47	-47	0,0	1,8	1,5	0,0	0,0	0,0	12,9	7,0	6,1	9,4	5,7	4,4	-0,5	-0,3	-0,5
cg2005		putative protein-plasmid encoded, conserved CGP3 region	340	139	0,0	2,7	1,8	2,0	0,0	0,0	15,8	14,8	11,9	15,8	14,2	9,1	0,0	-0,1	-0,4
cg2014		hypothetical protein CGP3 region	78	-78	0,0	12	6,6	4,9	0,0	0,0	109,7	122,2	54,1	50,9	57,2	33,9	-1,1	-1,1	-0,7
cg2021		putative protein, similar to p18, bacteriophage CP-1 streptococcus pneumoniae CGP3 region	298	298	0,0	3,3	1,5	1,4	0,0	0,0	14,9	12,8	9,0	12,0	10,9	6,5	-0,3	-0,2	-0,5
NCgl1731		hypothetical protein CGP3 region	523	245	0,0	1,8	1,2	1,5	0,0	0,0	1651,6	952,3	737,2	1404,5	786,8	620,6	-0,2	-0,3	-0,2
cg2031		hypothetical protein, conserved CGP3 region	164	7	0,0	3,0	1,7	1,5	0,0	0,0	91,8	112,3	78,4	96,8	72,4	62,2	0,1	-0,6	-0,3

cg2037		hypothetical protein, conserved CGP3 region	7	-44	0,0	3,3	1,8	1,5	0,0	0,0	89,9	92,4	82,1	81,6	98,5	68,9	-0,1	0,1	-0,3
NCgl1755		hypothetical protein CGP3 region	43	43	0,0	5,8	2,2	2,0	0,0	0,0	187,9	298,7	148,3	210,3	217,9	122,8	0,2	-0,5	-0,3
NCgl1787		hypothetical protein CGP3 region	14	-22	0,0	2,8	2,1	1,3	0,0	0,0	8,3	9,7	17,1	9,7	12,6	9,5	0,2	0,4	-0,8
NCgl1793		hypothetical protein CGP3 region	260	260	0,0	2,3	1,6	1,5	0,0	0,0	1,5	0,0	0,5	0,8	0,3	0,0	-1,0	NA	NA
NCgl1815		hypothetical protein CGP3 region	677	507	0,0	1,6	1,2	1,1	1,0	1,1	9,2	5,4	4,1	6,8	4,6	3,4	-0,4	-0,2	-0,3
cg2077	*aftC*	arabinofuranosyltransferase	367	271	0,0	3,0	1,9	1,3	0,0	0,0	271,9	331,4	130,5	162,6	263,7	113,2	-0,7	-0,3	-0,2
cg2079	*hemQ*	putative chlorite dismutase-family protein, conserved	133	13	2,0	19	11	6,9	1,7	0,0	177,1	109,0	460,8	630,7	773,5	1641,3	1,8	2,8	1,8
cg2080		hypothetical protein, conserved	140	67	2,0	19	11	6,9	1,7	0,0	692,7	882,1	402,4	448,6	636,8	338,1	-0,6	-0,5	-0,3
cg2085		hypothetical protein, conserved	164	96	0,0	0,0	1,5	1,4	0,0	0,0	281,8	252,3	351,3	259,5	252,7	257,4	-0,1	0,0	-0,4
cg2085		hypothetical protein, conserved	202	134	0,0	1,9	1,5	1,4	0,0	0,0	281,8	252,3	351,3	259,5	252,7	257,4	-0,1	0,0	-0,4
cg2090	*suhB*	myo-inositol-1or 4-monophosphatase (EC:3.1.3.25)	129	-129	2,3	266	104	70	1,6	0,0	166,2	117,0	181,7	287,2	242,2	164,6	0,8	1,0	-0,1
cg2091	*ppgK*	polyphosphate glucokinase (EC:2.7.1.63)	199	199	2,3	266	104	70	1,6	0,0	472,0	443,9	878,6	494,4	502,2	499,5	0,1	0,2	-0,8
cg2121	*ptsH*	phosphocarrier protein HPr, general component of PTS	25	-70	0,0	2,1	1,2	0,0	0,0	0,0	2765,7	3056,9	2443,1	3448,2	1299,4	1981,3	0,3	-1,2	-0,3
cg2155		hypothetical protein, conserved	326	326	0,0	5,0	2,6	1,9	0,0	0,0	464,3	371,5	396,7	644,6	640,5	329,9	0,5	0,8	-0,3
cg2181	*oppA*	ABC-type peptide transport system, secreted component	274	217	2,2	10	7,2	3,9	1,7	0,0	1304,7	133,3	1967,7	433,8	136,2	1525,0	-1,6	0,0	-0,4
cg2187		putative Mg-chelatase subunit D	279	279	0,0	2,1	0,0	0,0	0,0	0,0	88,0	55,0	41,6	36,9	39,0	40,4	-1,3	-0,5	0,0
cg2195		putative secreted or membrane protein	284	50	0,0	2,5	1,5	1,5	0,0	0,0	6624,2	8846,7	11679,9	8905,6	11651,9	11955,3	0,4	0,4	0,0
cg2201	*chrS (cgtS8)*	two component sensor kinase, control of heme homeostasis/export	4	4	0,0	2,5	1,4	1,0	0,0	0,0	36,8	490,1	23,7	11,6	363,7	57,5	-1,7	-0,4	1,3
cg2202	*hrtB*	ABC-type heme transport system, permease component	107	107	0,0	2,5	1,4	1,0	0,0	0,0	42,7	5528,5	12,0	4,7	2771,7	240,2	-3,2	-1,0	4,3
cg2208	*dxr*	1-deoxy-D-xylulose 5-phosphate reductoisomerase (EC:1.1.1.267)	44	44	0,0	3,2	2,4	1,8	0,0	0,0	48,8	32,4	96,3	51,3	58,8	72,1	0,1	0,9	-0,4
cg2211		putative membrane protein	200	121	0,0	3,2	2,4	1,8	0,0	0,0	1747,7	2114,1	2363,5	808,6	1629,5	1453,7	-1,1	-0,4	-0,7
cg2224	*xerC*	tyrosine recombinase	129	26	2,4	78	40	20	1,8	0,0	42,7	26,5	31,3	43,0	42,1	33,3	0,0	0,7	0,1
cg2311		putative SAM-dependent methyltransferase	113	113	0,0	4,2	2,8	2,1	0,0	0,0	99,7	50,0	135,3	47,2	48,7	163,2	-1,1	0,0	0,3
cg2343		putative decarboxylase	422	192	0,0	6,3	3,8	3,2	0,0	0,0	84,4	124,2	79,7	103,6	115,6	54,7	0,3	-0,1	-0,5
cg2398	*plsC*	1-acyl-sn-glycerol-3-phosphate acetyltransferase	153	75	0,0	2,3	1,8	1,4	0,0	0,0	441,4	656,1	325,5	243,1	242,3	147,8	-0,9	-1,4	-1,1
cg2406	*ctaE*	cytochrome aa3 oxidase, subunit 3	307	307	19	105	63	25	13	2,3	3935,0	4547,1	1818,0	965,4	1446,9	1039,4	-2,0	-1,7	-0,8
cg2409	*ctaC*	cytochrome aa3 oxidase, subunit 2	233	47	1,9	22	12	6,3	2,1	0,0	2698,8	3552,2	2684,1	1037,3	1403,6	1371,5	-1,4	-1,3	-1,0
cg2409	*ctaC*	cytochrome aa3 oxidase, subunit 2	270	84	1,9	22	12	6,3	2,1	0,0	2698,8	3552,2	2684,1	1037,3	1403,6	1371,5	-1,4	-1,3	-1,0
cg2410	*ltsA*	glutamine-dependent amidotransferase involved in formation of cell wall and L-glutamate biosynthesis (EC:6.3.5.4)	286	199	1,9	22	12	6,3	2,1	0,0	153,0	136,3	203,1	135,0	142,7	168,0	-0,2	0,1	-0,3
cg2410	*ltsA*	glutamine-dependent amidotransferase involved in formation of cell wall and L-glutamate biosynthesis (EC:6.3.5.4)	249	162	1,9	22	12	6,3	2,1	0,0	153,0	136,3	203,1	135,0	142,7	168,0	-0,2	0,1	-0,3
cg2423	*lipA*	lipoyl synthase/synthetase (EC:2.8.1.-)	127	33	0,0	3,3	2,3	1,9	0,0	0,0	677,5	1675,7	452,8	678,3	1702,6	462,5	0,0	0,0	0,0
cg2445	*hmuO*	heme oxygenase	149	43	0,0	5,4	2,8	3,1	0,0	0,0	185,3	80,4	263,1	8,3	9,6	19,1	-4,5	-3,1	-3,8
cg2445	*hmuO*	heme oxygenase	625	519	0,0	3,6	1,7	2,0	0,0	0,0	185,3	80,4	263,1	8,3	9,6	19,1	-4,5	-3,1	-3,8
cg2473	*acpM*	acyl carrier protein ACP	586	586	0,0	6,6	3,7	2,6	0,0	0,0	188,3	140,2	247,5	253,0	278,1	175,4	0,4	1,0	-0,5
cg2495		hypothetical protein, conserved	43	43	0,0	6,7	4,3	3,4	0,0	0,0	90,2	69,8	104,0	91,0	70,3	67,5	0,0	0,0	-0,6
cg2496		putative secreted protein	-1	-56	0,0	6,7	4,3	3,4	0,0	0,0	128,3	109,5	140,6	122,9	145,0	113,5	-0,1	0,4	-0,3
cg2521	*fadD15*	long-chain fatty acid CoA ligase (EC:6.2.1.3)	184	-15	0,0	1,3	1,6	1,5	0,0	0,0	284,8	254,5	209,6	250,1	244,5	204,5	-0,2	-0,1	0,0
cg2523	*malQ*	4-α-glucanotransferase (EC:2.4.1.25)	84	74	0,0	1,3	1,6	1,5	0,0	0,0	1629,8	1167,4	1339,1	1106,0	998,8	1039,7	-0,6	-0,2	-0,4
cg2537	*brnQ*	branched-chain amino acid uptake carrier, Na+-coupled?	345	235	0,0	3,9	2,9	2,0	1,5	0,0	178,7	133,9	150,6	158,3	187,0	169,8	-0,2	0,5	0,2
cg2546		putative secondary C4-dicarboxylate transporter, tripartite ATP-independent transporter, TRAP-T-family	183	162	0,0	8,6	5,3	3,5	1,3	0,0	5,3	4,0	12,1	3,2	3,7	16,2	-0,7	-0,1	0,4
cg2557		putative secondary Na+/bile acid symporter, bile acid:Na+ symporter BASS-family	114	37	0,0	1,8	1,3	0,0	0,0	0,0	25,4	20,2	114,8	15,5	21,9	125,7	-0,7	0,1	0,1
cg2625	*pcaF*	β-ketoadipyl-CoA thiolase (EC:2.3.1.174)	219	219	0,0	2,0	1,8	1,6	0,0	0,0	817,0	323,1	19,9	207,6	77,2	17,5	-2,0	-2,1	-0,2
cg2641	*benR*	transcriptional regulator, LuxR-family	295	229	0,0	5,6	4,0	3,1	0,0	0,0	24,0	26,5	45,7	22,3	24,3	20,4	-0,1	-0,1	-1,2

Table S4: Filtered dataset of time r
(w/v) glucose and 4 µM hemin and
(red) are shown (in transcripts per r
fold altered fold-change in one of th

Gene ID	Gene name
cg0012	*ssuR*
cg0061	*rodA*
cg0160	
cg0161	
cg0162	
cg0163	
cg0165	
cg0230	*gltD*
cg0256	
cg0314	*brnF*
cg0315	*brnE*
cg0318	*arsC1 (arsB2)*
cg0319	*arsC2 (arsX)*
cg0421	*wzx*
cg0445	*sdhC sdhCD*
cg0446	*sdhA*
cg0447	*sdhB*
cg0455	
cg0456	
cg0463	*csoR*
cg0464	*copA (ctpA, ctpV)*
cg0466	*htaA*
cg0635	*creA*
cg0676	
cg0683	
cg0755	*metY*
cg0793	
cg0898	*pdxS*
cg0922	
cg0923	
cg0926	
cg0927	
cg0951	*accD3*
cg1120	*ripA*
cg1225	*benK3 (pcaK)*
cg1226	*pobB (pobA)*
cg1313	
cg1405	
cg1411	*rbsA*

cg1412	*rbsC*
cg1424	*lysE*
cg1425	*lysG*
cg1537	*ptsG*
cg1555	
cg1695	
cg1705	*arsB1 (arsC2)*
cg1738	*acnR*
cg1759	
cg1760	*sufU*
cg1761	*sufS*
cg1762	*sufC*
cg1763	*sufD*
cg1778	*zwf*
cg1779	*opcA*
cg1780	*pgi (devB)*
cg1787	*ppc*
cg1861	*rel*
cg1962	
cg2012	
cg2014	
NCgl1729	
cg2106	
cg2117	*ptsI*
cg2118	*fruR*
cg2119	*pfkB (fruK)*
cg2120	*ptsF*
cg2121	*ptsH*
cg2204	*hrtA*
cg2329	
cg2381	
cg2397	
cg2398	*plsC*
cg2403	*qcrB*
cg2404	*qcrA (qcrA1)*
cg2405	*qcrC*
cg2406	*ctaE*
cg2408	*ctaF*
cg2409	*ctaC*
cg2438	
cg2445	*hmuO*
cg2559	*aceB*
cg2560	*aceA*
cg2624	*pcaR*
cg2625	*pcaF*

cg2626	*pcaD*
cg2629	*pcaB*
cg2630	*pcaG*
cg2636	*catA1 (catA)*
cg2638	*benB*
cg2639	*benC*
cg2674	
cg2675	
cg2676	
cg2677	
cg2678	
cg2697	
cg2732	*gntV (gntK)*
cg2739	
cg2780	*ctaD*
cg2810	*cynT*
cg2833	*cysK*
cg2836	*sucD*
cg2838	
cg2867	*mpx*
cg2925	*ptsS*
cg2939	*siaG*
cg2940	*siaI*
cg3101	
cg3109	
cg3112	*cysZ*
cg3141	*hmp*
cg3145	
cg3176	
cg3213	
cg3216	*gntP*
cg3226	
cg3227	*lldD*
cg3234	
NCgl2845	
cg3277	
cg3280	
NCgl2858a	
cg3281	*copB*
cg3282	
NCgl2861	
cg3284	*copS (cgtS9)*

cg3285	*copR (cgtR9)*
cg3286	
cg3287	*copO*
cg3334	*cepA*
cg3374	*cye1*
cg3385	*catA3 (rhcD2)*
cg3387	*iolT2*
cg3399	
cg3402	

esolved transcriptome analysis of *C. glutamicum* wild type and Δ*hrrA* with genes showing at lea
harvested 0 h, 0.5 h and 4 h after hemin addition. Column A and B show the gene locus (ID) and ge
nillion, mean of two biological replicates). Column J-L show the log2-fold change of Δ*hrrA* in comp
ıe measured time points and for a p-value <0.05.

Annotation
sulphonate sulphur utilization transcriptional regulator SsuR, activator of sulfonateester utilization, ROK-family, loss causes inability to utilize alkylsulfonates
putative FTSW/RODA/SPOVE-family cell cycle protein
hypothetical protein
putative membrane protein
putative membrane spanning protein
putative N-acetylglucosaminyltransferase
putative ABC-2-type transporter
glutamine 2-oxoglutarate aminotransferase NADPH small subunit, also glutamate synthase (EC:1.4.1.13)
putative protein, conserved
branched chain amino acid exporter Ile, Leu, Val, Met, large subunit
branched chain amino acid exporter Ile, Leu, Val, Met, small subunit
arsenite permease, arsenical resistance-3 (ACR3)-family
arsenate reductase, arsenical pump modifier (EC:1.20.4.1)
putative translocase involved in export of a cell surface polysaccaride, horizontally transferred
succinate:menaquinone oxidoreductase, cytochrome b subunit
succinate:menaquinone oxidoreductase, flavoprotein subunit
succinate:menaquinone oxidoreductase, iron-sulfur protein subunit
putative permease, major facilitator superfamily
putative permease, major facilitator superfamily
transcriptional repressor during copper starvation
copper-transporting P-type ATPase (EC:3.6.3.4)
secreted heme transport-associated protein
putative NAD+-dependent 4-hydroxybenzaldehyd dehydrogenase subunit (EC: 1.2.1.64), (N. Kallscheuer: why only 107 aa; too short)
hypothetical protein, conserved
putative permease
O-acetylhomoserine sulfhydrylase EC:2.5.1.49, loss causes methionine auxotrophy
putative secreted protein
pyridoxal 5-phosphate PLP synthase subunit
putative secreted siderophore-binding lipoprotein
putative membrane protein
putative putative iron-siderophore transporter, permease subunit
putative ABC-type putative iron-siderophore transporter, permease subunit
acetyl-coenzyme A carboxylase carboxyl transferase (EC:6.4.1.2)
transcriptional regulator of iron proteins and repressor of aconitase, AraC-family
putative benzoate transport transmembrane protein
4-hydroxybenzoate 3-monooxygenase (EC:1.14.13.2)
putative secreted lipoprotein
putative cytoplasmic siderophore-interacting protein
ribose/xylose transporter, ABC-type sugar aldose transport system, ATPase component (TC 3.A.1.2.1)

ribose/xylose transporter, ABC-type transport system, permease component (TC 3.A.1.2.1)
lysine efflux permease
transcriptional regulator of lysE, LysR-family
glucose-specific EIIABC component EIIGlc of PTS EC:2.7.1.69 fructose-specific enzyme II BC (EIIFru) component of PTS (EC:2.7.1.69)
putative superfamily I DNA or RNA helicase
putative plasmid maintenance system antidote protein, HTH-motif XRE-family
arsenite permease, arsenical resistance-3 ACR3-family
transcriptional regulator, represses aconitase, TetR-family
putative Fe-S cluster assembly protein, part of the sufBDCSU response
cysteine desulfhydrase
Fe-S cluster assembly protein
Fe-S cluster assembly ATPase
Fe-S cluster assembly membrane protein
glucose-6-phosphate dehydrogenase (EC:1.1.1.49)
putative subunit of glucose-6-phosphate dehydrogenase
6-phosphogluconolactonase (EC:3.1.1.31)
phosphoenolpyruvate carboxylase (EC:4.1.1.31)
ppGpp synthetase, ppGpp pyrophosphorylase (EC:2.7.6.5)
putative membrane protein CGP3 region
putative secreted protein CGP3 region
hypothetical protein CGP3 region
hypothetical protein CGP3 region
hypothetical protein, conserved
EI enzyme, general component of PTS (EC:2.7.3.9)
transcriptional regulator of sugar metabolism, presumably fructose responsive, DeoR-family
1-phosphofructokinase (EC:2.7.1.56)
fructose-specific enzyme II BC component of PTS (EC:2.7.1.69)
phosphocarrier protein HPr, general component of PTS
ABC-type heme transport system, ATPase component
putative coenzyme F420-dependent N5,N10-methylene tetrahydromethanopterin reductase or related flavin-dependent
hypothetical protein, conserved
putative membrane protein
1-acyl-sn-glycerol-3-phosphate acetyltransferase
cytochrome bc1 complex, cytochrome b subunit
cytochrome bc1 complex, Rieske iron-sulfur protein
cytochrome bc1 complex, diheme cytochrome c1 subunit
cytochrome aa3 oxidase, subunit 3
cytochrome aa3 oxidase, subunit 4
cytochrome aa3 oxidase, subunit 2
hypothetical protein
heme oxygenase
malate synthase (EC:2.3.3.9), part of glyoxylate shunt
isocitrate lyase (EC:4.1.3.1), part of glyoxylate shunt
transcriptional repressor involved in metabolism of 4-hydroxybenzoate, protocatechuate and p-cresol, IclR-family
β-ketoadipyl-CoA thiolase (EC:2.3.1.174)

β-ketoadipate enol-lactone hydrolase (EC:3.1.1.24)
β-carboxy-cis,cis-muconate cycloisomerase (EC:5.5.1.2)
protocatechuate dioxygenase α subunit (EC:1.13.11.3)
catechol 1,2-dioxygenase (EC:1.13.11.1)
benzoate dioxygenase small subunit (EC:1.14.12.10)
benzoate 1,2-dioxygenase ferredoxin reductase subunit (EC:1.18.1.3)
putative alkylhydroperoxidase AhpD-family core domain
putative ATPase component of ABC-type transport system, contains duplicated ATPase domains
putative ABC-type dipeptide/oligopeptide/nickel transport systems, permease component
putative ABC-type dipeptide/oligopeptide/nickel transport system, permease component
putative ABC-type dipeptide/oligopeptide/nickel transport systems, secreted component
putative single-strand DNA binding protein
putative gluconokinase (EC:2.7.1.12)
putative permease of the major facilitator superfamily
cytochrome aa3 oxidase, subunit 1
high affinity cysteine importer
O-acetylserine thiol-lyase, cysteine synthase (EC:2.5.1.47), loss causes cysteine auxotrophy
succinyl-CoA synthetase α subunit, ADP-forming (EC:6.2.1.5)
putative dithiol-disulfide isomerase
mycothiol peroxidase, GSH peroxidase-family (EC:1.11.1.9)
sucrose-specific EIIABC component EIISuc of PTS fructose-specific enzyme II BC (EIIFru) component of PTS (EC:2.7.1.69)
ABC-Transporter for sialic acid, fused permease and ATPase components
ABC-Transporter for sialic acid, contain duplicated ATPase domains
putative permease
putative membrane protein
Sulfate transporter, loss causes sulfide/cysteine auxotrophy
flavohemoprotein
BglG in CgR is 93 AA longer (belongs to BglG?), putative pseudo-gene
putative membrane protein
putative secreted protein
gluconate permease, gluconate:H+ symporter GntP-family
L-lactate permease, operon with lldD, MFS-type
menaquinone-dependent L-lactate dehydrogenase operon with cg3226
putative metal-dependent amidase/aminoacylase/carboxypeptidase
hypothetical protein
putative protein, ACR, double-stranded β-helix domain
putative secreted protein, horizontally transferred gene
hypothetical protein
Cu2+/cation-transporting ATPase transmembrane protein, horizontally transferred gene
putative Cu2+/heavy metal binding transport protein, horizontally transferred gene
hypothetical protein
two component sensor kinase, copper homeostasis, horizontally transferred gene

two component response regulator, copper homeostasis, horizontally transferred gene
putative secreted protein of unknown function, horizontally transferred gene
secreted multicopper oxidase, horizontally transferred gene
putative toxine efflux permease, MFS-type
putative NADH-dependent flavin oxidoreductase, Old Yellow Enzyme family, probably involved in oxidative stress response
catechol 1,2-dioxygenase (EC:1.13.11.37)
myo-Inositol transporter 2, MFS-type
putative permease of the major facilitator superfamily
putative copper chaperone or Hg2+ permease, MerTP-family

ıst two-fold alteration in gene expression. Wild type cells and a Δ*hrrA* strain were cultivated in CG
ene name. In green (D-F) and red (G-I), the measured mRNA levels of the corresponding genes in th
arison to the wild type after 0 h, 0.5 h, or 4 h of incubation in hemin containing medium. The prese

mRNA wt T=0h	mRNA wt T=30m	mRNA wt T=4h	mRNA DhrrA T=0h	mRNA DhrrA T=30m
783,2	319,1	5,9	160,5	103,2
146,9	344,0	222,8	169,4	166,3
7,8	2,0	3,6	2,4	0,6
494,5	397,9	287,3	80,6	88,9
306,1	327,4	201,3	66,6	50,4
165,9	302,2	181,6	56,6	50,7
31,6	114,3	88,2	26,0	26,2
57,0	427,7	8,4	147,6	96,4
42,1	5,4	39,3	9,4	0,3
37,5	47,5	14,2	29,1	19,8
50,5	39,6	16,2	34,2	19,4
39,6	90,2	19,4	29,6	32,9
86,2	116,4	34,9	77,2	50,3
69,7	36,7	60,2	20,7	14,8
1917,1	2911,0	2339,4	392,3	884,6
1156,2	2662,4	2224,9	278,2	768,3
458,1	2731,7	2527,3	229,8	798,8
634,7	578,7	24,9	364,1	261,3
276,6	580,5	17,8	320,0	253,6
537,5	3066,3	45,3	705,1	926,5
1863,7	4490,5	27,0	1442,6	1033,9
19,4	8,6	77,7	3,0	3,0
48,5	32,8	6,7	18,9	12,7
29,7	17,3	19,7	12,8	7,9
873,3	449,8	145,3	850,1	218,0
3615,4	2977,0	54,7	2088,5	1365,4
321,7	183,1	246,2	141,7	83,5
701,1	228,4	772,2	517,3	111,3
35,6	16,4	43,8	13,6	5,2
440,6	466,9	147,2	134,2	124,0
140,1	27,1	228,7	27,0	12,8
415,1	29,5	215,7	52,6	13,6
508,0	728,0	395,4	134,3	156,3
77,0	55,3	105,7	33,8	26,1
1672,9	600,3	42,2	1190,0	207,5
2600,5	682,1	60,3	1874,0	314,8
393,1	139,4	77,5	149,2	65,4
518,3	297,8	119,3	202,5	97,0
29,9	22,5	51,6	16,1	10,5

27,8	24,0	50,7	17,9	11,8
613,8	368,3	8,3	300,9	89,8
57,5	49,0	17,5	38,9	21,6
2393,3	1757,4	1855,8	2649,0	825,0
127,2	736,5	83,3	120,1	297,6
302,1	434,4	172,6	171,1	211,4
53,1	112,9	48,8	42,1	54,9
173,0	368,6	74,8	78,8	171,9
2544,1	4176,3	834,1	3478,9	1899,3
3043,1	4005,4	883,6	3669,2	1828,7
3417,4	3789,5	758,6	3412,6	1567,9
4638,9	4619,6	946,1	4230,5	1871,9
5218,2	4722,5	1051,6	4286,1	2202,4
411,2	728,0	294,8	316,8	321,9
382,6	823,1	302,5	338,8	342,5
184,5	399,9	181,9	208,7	198,5
1217,0	447,6	467,2	735,7	177,9
494,7	736,1	327,6	305,5	338,3
135,4	183,8	90,8	98,1	86,3
20,8	26,5	10,8	14,0	12,7
109,7	122,2	54,1	50,9	57,2
22,6	15,1	11,8	13,0	6,6
1096,6	3586,5	265,7	851,3	1615,4
1629,4	565,0	1067,6	1799,1	204,8
3069,0	1111,2	852,6	3750,8	251,3
2340,6	1037,4	848,4	2908,1	213,2
2834,9	2472,9	931,9	3460,9	431,2
2765,7	3056,9	2443,1	3448,2	1299,4
34,7	4329,7	11,2	2,8	2134,6
55,3	113,0	27,6	40,7	48,0
108,4	196,0	87,6	90,9	97,9
204,1	146,9	135,7	79,5	72,3
441,4	656,1	325,5	243,1	242,3
1531,9	4192,8	2001,6	533,1	1209,8
2308,3	4502,3	1893,6	612,3	1254,2
2729,9	4308,4	1782,9	692,9	1294,4
3935,0	4547,1	1818,0	965,4	1446,9
1375,0	2402,0	1615,9	575,2	824,0
2698,8	3552,2	2684,1	1037,3	1403,6
371,3	475,9	337,4	341,6	138,6
185,3	80,4	263,1	8,3	9,6
295,1	156,7	228,5	145,9	54,2
61,0	16,9	212,8	13,9	8,4
616,9	252,4	25,5	190,1	106,2
817,0	323,1	19,9	207,6	77,2

1150,5	606,2	36,7	349,9	132,0
2832,7	1115,4	156,2	2377,9	555,3
5111,6	2096,4	232,9	5046,4	999,5
143,3	298,3	821,6	49,7	62,5
4,4	6,6	7,3	3,9	1,6
5,2	6,7	5,9	1,8	1,5
349,7	1095,0	285,3	877,5	491,2
571,8	1357,7	18,0	859,1	399,3
891,9	1635,4	12,3	855,5	432,6
1213,2	1710,5	11,0	845,1	438,1
1362,4	1661,0	15,7	756,1	465,6
26,5	20,5	12,0	14,0	9,9
61,2	33,8	6,5	36,9	8,0
32,7	59,3	9,0	21,7	29,2
3107,7	5452,0	3251,3	1682,3	2653,4
212,1	944,4	26,1	94,1	164,4
8886,8	7276,4	611,9	4250,2	2372,2
45,7	35,7	576,0	87,0	16,6
283,1	1219,4	86,3	197,3	579,0
284,8	487,7	311,2	195,9	172,1
3076,8	629,6	1200,2	4006,3	144,1
35,4	22,2	36,7	41,0	9,9
19,8	23,7	33,5	31,4	9,4
393,2	430,1	327,3	106,2	126,7
12,4	12,0	4,8	8,2	5,2
4747,4	5718,7	15,8	4079,5	2666,5
825,6	454,8	8,7	238,8	170,1
7,5	9,4	5,8	5,7	2,2
430,2	422,9	189,2	92,0	98,6
74,6	260,6	15,5	104,4	122,7
383,5	166,1	178,6	212,9	60,1
2579,1	569,4	83,9	1161,8	178,5
4147,0	905,9	134,2	1808,7	311,1
129,2	557,6	59,9	89,6	262,7
1,5	7,1	10,4	1,5	2,4
181,8	804,8	57,2	198,6	265,1
1436,3	6136,9	43,1	1447,1	2940,8
459,2	4055,7	22,0	685,8	1736,3
1250,1	2882,3	27,1	647,3	1133,8
1870,4	2441,3	31,0	957,1	923,6
779,6	978,2	23,3	474,2	440,8
15,5	22,6	22,4	6,2	8,7

25,0	31,0	19,7	7,3	14,2
107,6	212,5	77,3	17,8	56,2
45,5	91,0	37,4	6,6	24,3
310,8	263,7	22,4	17,4	18,8
993,8	1177,7	27,2	610,7	554,7
94,1	35,1	49,3	86,0	16,5
127,1	33,4	56,0	62,0	13,6
1182,9	1521,5	10,6	602,5	241,8
1464,6	2591,0	28,3	1863,5	1236,0

XII minimal medium supplemented with 2%
e wild type strain (green) and a Δ*hrrA* strain
ented genes were filtered for at least two-

mRNA DhrrA T=4h	Log2 DhrrA/WT T=0h	Log2 DhrrA/WT T=30m	Log2 DhrrA/WT T=4h
20,4	-2,3	-1,6	1,8
155,6	0,2	-1,0	-0,5
18,7	-1,7	-1,7	2,4
133,9	-2,6	-2,2	-1,1
99,2	-2,2	-2,7	-1,0
87,6	-1,6	-2,6	-1,1
43,6	-0,3	-2,1	-1,0
6,4	1,4	-2,1	-0,4
20,8	-2,2	-4,1	-0,9
6,9	-0,4	-1,3	-1,0
11,0	-0,6	-1,0	-0,6
15,2	-0,4	-1,5	-0,4
25,5	-0,2	-1,2	-0,5
14,4	-1,8	-1,3	-2,1
760,6	-2,3	-1,7	-1,6
774,9	-2,1	-1,8	-1,5
839,3	-1,0	-1,8	-1,6
24,2	-0,8	-1,1	0,0
19,4	0,2	-1,2	0,1
39,9	0,4	-1,7	-0,2
30,1	-0,4	-2,1	0,2
72,5	-2,7	-1,5	-0,1
5,4	-1,4	-1,4	-0,3
17,5	-1,2	-1,1	-0,2
148,4	0,0	-1,0	0,0
304,6	-0,8	-1,1	2,5
153,9	-1,2	-1,1	-0,7
907,8	-0,4	-1,0	0,2
106,2	-1,4	-1,7	1,3
92,2	-1,7	-1,9	-0,7
718,5	-2,4	-1,1	1,7
644,6	-3,0	-1,1	1,6
119,4	-1,9	-2,2	-1,7
339,2	-1,2	-1,1	1,7
27,4	-0,5	-1,5	-0,6
37,4	-0,5	-1,1	-0,7
33,4	-1,4	-1,1	-1,2
135,6	-1,4	-1,6	0,2
61,5	-0,9	-1,1	0,3

69,2	-0,6	-1,0	0,4
9,1	-1,0	-2,0	0,1
14,7	-0,6	-1,2	-0,3
1779,5	0,1	-1,1	-0,1
71,6	-0,1	-1,3	-0,2
62,1	-0,8	-1,0	-1,5
45,0	-0,3	-1,0	-0,1
60,3	-1,1	-1,1	-0,3
830,8	0,5	-1,1	0,0
869,8	0,3	-1,1	0,0
766,3	0,0	-1,3	0,0
954,6	-0,1	-1,3	0,0
1067,8	-0,3	-1,1	0,0
243,7	-0,4	-1,2	-0,3
267,3	-0,2	-1,3	-0,2
157,0	0,2	-1,0	-0,2
332,6	-0,7	-1,3	-0,5
227,1	-0,7	-1,1	-0,5
63,5	-0,5	-1,1	-0,5
6,3	-0,6	-1,1	-0,8
33,9	-1,1	-1,1	-0,7
10,4	-0,8	-1,2	-0,2
206,4	-0,4	-1,2	-0,4
910,0	0,1	-1,5	-0,2
510,3	0,3	-2,1	-0,7
510,7	0,3	-2,3	-0,7
548,2	0,3	-2,5	-0,8
1981,3	0,3	-1,2	-0,3
185,5	-3,7	-1,0	4,0
14,6	-0,4	-1,2	-0,9
87,7	-0,3	-1,0	0,0
106,6	-1,4	-1,0	-0,3
147,8	-0,9	-1,4	-1,1
1227,5	-1,5	-1,8	-0,7
1153,9	-1,9	-1,8	-0,7
1034,6	-2,0	-1,7	-0,8
1039,4	-2,0	-1,7	-0,8
934,6	-1,3	-1,5	-0,8
1371,5	-1,4	-1,3	-1,0
169,3	-0,1	-1,8	-1,0
19,1	-4,5	-3,1	-3,8
159,1	-1,0	-1,5	-0,5
260,7	-2,1	-1,0	0,3
15,4	-1,7	-1,2	-0,7
17,5	-2,0	-2,1	-0,2

34,0	-1,7	-2,2	-0,1
60,4	-0,3	-1,0	-1,4
93,3	0,0	-1,1	-1,3
230,6	-1,5	-2,3	-1,8
1,1	-0,2	-2,0	-2,7
2,1	-1,6	-2,2	-1,5
225,6	1,3	-1,2	-0,3
61,0	0,6	-1,8	1,8
63,4	-0,1	-1,9	2,4
72,0	-0,5	-2,0	2,7
79,0	-0,8	-1,8	2,3
8,1	-0,9	-1,1	-0,6
10,6	-0,7	-2,1	0,7
9,0	-0,6	-1,0	0,0
1786,1	-0,9	-1,0	-0,9
35,7	-1,2	-2,5	0,5
2635,8	-1,1	-1,6	2,1
171,2	0,9	-1,1	-1,8
93,3	-0,5	-1,1	0,1
208,8	-0,5	-1,5	-0,6
674,8	0,4	-2,1	-0,8
26,8	0,2	-1,2	-0,5
25,5	0,7	-1,3	-0,4
178,9	-1,9	-1,8	-0,9
2,6	-0,6	-1,2	-0,9
166,0	-0,2	-1,1	3,4
12,5	-1,8	-1,4	0,5
2,2	-0,4	-2,1	-1,4
137,5	-2,2	-2,1	-0,5
9,7	0,5	-1,1	-0,7
89,0	-0,8	-1,5	-1,0
151,9	-1,2	-1,7	0,9
408,9	-1,2	-1,5	1,6
56,7	-0,5	-1,1	-0,1
14,2	-0,1	-1,6	0,4
43,7	0,1	-1,6	-0,4
26,3	0,0	-1,1	-0,7
13,0	0,6	-1,2	-0,8
16,0	-0,9	-1,3	-0,8
23,4	-1,0	-1,4	-0,4
20,7	-0,7	-1,2	-0,2
10,7	-1,3	-1,4	-1,1

5,6	-1,8	-1,1	-1,8
59,4	-2,6	-1,9	-0,4
32,9	-2,8	-1,9	-0,2
6,8	-4,2	-3,8	-1,7
26,2	-0,7	-1,1	-0,1
30,8	-0,1	-1,1	-0,7
37,2	-1,0	-1,3	-0,6
47,0	-1,0	-2,7	2,1
24,2	0,3	-1,1	-0,2

Predicted function
Signal transduction mechanisms
Cell division, chromosome partitioning
Unknown function
Unknown function
Unknown function
General function prediction only
General function prediction only
Amino acid transport and metabolism
Unknown function
Amino acid transport and metabolism
Amino acid transport and metabolism
Inorganic ion transport, metabolism, and storage
Inorganic ion transport, metabolism, and storage
Cell wall/membrane/envelope biogenesis
Central carbon metabolism; Anaerobic metabolism; Respiration and oxidative phosphorylation
Central carbon metabolism; Anaerobic metabolism; Respiration and oxidative phosphorylation
Central carbon metabolism; Anaerobic metabolism; Respiration and oxidative phosphorylation
General function prediction only
General function prediction only
Signal transduction mechanisms; Inorganic ion transport, metabolism, and storage
Inorganic ion transport, metabolism, and storage
Transport and metabolism of further metabolites
General function prediction only
Unknown function
General function prediction only
Amino acid transport and metabolism
Unknown function
Coenzyme transport and metabolism
Inorganic ion transport, metabolism, and storage; Transport and metabolism of further metabolites
Unknown function
Inorganic ion transport, metabolism, and storage; Transport and metabolism of further metabolites
Inorganic ion transport, metabolism, and storage; Transport and metabolism of further metabolites
Lipid transport and metabolism
Signal transduction mechanisms
Carbon source transport and metabolism
Carbon source transport and metabolism
Unknown function
Transport and metabolism of further metabolites
Carbon source transport and metabolism

Carbon source transport and metabolism
Amino acid transport and metabolism
Signal transduction mechanisms
Carbon source transport and metabolism; signal transduction mechanisms
DNA replication, recombination, repair, and degradation; Transcription including sigma factors, RNA processin
General function prediction only
Inorganic ion transport, metabolism, and storage
Signal transduction mechanisms
Coenzyme transport and metabolism
Coenzyme transport and metabolism
Coenzyme transport and metabolism
Coenzyme transport and metabolism
Coenzyme transport and metabolism
Central carbon metabolism
Central carbon metabolism
Central carbon metabolism
Central carbon metabolism
Signal transduction mechanisms
Prophage genes
Prophage genes
Prophage genes
Prophage genes
Unknown function
Carbon source transport and metabolism
Signal transduction mechanisms
Central carbon metabolism
Carbon source transport and metabolism
Carbon source transport and metabolism
Transport and metabolism of further metabolites
Coenzyme transport and metabolism
Unknown function
Unknown function
Cell wall/membrane/envelope biogenesis
Respiration and oxidative phosphorylation
Respiration and oxidative phosphorylation
Respiration and oxidative phosphorylation
Respiration and oxidative phosphorylation
Respiration and oxidative phosphorylation
Respiration and oxidative phosphorylation
Unknown function
Transport and metabolism of further metabolites
Central carbon metabolism
Central carbon metabolism
Signal transduction mechanisms
Carbon source transport and metabolism

Carbon source transport and metabolism
Carbon source transport and metabolism
Carbon source transport and metabolism
Carbon source transport and metabolism
Carbon source transport and metabolism
Carbon source transport and metabolism
General function prediction only
General function prediction only
General function prediction only
General function prediction only
General function prediction only
DNA replication, recombination, repair, and degradation
Central carbon metabolism
General function prediction only
Respiration and oxidative phosphorylation
Amino acid transport and metabolism
Amino acid transport and metabolism
Central carbon metabolism
Protein turnover and chaperones
Transport and metabolism of further metabolites
Carbon source transport and metabolism
Carbon source transport and metabolism
Carbon source transport and metabolism
General function prediction only
Unknown function
Amino acid transport and metabolism; Inorganic ion transport, metabolism, and storage
Inorganic ion transport, metabolism, and storage
Unknown function
Unknown function
Unknown function
Carbon source transport and metabolism
Carbon source transport and metabolism
Carbon source transport and metabolism; Respiration and oxidative phosphorylation
Protein turnover and chaperones
Unknown function
General function prediction only
Unknown function
Unknown function
Inorganic ion transport, metabolism, and storage
Inorganic ion transport, metabolism, and storage
Unknown function
Post-translational modification; Signal transduction mechanisms

Signal transduction mechanisms
Unknown function
Inorganic ion transport, metabolism, and storage
Transport and metabolism of further metabolites
General function prediction only
Transport and metabolism of further metabolites
Carbon source transport and metabolism
General function prediction only
Inorganic ion transport, metabolism, and storage

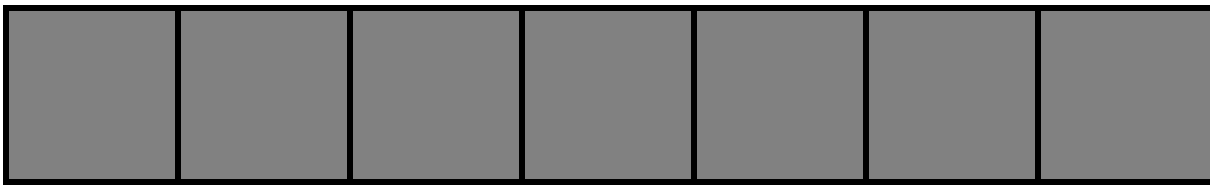

g and modification